Fall 2014

Impact of slickwater fracturing fluid compositions on the petrophysical properties of shale and tightsand

Yongpeng Sun

Department: Geosciences and Geological and Petroleum Engineering

IMPACT OF SLICKWATER FRACTURING FLUID COMPOSITIONS ON THE PETROPHYSICAL PROPERTIES OF SHALE AND TIGHTSAND

by

Yongpeng Sun

A DISSERTATION

Presented to the Faculty of the Graduate School of the

MISSOURI UNIVERSITY OF SCIENCE AND TECHNOLOGY

In Partial Fulfillment of the Requirements for the Degree

DOCTOR OF PHILOSOPHY

in

PETROLEUM ENGINEERING

2014

Approved
Baojun Bai, Advisor
Yinfa Ma, co-Advisor
Ralph Flori
Runar Nygaard
Mingzhen Wei

ABSTRACT

A tight reservoir always requires hydraulic fracturing before production to increase production rate. The additives in hydraulic fluids are highly considerable for a successful stimulation. A friction reducer is often used to reduce the flowing friction in the wellbore during hydraulic fracturing. Extensive researches have been conducted to examine the extent it can reduce the fluid friction in tubings; however, no research has been reported on its behavior in a reservoir, which is related to the fracture extension. A breaker is also pumped into the formation to degrade the friction reducer. However, it is not clear that what is the best time to break it. After the hydraulic fracturing, the existence of liquid in matrix reduces the gas phase permeability. A surfactant is added to reduce water block by providing a low surface tension. However, the effect of the surfactant on the petrophysical properties of tight rocks is not clear.

In this dissertation, the following four researches have been carried out, and significant findings have been summarized in conclusions. The friction reducer flow behavior in microfractures was studied firstly, including size effect, concentration effect, wettability effect, and etc. Consequently, various additives impact on the petrophysical properties on tight sand was examined, such as surface contact angle, gas phase permeability, liquid imbibition, and gas transportation. Then, formation damage of FR and breaker in tight sand was systematically investigated. The impact factors were disclosed in detail, including fluid concentration, sample length, breaking time, and permeability regain. Finally, surfactant wettability impact on liquid intake in shale was carried out carefully. The liquid intake rate affected by the existence of fractures, fluid concentration, sample length, and treatment method were specified in detail.

ACKNOWLEDGMENTS

First I would like to express sincere thanks to my advisor, Dr. Baojun Bai, not only for this dissertation, but also for helping me develop a scientific mind to do research. You have a great influence throughout my Ph.D. career. You have supported me not only by providing research assistantship, but also academically and emotionally throughout the rough road. You helped me come up with the research topics, guided me over difficulties and enrich me freedom during research. Your ability to select and to approach compelling research problems, high scientific standards, and hardworking personality set an example. Above all, you made me feel a friend, which I appreciate from my heart.

I am particularly thankful to Dr. Yinfa Ma, my co-Advisor. I have learned invaluable experience about thinking and learning from you. Your background in chemistry can always brighten me new ideas. Thank you for the comments, motivating discussions, support, and the kind encouragement for my research.

Special thanks go to my dissertation committee: Dr. Ralph Flori, Dr. Runar Nygaard and Dr. Mingzhen Wei. They guided me through all these years. Your insightful comments and discussions always bring me new view in my study.

I am also indebted to dozens of people, who have helped and taught me immensely. Dr. Yongfu Wu's chemistry background and experience is impressive. Fang Yang welcomed me to the lab and found me my first apartment. Jia Zhou gave me really constructive comments. Your industry insight is a valuable source of motivation. Hao Zhang helped me fabricate and build the setup with his multi discipline knowledge. Qihua Wu‘s writing and presenting skills benefit me a lot these years. Farag Muhammed always provides help whenever I am asking. My other great office mates have been supportive in every way. Department secretaries: Paula Cochran, Patti Robertson, Patti Adams have been amazing help all this time.

Sincere gratitude and very special thanks go to family. My wife Lingke Meng provides me love, encouragement and support when I have needed them the most. My son Justin always brings me fun and happiness. Thank you with all my heart!

Finally, Thanks also are due to RPSEA and China Scholarship Council for their financial supporting these years.

TABLE OF CONTENTS

Page

LIST OF ILLUSTRATIONS

LIST OF TABLES

NOMENCLATURE

Symbol	Description
A	Cross-sectional area
AP	Ammonium persulfate
c_1	Conversion factor, $c_1=7.32\times10^{-7}$
c_2	Conversion factor, $c_2=1489.6$
cP	centi-poise
D	Equivalent diameter of microfracture, m
DIW	deionized water
dP/dL	Pressure gradient
EIA	US Energy Information Administration
FR	Friction reducer
F_r	Resistance factor
F_{rr}	Residual resistance factor
gpt	Gallon per thousand gallon
GTI	Gas Technology Institute
h	Fracture height, m
ID, D	Inner diameter of microchannel in μm
K	Permeability
k	Flow consistency index in cP
K_a	absolute permeability
KCl	Potassium Chloride
K_g	gas phase permeability
K_{ga}	gas phase permeability after treated with additives
K_{rg}	relative gas permeability
L	Microchannel length in ft
M	Fluid mobility
mD	Milli-Darcy
n	Dimensionless flow behavior index
nD	nano-Darcy

nm	nanometer
pm	picometer
pptg	Pound per thousand gallon
PV	Pore volume
q	Fluid flow rate
r	Edge radius of the microfracture, m
R	Microchannel radius in ft
Re	Reynolds number
RPM	Rotary per minute
S_L	Liquid saturation, %;
SEM	Scanning Electron Microscope
SEM/FIB	Focused Ion Beam/Scanning Electron Microscope
tcf	Trillion cubic feet
TOC	Total organic carbon
USGS	United States Geological Survey
v	Fluid velocity
w_L	Sample weight at certain time, g
w_{wet}	Sample weight after humidified Nitrogen flooding, g
x	Boundary layer development length, m
XRD	X-ray diffraction
γ	Shear rate, s^{-1}
δ	Boundary-layer thickness, m
$\Delta dP/dL$	Pressure gradient difference in psi/ft
ΔP	Pressure drop
η_{app}	Apparent viscosity
μ	Fluid dynamic viscosity
μD	micro-Darcy
ρ	Fluid density
υ	Fluid kinematic viscosity, m^2/s

1. INTRODUCTION

1.1. ENERGY DEMANDS

With the increasing demand of energy all around the world, renewable and environmental friendly energy is booming in the past decade, such as: solar energy, wind power, geothermal energy, hydropower, etc. However, due to the problems of technical feasibility, availability, economical and ecology concerns in the development of renewable energy, fossil fuels, such as crude oil, natural gas and coal, will still be the major energy source of the world in the next several decades, as illustrated by the U.S. Energy Information Administration (EIA) in Figure 1.1.

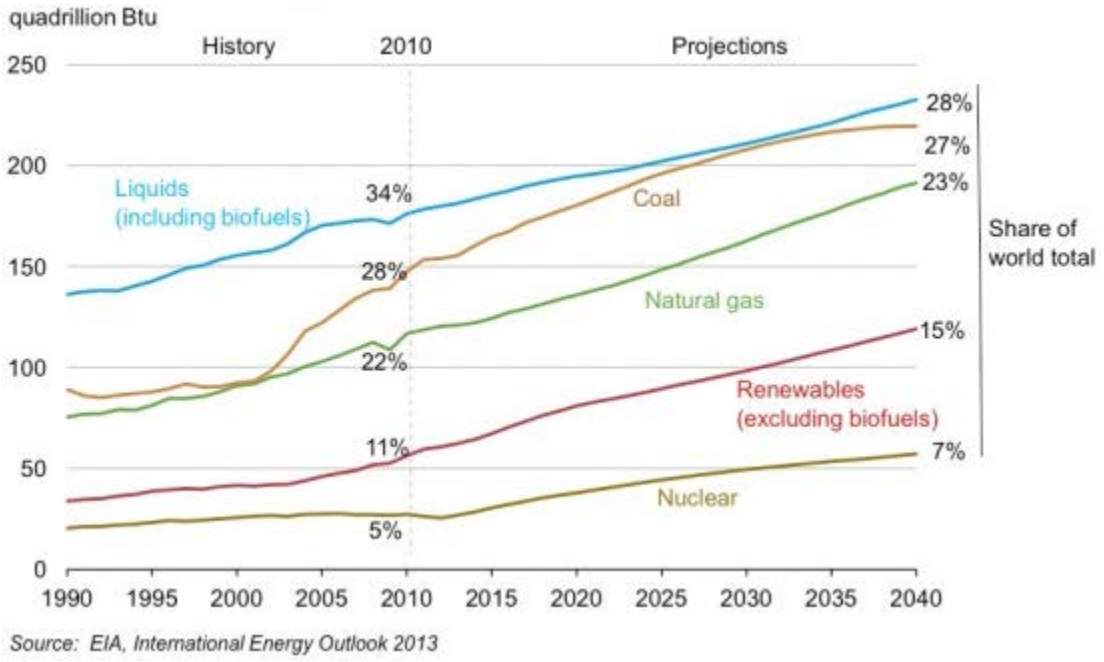

Figure 1.1. World energy consumption by fuel
(EIA, International Energy Outlook, 2013)

Natural gas, which produces the least greenhouse gas emission among the fossil fuel, is considered as a green energy. With the huge demanding, technical development and declining production from conventional gas reservoir, the large volume reserve of natural gas stored in tight formation, such as tight sand and shale, is practical to develop recently.

1.2. UNCONVENTIONAL GAS

The unconventional gas majorly includes tight gas, shale gas, and coalbed methane. Tight gas is the natural gas store in conventional sandstone or limestone reservoir, featuring less than 0.1 Millidarcy (mD) matrix permeability and less than ten percent matrix porosity. Shale gas is natural gas that is found trapped within shale formations. Coalbed methane is the natural gas extracted from coal beds. It is usually ‘sweet gas' because of its lack of hydrogen sulfide, and distinct from the typical sandstone or other conventional gas reservoir. This dissertation will focus on the first two types of unconventional gas: tight gas and shale gas.

EIA estimates that there is 7,299 trillion cubic feet (Tcf) technically recoverable shale gas in the world**.** In the United States in 2011, about 7.85 Tcf of dry natural gas was produced directly from shale deposits. This was approximately 34% of total U.S. dry natural gas productions in 2011. The Gas Technology Institute (GTI) estimates that the gas in place in the U.S. tight gas basins is over 5,500 Tcf (Gas 2001).

Tight sand and shale gas exists in underground reservoirs with micro-Darcy (μD) and nano-Darcy (nD) range permeability and are characterized by nanometer sized pore throats and crack-like interconnections between pores (Wells and Amaefule 1985). These microscopic features result in some macroscopic characteristic features such as high capillary pressures, low porosities, high irreducible wetting phase saturation and extremely low permeability. In order to achieve commercial production from these extremely low permeability gas reservoirs, horizontal drilling combined with hydraulic fracturing stimulation is generally executed.

1.3. HYDRAULIC FRACTURING

Hydraulic fracturing is the fracturing of rock by a pressurized liquid to increase the fracture-face surface area, and increase the production rate. It is a formation stimulation technique.

The basic hydraulic fracturing process is illustrated in Figure 1.2.

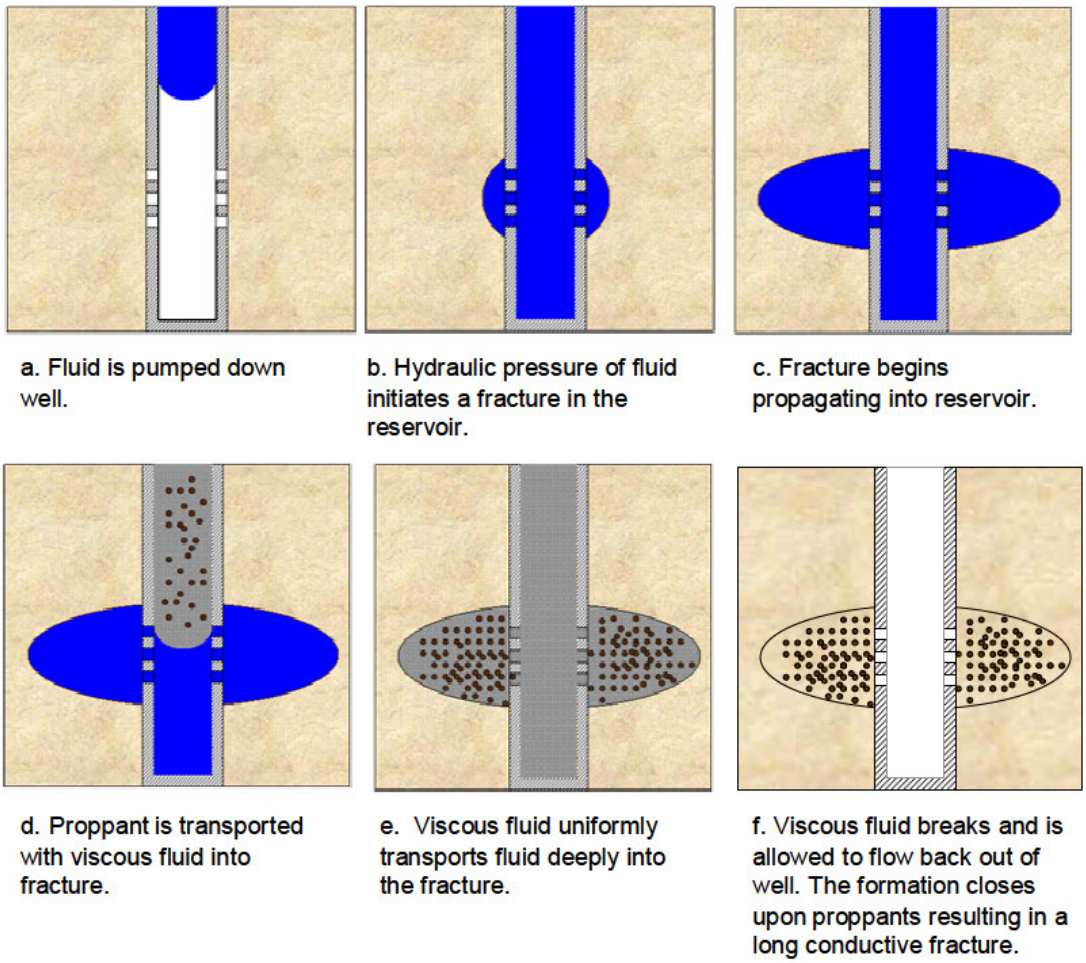

Fig. 1 – Basic Hydraulic Fracturing Process

Figure 1.2. Basic Hydraulic Fracturing Process
(Tschirhart 2005)

In the first stage, a small quantity of fluid is pumped down the well, known as "pre-pad," to fill up the well and initiate a fracture into the reservoir through the perforations in the well casing.

Then, a neat fluid known as “pad” is pumped. When the hydraulic pressure exceeds that of the fracture gradient, the rock cracks and the fracture extended further as the fluid continues pumping.

Subsequently, slurry consisting of fluid and proppant is pumped in the fracture to maintain the fracture width or slow its decline. The proppant could be grains of sand, ceramic, or other particulates. It will hold the fracture open when pumping is stopped and the pressure of fluid is removed. It also provides a conductive path for gas to flow to the wellbore. High fluid viscosity is required to carry proppant deep into the fracture and prevent proppant from settling down at near wellbore location.

The last and most important stage of fracturing is to break the polymer carrying the proppant. When the polymer is degraded, the low viscosity fluid can flow back to the ground surface. Then the fracture is created where proppant is holding the fracture against closing.

1.4. OBJECTIVE

The objective of the study is to improve the understanding of the flow behavior of introduced fluids (water, polymers, breaker, and surfactant solutions) in micro-Darcy to nano-Darcy range of tight gas and shale formations by a series of experiments. The specific objectives are to:

1) Develop a fast, steady state method to measure the absolute permeability of unconventional tight sand;
2) Analysis the major fracturing fluid component properties, such as particle size distribution in fluid, viscosity, surface tension, and etc;
3) Study the friction reducer flowing behavior in microchannel and microfracture, including size effect, concentration effect, wettability effect, and residual resistance factor to water;
4) Investigate the petrophysical impact of brine, friction reducer, breaker and surfactant consecutively treating on tight sand samples, including relative permeability, surface wettability, and in-depth wettability, and etc;
5) Examine the formation damage caused by friction reducer and breaker in tight sand samples, including permeability regain after treated with additives, and gas transport phenomenon in these samples;

6) Study the liquid intake condition of surfactant in shale samples using co-current imbibition method

1.5. RESEARCH SCOPE

This fundamental research will comprehensively investigate the hydraulic fracturing fluid transport in unconventional tight gas and shale gas formation by multiple-disciplinary research methods as follows: (1) Novel method to determine tight sample absolute permeability; (2) Integrated hydraulic fluid additives analysis, including brine, friction reducer, breaker, and surfactant; (3) Friction reducer flows in different shaped microchannel and microfracture model to represent the microfracture after fracturing; (4) Combined imbibition and core flooding tests to study the rock, fluid, and gas interaction during hydraulic fracturing.

Figure 1.3 shows the scope of the project.

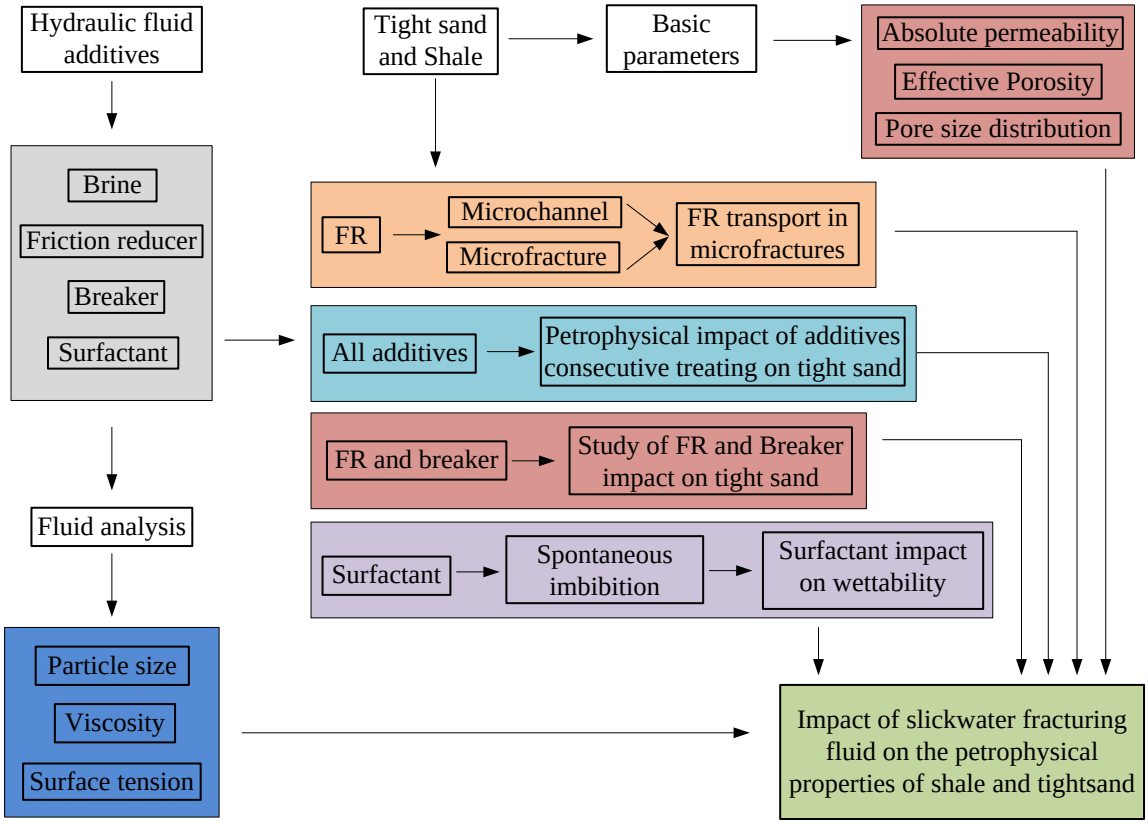

Figure 1.3. Whole study flowchart

1.6. DISSERTATION OUTLINE

Section 2 presents a literature review of unconventional rock basic parameter measurement, and hydraulic fluid composition.

Section 3 describes the rock preparation method and their basic parameters, including: rock permeability, porosity, pore size distribution, surface examination using SEM. It also provides the surface tension of the surfactant and emulsion particle size of the friction reducer used in this dissertation.

Section 4 displays the friction reducer transport phenomenon in microchannel and microfracture. Friction reducer is found to behave different from that in macro tubing during hydraulic fracturing.

Section 5 illustrates the petrophysical impact when a rock is consecutively treated with several additives. It shows how the fluid influence in the near fracture matrix during each stage of hydraulic fracturing, such as permeability, surface wettability, liquid intake, and gas transportation.

Section 6 discusses the friction reducer and breaker interaction in near fracture matrix through comprehensive experiment. Several impact factors are studied in detail, such as sample length effect, fluid concentration, treating method.

Section 7 exhibits the shale rock liquid intake condition before and after treated with surfactant. The impact of fractures existence, solution concentration, and sample length are all discussed carefully.

Section 8 presents the conclusions founded on all the experimental work. Recommendations for the next step are listed based on experience.

2. LITERATURE REVIEW

2.1. TIGHT SAND AND SHALE BASIC PARAMETERS MEASUREMENT

Many petro-physical properties of unconventional tight gas and shale gas formation are significantly different from those of conventional reservoirs because of their nanometer sized pore, unique pore structure, and the resulted wettability, transport, and gas storage properties.

Although shale and tight sand are both very tight formations, they are still very different. Tight sand is from a tight sandstone reservoir, dominantly composed of quartz, followed by feldspar and rock fragment and others (Rushing, Newsham et al. 2008). The tight gas sandstone is completely water wet, and gas is stored in the pore space as free gas. On the other hand, the pore space in gas shale consists of pores in the organic matter, Kerogen, and pores in the inorganic matrix (Wang and Reed 2009, Elgmati, Zhang et al. 2011, Georgi, Jin et al. 2013). While organic matter is oil wet, and the inorganic matrix is water wet. The adsorbed gas resides mainly in the small Kerogen pores whose characteristic lengths are usually less than 100 nm. The free gas is mainly stored in the inorganic matrix pores, and microfractures. The pore size could be only slightly one order of magnitude larger than that of Methane molecules. Flow behavior of introduced fluid should be different from that in conventional gas reservoir. Permeability and porosity are critical parameters controlling fluid transport in porous rocks.

2.1.1. Permeability Measurement. Due to the extremely small pore size and low porosity, traditional steady state method to measure absolute permeability is time consuming. Unsteady state method, such as pulse decay method with whole core plug or crush sample, 3D imaging method are usually used for tight formation permeability measurement in lab.

Pulse decay method with core plug for the tight sample permeability measurement is initially brought in the 1970s (Byrnes, Sampath et al. 1979). After the sample placed in a core holder, shut in the system, the upstream and downstream pressures of the core are allowed to equilibrate. A pressure approximately 50 psi higher than the pore pressure is generated in the vessels upstream of the core and then, by opening the upstream valve, a differential pressure is instantly induced across the core. By monitoring the upstream

pressure decay as a function of time, permeability was calculated. Permeability measured with pulse decay method as they reported are very close to the steady state method (Byrnes, Sampath et al. 1979).

Pulse decay method with crushed samples could be employed when the whole core plug is not available. This method is more focusing on matrix permeability, without any fracture, parallel to bedding or coring induced. It crushes the sample first, and a narrow sieve cut is used in pulse pressure tests with helium to derive both K and ϕ_g. Advantages of this method are that it is quick to run (roughly one hour), less expensive, can be used on drill cuttings. And since shale is likely to part along microfractures and bedding planes during crushing, individual chips are unlikely to contain microfractures. A disadvantage is that the test is running at no overburden stress (Luffel, Hopkins et al. 1993). The lab procedure is as followed. A measured weight of crushed shale (15 to 30 g) is placed in a sample cell. Helium is then expanded into the sample cell from a reference chamber at 200 psig. Pressure instantly drops to a level dictated by the dead space in the sample cell, and then decays with time to a lower pressure as helium moves into the pores within each shale chip. In addition, selected pulse tests were implemented in shale chips of various sieve cuts (10/20, 20/35, and 35/60 mesh).

Other method could also obtain the permeability of tight samples, such as 3D imaging method with Focused Ion Beam - Scanning Electron Microscopy (FIB-SEM). The 3D imaging method could characterize the nano-scale pores and mineral structure of the low permeability rocks by using the FIB-SEM, which is focused on up to μm size scale samples. During measurement, FIB is milling at nanometer sized increment in depth, and SEM is taking imaging of a certain area after each milling. Through combining the hundreds of images, a 3D model will be generated, with numerical simulation software, permeability, porosity, and pore connectivity could be obtained (Elgmati, Zhang et al. 2011, Zhang, Klimentidis et al. 2011).

However, pulse decay with core plug and the 3D imaging method are expensive, pulse decay with crushed sample does not have confining pressure, and it does not consider the fracture in sample. And steady state method is usually recommended in lab permeability measurement, but for unconventional tight rock, it will take very long time to achieve this. In this proposal, a coating and slicing method will be studied to measure

the absolute permeability of tight rock. It does not require whole core plug or regular shape sample. It has confining pressure and runs fast.

2.1.2. Porosity Measurement. There are two types of porosity in porous media, total porosity and effective porosity. Total porosity is defined as the ratio of the volume of all pores to the bulk volume of a porous media, regardless of whether or not if the pores are interconnected. While effective porosity is defined as the ratio of the interconnected pore volume to the bulk volume of a porous media, which is more often used to study the fluid behavior in porous media. The matrix pore spaces in shale are poorly connected. The general effective porosity estimates of the US shale matrix are in the range 1– 9% (Curtis 2002, Boyer, Kieschnick et al. 2006, Arthur, Bohm et al. 2009, Yu and Lau 2013). For tight sand, the effective porosity generally could be ranging from 5% to 12% (Fredrich, Greaves et al. 1993, MacBeth and Schuett 2007, Wang, He et al. 2013). Generally, there are two kinds of methods to measure the effective porosity: Helium method and Mercury method.

The Helium method is based on Boyle's law. This method is usually used to determine the effective porosity of conventional reservoir. The porous sample need to stay in oven at temperature over 100 ℃ for some time to vaporize the water and moisture before loaded in the sample cell. Time varies on sample condition. Measure the sample dimension, dry weight, bulk volume. The setup mainly consists of 2 cells: reference cell and sample cell. Before measuring the porosity, reference volume and dead volume have to be calibrated first. After applied a certain pressure to the reference cell, shut in the inlet valve, open the valve between the two cells, and observe the pressure before and after Helium goes into the sample cell, calculate the reference volume and dead volume based on Boyle's law. Then the porosity measurement can be started. After the sample is loaded in sample cell, fill the reference cell with Helium at certain pressure, release it to the sample cell and monitored the pressure before and after. Then calculate the porosity based on the pressure data. This method is also used to estimate the effective porosity of shale. Luffel and Guidry (1992) introduced a crushing technique to increase the surface area of the available pore networks for various gas shales. They argued that the pores were all connected, but the connections were so small even helium required substantial times to

equilibrate and reach all the pore space. They conducted measurement with 5 samples of Devonian Shales that were known to be well within the dry gas window, thereby eliminating any residual liquid hydrocarbon issues. Initially, bulk volume, grain volume, and dry bulk density were determined using standard helium techniques on the 1 in diameter core plugs. The core plugs were subsequently crushed into chips around ½ in. Grain volumes and weights were measured on the chips and porosity was calculated using a combination of the dry density (measured on plugs) and weight. They also conducted the experiment with whole core plug. Their results show that crushed rock porosities were generally 0.1 % higher than the whole core samples, presumably due to the fact that helium did not completely infiltrate the uncrushed whole samples (Luffel and Guidry 1992, Sondergeld, Newsham et al. 2010)

Mercury method: high pressure mercury injection capillary pressure (MICP) is also a direct method to obtain the porosity of a porous media. Due to the high pressure capacity of the instrument, this method could work on all rocks, sandstone, shale, dolomite, carbonate, and etc. Determining porosity using MICP involves measuring bulk volume and pore volume by measuring the amount of mercury injected into the sample under a pressure as high as 60,000 psia. Due to the limited sample employed during measurement, the result has turned out to be highly dependent upon the accuracy and precision of making bulk density and grain density measurements on crushed rock. The sample used in MICP will not be able to perform other experiments. This method could also obtain the pore size distribution of a porous media.

In this dissertation, Helium method will be employed for the porosity measurement. Careful sample surface preparation removes the contamination and blocking introduced during cutting. Mercury injection experiment is conducted to study the pore size distribution in tight rocks.

2.2. HYDRAULIC FRACTURING FLUID ADDITIVES

Among the various fracturing methods, slickwater fracturing has been proved to be an effective method by which to increase the recovery of tight gas and shale gas reservoirs (Grieser, Hobbs et al. 2003, Palisch, Vincent et al. 2010, Sun, Wood et al. 2011). By adding a very small amount of chemical to the fluid (<1 vol% of the liquid volume) (Kaufman, Penny et al. 2008, Arthur, Bohm et al. 2009, Paktinat, O'Neil et al.

2011), slickwater fracturing fluid can lower the surface pumping pressure below that achieved with the traditional cross-linked fracturing fluid. This fluid also demonstrates a relatively low viscosity during fracture extension, which would significantly reduce the gel damage and easier to flow back.

The slickwater fracturing fluid contains some specially designed additives. Their name, generic product, typical concentration, and function are shown in Table 2.1 (Arthur, Bohm et al. 2009, Paktinat, O'Neil et al. 2011, Paktinat, O'Neil et al. 2011).

Table 2.1. Slickwater fracturing fluid composition

Additives	Generic chemistry	Typical concentration	Function and purpose
Water	Mixing fluid	~95-99%	Majority of frac fluids
Brine	KCl	0.2%	Create a brine carrier fluid that prohibits fluid interaction with formation
Friction reducer	Polyacrylamide (anionic, cationic or nonionic), Mineral oil	0.25-1 gpt	Reduce the flowing friction by changing the turbulent flow to laminar flow
Surfactant	Ethoxylated alcohols, Isopropanol	0.02-0.1%	Reduce the frac fluid surface tension, and improve the liquid recovery from the well after frac
Breaker	Peroxide, Enzyme complexes	0.009%	Allow a delayed break down of the polymer and gel
Biocide	Glutaraldehyde, DBNPA, THPS, Dazomet.	0.01%	Eliminates bacteria in the water that produce corrosive byproducts
Crosslinker	Borate salts	0.006%	Maintain the fluid viscosity as temperature increase

Table 2.1. Slickwater fracturing fluid composition (cont.)

Additives	Generic chemistry	Typical concentration	Function and purpose
Gel	Guar gum or Hydroxyethyl cellulose	0.05%	Thicken the water and suspend the proppant
Scale inhibitor	Phosphonates, polymeric, Ethylene glycol	0.05%	Prevent mineral scale deposition

Moreover, according to the various formation properties, these additives should be carefully designed before Frac operation. The tight gas and shale gas reservoir, where the slickwater fracturing is generally applied, usually displays micro-Darcy to nano-Darcy range permeability, and small pore throats and crack-like interconnections between pores. They are different from traditional sandstone, carbonate reservoir. The mechanism of how these fluids interact with the tight formation is not completely understood. Therefore, it is prominent important to find out how these fluids impact on tight formation. Since brine, friction reducer, surfactant, and breaker are mostly widely employed during slickwater fracturing, they will be carefully studied in this project.

2.2.1. Clay Stabilizer. Formation clay and shale will swell in the presence of fresh water. KCl helps control clay swelling in the presence of water and helps minimize fines migration and is compatible with most chemicals used for fracturing operations. It is effective at temperatures between 50° and 400°F (10° and 204°C). Typical KCl concentrations for fracturing applications are 2 to 7 wt% of the base fluid, depending on the clay content of the formation (van Gijtenbeek, Neyfeld et al. 2006).

Capillary Suction Time (CST) test is a way to examine fluid sensitivity in particulate samples. The CST_{Time} measures the retention time (sec) it takes a fluid to pass through the core sample and filter paper. The $Blank_{Time}$ is the retention time (sec) for a fluid to pass through the filter paper without a core sample present. CST ratio is a factor that defines the possibility of sample swelling condition in present with a fluid:

$$CST\ Ratio = \frac{CST_{Time} - Blank_{Time}}{Blank_{Time}} \quad (1)$$

High CST ratio indicates more potential formation damage caused by this fluid.

Shale formation is generally very rich in clay. The North American gas shale has a clay content of 15%-50% (Kaufman, Penny et al. 2008, Conway, Venditto et al. 2011). The clay stabilization is even more important with any fluid introduced into the formation. KCl and other salts could inhibit clay from swelling in shales. CST measurement had been conducted with 170 North American shale samples (Conway, Venditto et al. 2011). It was found for concentrations approaching 3-5%, neither $CaCl_2$ nor $(NH)_4Cl$ has performed better than 7% KCl on average. However, each shale reservoir gets its unique properties, especially the mineralogy. The impact of different salt type and concentration of brine on shale sample is highly variable. Many flow tests and CST evaluations show that 2% KCl has a marginal effect on swelling clay (Paktinat, Pinkhouse et al. 2007, Kaufman, Penny et al. 2008, Arthur, Bohm et al. 2009).

2.2.2. Friction Reducer. Friction reducer was firstly observed by field personnel to exhibit low friction pressure since mid-1950s (White 1964). It could lower surface treating pressures or increase the injection rates. Friction reducer is also known as drag reducer. While flowing in a pipeline, it disrupts the near-wall turbulence regeneration cycle and reduces the turbulent friction drag by directly interacting with the vortex, thereby decreasing the flow friction in the pipeline (White 1964, Ram, Finkelstein et al. 1967, White and Mungal 2008).

There are many types of it. But they have a couple of properties in common. They are large polymers; the longer the polymer chain, the more effective the material; they tend to build non-Newtonian gel structure and, to varying degrees, they lose some of their effectiveness with prolonged agitation (i.e. they are shear sensitive) (White 1964, Sharp and Adrian 2004). The agents employed to reduce friction in aqueous systems (water, brine and hydrochloric acid solutions) are guar, anionic and nonionic polymers. And the agents used in hydrocarbon systems (kerosene, diesel fuel and crude oils) could be synthetic polymer solutions and in-situ soap gels. There are 3 major factors to evaluate a

friction reducer: friction reduction, leak-off control and apparent viscosity. Five types of friction reducer are compared in Table 2.2 (White 1964).

Table 2.2. Five types of friction reducer

	Base fluids	Friction reduction	Leak-off control	Apparent viscosity	Concentration
Guar	Aqueous	Not the most efficient	Good	Good	5 to 50 lb/ 1,000 gal
Anionic synthetic polymers	Aqueous	Most efficient in fresh water	Not good	More shear sensitive	2 to 4 lb/1,000 gal
Nonionic synthetic polymers	Aqueous	Between Anionic and Guar	Poor	Poor	2 to 4 lb/1,000 gal
Synthetic polymer solutions	Hydrocarbon	Efficient	No	No	3 to 8 lb/1,000 gal
In situ soap gels	Hydrocarbon	Not the most efficient	Good	Good	

There are also cationic friction reducers, which are usually used in acidizing, and can also be used in hydraulic fracturing fluids, but their cost is significantly higher than the conventional anionic types. Uncharged polysaccharide polymers like guar will need necessary concentrations, usually an order of magnitude greater resulting in substantially higher cost (Rimassa, Howard et al. 2009).

Therefore, within the hydraulic stimulation in tight formation, such as shale gas and tight gas reservoir, synthetic anionic polymers would be a good choice. One thing

noted, the synthetic anionic polymers are not recommended for use in highly ionic systems, because cations greatly reduce their efficiency, true of divalent cations, such as calcium and magnesium (White 1964). In slickwater fracturing fluid, the most common friction reducers used presently are polyacrylamide-based polymers (Kaufman, Penny et al. 2008, Kundert and Mullen 2009, Sun, Stevens et al. 2010, Zhou, Sun et al. 2011), usually manufactured as water-in-oil emulsions and added to the fracturing fluids (hydration) “on the fly”.

2.2.3. Breaker. After proppant is placed in fracture, the cross linked transport fluid need to be thinned, and the high molecular weight polymer filter cake on fracture face need to be removed to facilitate clean-up (Rae and Di Lullo 1996). Breakers degrade polymers by cleaving the polymeric macromolecule into small fragments which can be produced after the hydraulic fracturing during fluid recovery.

The most common breakers are oxidizing agents like peroxides and persulphates. These reactive species decompose to produce “free radicals” which attack the polymer chains and bring about degradation. A study of oxidative breakers was performed on fresh water and brine-based polyacrylamide friction reducer. The result showed that the persulfate breakers worked best at 180°F, and are effective at 100°F at concentrations of 5 and 10 pptg of water. Flow loop data showed no degradation of polymer at a persulfate concentration of 1 pptg up to 105°F, nor did the breaker have detrimental effects on hydration of the polymer (Kaufman, Penny et al. 2008).

Enzymes have also been applied to break fracturing fluids for many years. Enzymes are biological catalysts elaborated by living organisms and they perform very specific functions associated with the processes of cellular metabolism. Each enzyme has high specificity for only one or, at most, a very few substrates, e.g. cellulose-based, guar-based, or starch-based polymer (Tjon-Joe-Pin, Brannon et al. 1993). These enzymes attack the guar molecule and reduce its molecular weight, but unlike oxidizing agents, they are not consumed in the process. In principle, a single enzyme molecule is capable of degrading an unlimited number of guar molecules. At the limit, under optimum conditions, some enzymes can degrade complex polysaccharides, like guar and its derivatives, to simple sugar solutions (mono- and di-saccharides)

Moreover, when temperatures are higher, normal breakers may be too active. In such cases, the fluid may degrade too fast and its initial (or “front-end”) viscosity may be compromised. This problem can be overcome by wrapping or “encapsulating” the breaker in a low permeability film (Rae and Di Lullo 1996). This technique was first proposed in 1964 to use the water-insoluble, oil-soluble coatings, like resin or parafilm, to slow the release of breaker (Wyant, Perkins et al. 1964). Encapsulation has the added benefit of concentrating breaker in the polymer filter cake within the fracture i.e. it does not leak-off into the adjacent fracture matrix and stays in the fracture.

Ammonium persulfate are proved to be able to coexist with polyacrylamide friction reducer during the early part of the treatment. It allows the friction to be reduced in the tubing where the friction reducer is most effective (Kaufman, Penny et al. 2008) and a delayed broke down in formation when stimulation is finished or fluids are heated up to reservoir temperature (Sun, Stevens et al. 2010).

2.2.4. Surfactant. In a water-wet tight sand, and mix wet shale gas reservoir, water strongly associates with sandstone and clay surfaces. During cleanup in these conditions after fracturing, the hydrocarbon tends to break through the water, the remaining fluid is held in place by high capillary pressures, leaving high water saturation and low relative permeability to gas (Ford, Penny et al. 1988). The amount of frac fluid recovered on flowback in shale gas reservoir may range from as little as 5% in the Haynesville shale to as much as 50% in areas of the Barnett and the Marcellus shales (King 2012).

Surfactants are generally added in the fracturing fluid to enhance the fluid flow back by reducing the interfacial and surface tension. They consist of an oil soluble hydrophobic tail covalently bonded with a water soluble hydrophilic head group (Sheng 2010). When a surfactant is dissolved in an aqueous solution, the molecule will migrate to the surface of the water or the interface between water and oil, thus altering the surface properties between water/air and water/oil (Paktinat, O'Neil et al. 2011). Not only will this reduce the interaction between immiscible liquids, but also between the injected fluids and the reservoir rock.

The classification of surfactants comes from the specific surfactant hydrophilic group, as this identifies them as anionic, cationic, non-ionic, or zwitterionic. Anionic

surfactants are most commonly used in chemical EOR processes because they exhibit relatively low adsorption on sandstone rocks whose surface charge is negative. Cationic surfactants can strongly adsorb in sandstone rocks; therefore, they are generally not used in sandstone reservoirs, but they can be utilized in carbonate rocks to change wettability from oil-wet to water-wet. Zwitterionic surfactants contain two active groups. Zwitterionic surfactants can be nonionic-anionic, nonionic-cationic, or anionic-cationic. Such surfactants are temperature and salinity tolerant, but they are expensive. Nonionic surfactants primarily act as co-surfactants to improve system phase behavior. They are more tolerant of high salinity (Sheng 2010).

A micelle may consist of two or three molecules or ions, or as many as several millions. Micelles in surfactant are not present at all concentrations. Below the critical concentration, the solute is presented as single molecules or ions, and the micelles begin to form above a particular concentration. The changes in properties of surfactants, which occur as micelles form, are characterized by sudden transitions in many physical quantities such as: surface tension, viscosity, and conductivity (Abe 2005).

In this study, a non-anionic surfactant, which is commonly used in unconventional gas reservoir, will be used to study its impact on the wettability of tight rocks.

2.3. FRICTION REDUCER TRANSPORT IN PIPELINE

Slickwater fracturing had been more and more adopted over the past decade, especially with the booming of shale gas production. Friction reducer is the major composition of this fluid, which could lower the surface pumping pressure below that achieved with traditional cross-linked fracturing fluid. It also demonstrates a relatively low viscosity, which could significantly reduce the gel damage during hydraulic stimulation.

Different friction reducers have various hydration times. Flowloop experiments were conducted to evaluate their efficiency over time under such conditions (Kaufman, Penny et al. 2008): 6 commercial available friction reducer were selected first, concentration of 0.25 gpt of FRs were prepared with in 2 wt% KCl, then they were flowing at 5 gal/min through a tubing of 50 ft long with 0.402 in inner diameter. At 20 secs, when they made two complete pass through the loop, the polymers hydrate at

different rates; the friction reduction between the lowest and highest values is roughly 50%. At 600 secs, or 60 passes, the difference between the lowest and highest values is roughly 20%. Therefore, most friction reducer could work or partial work after 30 secs (Kaufman, Penny et al. 2008, Zelenev, Gilzow et al. 2009, Sun, Wood et al. 2011, Zhou, Sun et al. 2011).

The friction reducer function will also be affected by the fluid salinity. As noted before, the anionic synthetic friction reducer are not recommended for use in highly ionic systems, because cations greatly reduce their efficiency, true for the divalent cations, such as calcium and magnesium. And the anionic polyacrylamides give greater friction reduction in fresh water. Water with added KCl or produced water usually requires additional friction reducer to attain the same level of drag reduction as in fresh water. With the salinity increase, the friction reduction decreased (Aften and Watson 2009, Rimassa, Howard et al. 2009, Zelenev, Gilzow et al. 2009). Based on lab flowloop experiment, KCl will get a best friction reduction, and $CaCl_2$ functions the worst, while NaCl behaves in between them (Rimassa, Howard et al. 2009, Zelenev, Gilzow et al. 2009). It would be best if a proper friction reducer and brine can be optimized based on hydraulic fluid design and reservoir condition before operation, such as a performance test with the flowback water. If a wrong friction reducer is used, then a higher concentration has to be pumped to achieve the same effect, and potentially more formation damage will occur or more breaker is needed.

Concentration is also a major factor which will result in different drag reduction. For most of the friction reducer, the friction reduction with increase at higher concentration (Rimassa, Howard et al. 2009, Rimassa, Howard et al. 2009, Zelenev, Gilzow et al. 2009, Baser, Shenoy et al. 2010, Paktinat, O'Neil et al. 2011), e.g. their friction reduction will increase from 55% to 75% with concentration increase from 0.25 gpt to 1 gpt. But there is also a specially designed product which could give the same friction reduction at a concentration from 0.5 gpt to 1 gpt.

The anionic polyacrylamide friction reducer is a shear thinning fluid. But it is not strong shear sensitive (Rimassa, Howard et al. 2009). During its application in tight reservoir stimulation, very small loading is generally used. Its viscosity generally remains in 1- 2 cP, even though the shear rate increased 2 magnitude (Sun, Wu et al. 2013).

Beyond flowloop experiment in lab, field tests were conducted at tight gas sandstone reservoir. During the slickwater fracturing, it is not applicable to run with water first, and then use friction reducer to frac the same well. Therefore, the field test was conducted with decreasing friction reducer concentration. In the Granite Wash formation tight gas reservoir, located in the Texas Panhandle, the job was pumped down the 5.5 in OD casing at 90 bpm (Sun, Stevens et al. 2010, Zhou, Sun et al. 2011). Once the friction reducer concentration reduced from 1.0 gpt to 0.75 gpt, the pressure increase was in the range of 150 psi (over 14,000 ft tubular). When the loading was reduced from 0.75 gpt to 0.5 gpt, the pressure increase was in the range of 500 psi. It tells the pressure is increasing with the agent concentration reducing, which shows the friction reducer function well in the real field condition.

However, micro-sized fractures generated near the main fractures have much more contact area with the matrix, therefore hold the majority of the productivity potential of shale gas (King 2010, Odusina, Sondergeld et al. 2011, Apaydin, Ozkan et al. 2012). When this fluid comes into the microfractures, extending micro sized fracture network, its flow characteristics are not clear. The present study attempts to represent how this fluid flows in microfractures by considering how it flows in long circular microchannels and microfracture model.

2.4. FRICTION REDUCER FORMATION DAMAGE EVALUATION

All wells drilled in tight gas and shale reservoir require stimulation through hydraulic fracturing to enhance production rate (Malpani 2007). Slickwater frac had been successfully applied in tight sand gas reservoir by providing adequate conductivity at comparatively low costs than those treated with cross-linked fluids. Its application in Cotton Valley of Texas, Sultanate of Oman, , Piceance Creek and Wattenberg of Colorado demonstrates a promising production (Clark, Mullen et al. , Malayalam, Faz et al. , Mayerhofer and Meehan , Perez, Benish et al. , Woodworth and Miskimins , Yang, Hu et al.).

Hydraulic stimulation will result in economical production by increasing the drainage area with high conductivity micro fracture network. However, during slickwater fracturing in tight gas sandstone reservoir, friction reducer will cause formation damage. Breaker will then be able to degrade the friction reducer polymer or emulsion (Kaufman,

Penny et al. 2008, Sun, Wood et al. 2011). Formation damage evaluation is used to estimate the effect on the permeability of reservoir rock samples from various fluids at reservoir pressure and temperature. For the hydraulic fracturing stimulation, formation damage evaluation could evaluate the effect on the producing permeability after introduced fluid is applied on reservoir rock samples. The effect of fines migration caused by clay sensitivity, brine salinity changes, high production flow rates could also be considered as formation damage evaluation.

Gas permeability regain test with rock sample evaluates the solution impact on sample gas permeability before and after the liquid is introduced into the samples. At temperature of 150 °F, the gas permeability regain test was conducted with Ohio sandstone (permeability less than 1mD), friction reducer and breaker solution (Sun, Wood et al. 2011). Before and after the solution was injected into the core samples, the gas phase permeability results revealed the friction reducers had some kind of damage to the sample permeability by around 20%, however, with the breaker loaded in the solution, its damage decreased. Some friction reducer with ammonium persulfate could regain 94.9 to 99.9% of its original permeability.

Gas permeability regain test can also be used with fracture model to investigate the friction reducer permeability impact in fracture. Bossier shale core plug was used as fracture model by cutting the sample through at axial direction from center (Sun, Wood et al. 2011). Some friction reducers can regain 100% (no reduction in fracture permeability), while some friction reducer can regain only 56% due to the noneffective degradation of breaker to friction reducer, the residue polymer deposited on the fracture faces decrease the flowing capability of gas through the fracture. Therefore, the compatibility of breaker to friction reducer is prominent importance before it is applied to field.

Viscosity test is a fast method to evaluate the polymer breaking after interacting with breaker. Breakers are usually used to break the friction reducer by reducing it viscosity after reaction. A viscosity test at 120 °F showed that the A-1 persulfate breaker effectively reduces the viscosity of the polyacrylamide friction reducer even at low concentrations (Carman and Cawiezel). As the breaker concentration is increased, the fluid break time decreases. The A-1 persulfate breaker also effectively reduces the viscosity of the friction reducer at 100°F at concentrations of 5 and 10 ppt. High

temperature will usually make the breaker work faster (Sun, Wood et al. 2011). For the ammonium persulfate to react with a friction reducer at 100°F, the solution viscosity takes 22 hrs to reach to that of water. However, at temperature of 150 °F, it takes only 75 min, the solution viscosity becomes very close to that of water.

In the last decade, slickwater fracturing had been successfully applied in unconventional tight gas and shale gas reservoir. The paths for fluid flow in these tight and shale gas reservoirs are primarily the fractures network generated by hydraulic fracturing or inborn fracture connected with each other. Adjacent to the fracture, the unfractured matrix rocks contain the majority of the production potentials of the reservoir. The fractures provide the easiest way for fluid flow, and the matrix is source of the fluid or the fluid is passing through the matrix with nano Darcy to micro Darcy permeability into the fractures, which means the matrix in unconventional gas reservoir play a more prominent role in gas production. The cleanup of breaker to polymer in fractures is supposed to be very well, because the fractures have at least thousand times higher permeability than that in the adjacent matrix. However, to date, no existing publications discussed the magnitude and mechanism of FR and breaker impact on the unfractured matrix in unconventional gas reservoir. Thus, the understanding of formation damage of gas/water transport phenomenon through tight gas sandstone in the presence of FR and breaker is crucial for hydraulic stimulation operation and design. The proposed research will target to expand the knowledge of formation damage evaluation with FR and breaker introduced into tight sand.

2.5. WETTABILITY EVALUATION

If the drawdown pressure is greater than the capillary pressure, the water retention is small (Abrams and Vinegar 1985, Adibhatla, Mohanty et al. 2006). Otherwise, this retained brine can block the flow of gas and impair productivity.

There are many wettability evaluation methods for reservoir rock: direct method and indirect method. Contact angle method is a direct measurement of a reservoir rock intrinsic wettability. It measures the contact angle that a liquid-air or liquid-liquid interface makes with a solid surface. Several indirect methods provide indexes of the relative wetting properties. Amott method is a based on the amounts of fluids imbibed by

a rock sample under various conditions. The USBM method is area comparison under capillary pressure curves obtained using a centrifuge (Tiab and Donaldson 2011).

Tight gas sandstone reservoir is dominantly composed of quartz, followed by feldspar and rock fragment and others (Rushing, Newsham et al. 2008). Numerous tight gas formations are under-saturated where the initial water saturation in the reservoir is less than the capillary equilibrium irreducible water saturation. Tight rock is completely water wet. The use of water-based fracturing fluids causes water to be trapped in the near wellbore region, resulting low gas phase permeability, thereby significantly impairing the ability of gas production rate.

Shale is mixed with quartz, feldspar, calcite, dolomite, clay (Yu and Lau 2013). The pore space in gas shale consists of pores in the organic matter, Kerogen, and pores in the inorganic matrix (Wang and Reed 2009, Elgmati, Zhang et al. 2011, Georgi, Jin et al. 2013). When in contact with liquids, the exposed surfaces support a broad range of surface forces that bound the liquids to vary degrees. The pores with organic surfaces (oil wet) and inorganic surfaces (water wet) develop strong capillary forces that bound liquids with strengths, and they are inversely proportional to the pore radius. The wettability of shale can be more water wet, more oil wet, mixed wet, or intermediate wet (Rimassa, Howard et al. 2009, Sondergeld, Ambrose et al. 2010, Lakatos, Bódi et al. 2011, Odusina, Sondergeld et al. 2011, Roychaudhuri, Tsotsis et al. 2013). This is highly depending on shale heterogeneity, such as mineral distribution and composition. In shale gas reservoir, water wet can easily generate a water block in the near wellbore matrix.

For an unconventional gas reservoir, due to their micro-Darcy to nano-Darcy permeability and low porosity, some indirect method did not work well on these rocks, especially for shale. Nuclear Magnetic Resonance (NMR) is a technique which directly senses fluids in a formation almost independent of the lithology. Fluids containing hydrogen become the prime target for NMR because hydrogen has one of the highest gyromagnetic ratios and produces a strong signal which can be easily detected by the NMR tool: T_1 and T_2. The T_2 measurement requires less time and is more commonly used in shale wettability estimation (Odusina, Sondergeld et al. 2011, Chen, Zhang et al. 2012). For Barnett, Eagle Ford, Floyd, Woodford shale, NMR method indicted both brine and Dodecane could wet the shale (Odusina, Sondergeld et al. 2011).

After the well is completed, hydraulic fracturing is generally required for the tight formation to enhance the production rate and recover investment. During a hydraulic fracturing process, millions of gallons of liquid is injected in the formation, but more than 50% could not be recovered after the stimulation. The fluid flow back could be 5% in the Haynesville shale, and 50% in areas of the Barnett (King 2012). The retention of the injected fluids would impair the formation matrix and production in long term, even though the production rate will generally increase immediately after the stimulation.

Contact angle and spontaneous imbibition are two methods usually used to evaluate the sample wettability change, especially when fluid is introduced.

2.5.1. Contact Angle Measurement. Contact angle measurement is an experimental approach which could determine the wettability and wettability alteration condition of a sample surface by placing a liquid drop.

Many surfactants have been identified to be able to change the wettability of sandstone and shale rocks from water-wet to intermediate-wet in water-air-rock systems (Adibhatla, Mohanty et al. 2006, Roychaudhuri, Tsotsis et al. 2013). They treat the sample surface to be smooth first, then soak in surfactant solution for a certain time (e.g. 1day), then use KCl or NaCl to conduct the contact angle measurement.

The wettability of aged quartz surface could also be altered from intermediate wet to water wet with the various agents, such as: sodium dodecyl alcohol ether sulfate (AES,99.5%), sodium dodecyl sulfate (SDS, Anionic, 99.5%), alkyl glucoside (GD70, non-ionic) and cetyl trimethyl ammonium bromide (CTAB, 99.5%). And they all behave a trend that the contact angle is decreasing with the agent concentration increasing (Qi, Wang et al. 2014).

The salinity of surfactant could have very a big impact on the contact angle of carbonate and sandstone. Where calcite and mica were used to represent carbonate and sandstone, respectively, four types of surfactants give a contact angle between 65°-120° on both calcite and mica. When surfactants were prepared with field brine, their contact angle displayed a sharp decreased to 16.7°-27.2° (Qi, Wang et al. 2014).

The type of gas will also impact on surface wettability, even without surfactant. Experimental evidence proved that the water-wettability of minerals representative of shales, such as mica and quartz, is significantly altered in the presence of CO_2 under

pressure typical of geological storage conditions (Chiquet, Broseta et al. 2005). Those minerals, known to be strongly water-wet in the presence of oil, turn out to be intermediate-wet in the presence of dense CO_2.

The surfactant treated sandstone also displayed a relative permeability increasing compare with untreated one (Wu and Firoozabadi 2011). The Berea sandstone was treated with fluorinated polymeric surfactants, the wettability of the rock was altered from liquid-wetting to intermediate gas-wetting by the adsorption of the chemical molecules composed of various functional groups (fluoro, silanol, or ionic) with the ability to form chemical bonds with the solid surface and to repel the liquid phase (Tang and Firoozabadi 2002). The relative water permeability increased by a factor of two.

2.5.2. Spontaneous Imbibition. Due to the micro-Darcy to nano-Darcy permeability and very low porosity, the conventional Amott cell imbibition method will not be a best choice to evaluate the liquid intake condition of tight sand and shale. Spontaneous imbibition setup equipped with digital balance could measure the imbibition rate of an imbibing core by continuously recording the increase in mass. It provides the basis for accurate measurement of imbibition rates, even when the total mass of imbibed water is small or the duration of the experiment is long (Humphrey, Istok et al. 1996). It is a process where only capillary forces drive imbibition. The imbibition amount and rate are related to the overall wettability of the pore system in deep matrix, rather than at the sample surface.

There are two types of spontaneous imbibition: counter-current imbibition and co-current imbibition. Counter-current imbibition differs from co-current imbibition in the flow direction of wetting phase and non-wetting phase. If wetting phase flows in the same direction as the non-wetting phase, this imbibition process is called co-current imbibition. This is generally used to study the water flooding process in oil reservoir, or gas-fluid interaction in gas reservoir, through hang the sample over the liquid, where only one face contacted with the liquid and other faces exposed to air. Counter-current imbibition is the process in which the displacing and the displaced phases flow in opposite direction. This is usually used to study the fluid-fluid interaction in oil reservoir with Amott cell or similar imbibition setup, where the sample is totally immersed in liquid, water or surfactant is imbibed into the sample and oil is going out of the sample.

Co-current imbibition would be more applicable in the fluid-gas interaction study of unconventional tight gas and shale gas reservoir during hydraulic fracturing. The co-current water imbibition into gas-saturated rocks was studied for the effect of initial water saturation on imbibition rate, residual gas saturation, and the gas recovery through experimental analysis (Li and Horne 2000). It has been reported that the maximum water saturation by spontaneous imbibition is almost unaffected by initial water saturation in Berea sandstone. But the ultimate gas recovery declines with the increase of initial water saturation.

The co-current imbibition method could also evaluate the water imbibition rates of various samples. The different intake amount can be explained, in part, by the clay content, the total organic content (TOC), porosity and permeability of the samples (Li and Liu 2007, Roychaudhuri, Tsotsis et al. 2011). The experiment conducted with Berea sandstone tells high permeability samples display higher imbibition rate. The initial water saturation impact on imbibition rate could also be studied with co-current imbibition method. Experiment shows lower initial water saturation would result in higher imbibition rate, and a higher imbibition amount (Kewen and Abbas 2000, Li, Chow et al. 2002, Li and Liu 2007, Li and Zhao 2012).

The imbibition of surfactant could result in a lower imbibition rate than that with deionized water in gas shale at the very beginning several minutes. Then with experiment continues, the imbibition rate is almost the same for both surfactant and water (Lakatos, Bódi et al. 2013, Roychaudhuri, Tsotsis et al. 2013). If sample is treated with surfactant, e.g. Berea sandstone soaking in surfactant (Kewen and Abbas 2000), the sample surface, which is initially strong water wet, could attain a contact angle of 120° with water drop and 60° with oil drop, which changed to be oil wet. Before the agent treatment, water could take in 0.56 PV, after treatment, water could only take in less than 0.05 PV. Wettability altered by surfactant gets a prominent impact on the spontaneous imbibition in Berea sandstone.

The summary of the previous literature review has indicated that there are many petrophysical properties are affected the reservoir rock wettability condition after surfactant treatment, such as absolute permeability, relative permeability, initial water saturation, irreducible water saturation and residual gas saturation. However, it is still

unclear how the different factors impact on tight rock contact angle and imbibition rate. The project will address on the effect of water and surfactant on gas flow in the nano sized pores or cracks with co-current imbibition method.

3. BASIC PARAMETER OF ROCK SAMPLES AND FLUIDS

3.1. TIGHT SAND AND SHALE SAMPLES INTRODUCTION AND THEIR PARAMETERS

3.1.1. Rock Sample Introduction. The rock samples used here contain unconventional tight gas sandstone and shale gas rock, all from underground gas reservoir.

SL Gas field is located in Erdos, Inner Mongolia, China, as shown in Figure 3.1. It is the largest gas-producing area in China, contains over 35 trillion cubic feet (Tcf) of proven gas reserves. Its reservoir depth is around 11,500 ft. The gas production in this region is both geologically and technically challenging, and most of the reserves are tight gas. The tight gas sandstone sample used here is acquired at depth of 12800 ft.

Figure 3.1. Location of SL Gas Field
(Base map is adopted from http://www.china-tour.cn/China-Maps)

Marcellus is the lowest unit of the Devonian age Hamilton Group. It runs across the Southern Tier and Finger Lakes regions of New York, in northern and western Pennsylvania, eastern Ohio, through western Maryland, and throughout most of West Virginia extending across the state line into extreme western Virginia (PSU 2008), as shown in Figure 3.2. It extends throughout much of the Appalachian Basin. The Energy Information Administration (EIA) estimates the Marcellus shale contains 410 Tcf undeveloped technically recoverable shale gas in 2011 (EIA 2011). Marcellus shale occurs as deep as 9,000 feet below ground surface, and the outcrops appear along the northern margin of the formation in central New York. Its thickness could be as high as 890 ft in New Jersey and as low as 40 ft in Canada. The surge in drilling activity in the Marcellus Shale since 2008 turns it into the largest source of natural gas in the United States. The shale sample employed here is from a depth of 6982 ft.

Figure 3.2. Marcellus Shale Geographic Map
(Source: http://oilshalegas.com)

3.1.2. Rock Sample Preparation. Bulk shale is used for fluid rock interaction by previous researchers (Dehghanpour, Zubair et al. , Wang, Butler et al. 2011). Their results show bulk shale is very easy to crack and become small pieces once fluid is introduced. Our test also proved this phenomenon, as shown in Figure 3.3. Shale is deposited in layer by layer condition, and featured of high clay content. The bond between each layer is generally not strong. Once shale encountered with liquid, clay would be easy to swell and the layers would be separated from each other. Moreover, the wetted thin layer is very fragile. It almost cannot hold its integrity from any force or even gravity.

Figure 3.3. Bulk shale cracked when fluid is introduced

The tight sand and shale rock samples all came in bulk condition with diameter of 4 in. If conventional 1 in diameter sample is cored and then used for experiment, the rock in our hand would not be enough. A new core preparation method is developed here.

The detailed preparation method is as followed:

1) Slice a piece from the 4 in bulk rock, and then cut it into a cubic shape, as shown in Figure 3.4. Polish each surface with 60 grit sandpaper, and clean the surface dust with strong air flow;

Figure 3.4. Tight sand in cubic shape

2) Measure its dimension and put it in oven at temperature oven 212°F to vaporize the water. Measure its effective porosity using Helium Porosimeter;
3) Cut the acrylic tube to desired length, and load the cubic rock into the tube. Prepare epoxy, and pour it into the tube when its viscosity becomes relatively high, as shown in Figure 3.5. Cool down for 24 hrs;

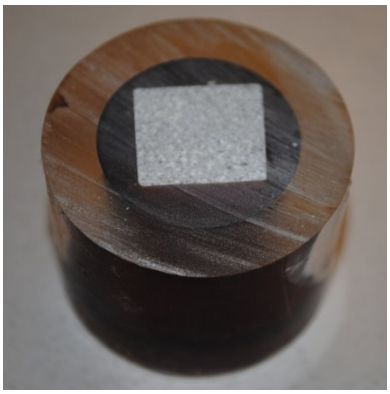

Figure 3.5. Tight sand sample coated in 1 inch ID acrylic tube with epoxy

4) Slice the rock from the acrylic tube with coated epoxy, and push it out, as shown in Figure 3.6. Then polish it with 60 grit, 180 grit and 320 grit of sandpaper in sequence.

Figure 3.6. Slice tight sand sample

5) Since original cubic rock cannot guarantee to be perfectly shaped, the opposite sides may not be parallel, we use a camera to take pictures of each side of each slice, then analyze the effective area of the rock by Adobe Photoshop. Then put the samples in oven at temperature of 170 °F for 4 days+ to vaporize the water. Then samples are ready to use.

Since this study is focusing on the hydraulic fluid interaction with rock during the fracturing process. The sample orientation is carefully considered to simulate that underground during sampling process, as shown in Figure 3.7. The final thin slice sample is designed to parallel to wellbore direction, so when the rock is encountered with any liquid, then, the fluid flow direction would be the same during injection hydraulic fluid into the rock formation along the wellbore.

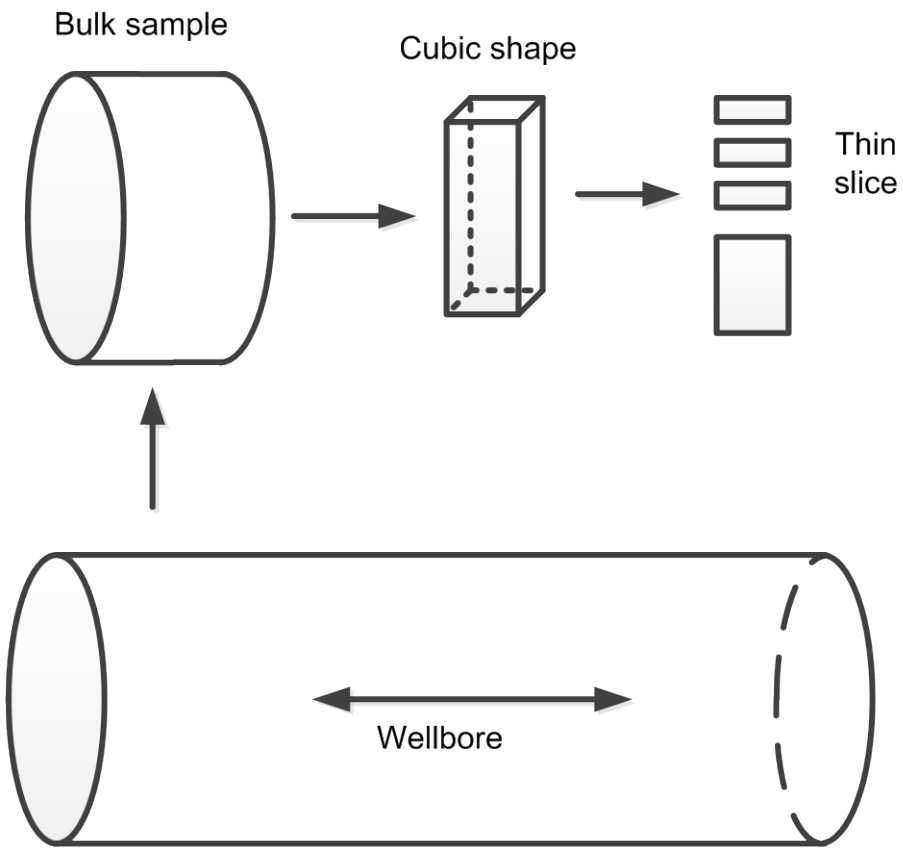

Figure 3.7. Sampling procedure to obtain representative sample for test

3 brands of Epoxy adhesive are tested during coating, they are: Sikadur 35, (Sika, Lyndhurst, NJ). Their properties are listed in Table 3.1. After many try and error, Sikadur 35 is supposed to be best fit in this study. Its strength is not too high, so it is not easy to break during slicing. It also allows some contraction compares with the other 2 adhesives. It does not get strong interaction with smooth surface in acrylic tube.

Table 3.1. Epoxy adhesive comparison

Epoxy adhesive	Color	Temperature	Strength	Other properties
Sikadur 35	Brown, half transparent	Below 170 °F	Middle	

Table 3.1. Epoxy adhesive comparison (cont.)

Epoxy adhesive	Color	Temperature	Strength	Other properties
Duralco 4525 Resin Epoxy	Black, Nontransparent	up to 500 °F	High	Easy to generate fracture during cutting and temperature changing,
Buehler EpoHeat Epoxy	Light yellow, Transparent,	up to 149 °F	Middle to high	Very easy to generate gas bubble during coating

3.1.3. Porosity. Porosity is measured with Helium in order to calculate how many pore volumes (PV) of liquid are injected or imbibes into the sample. Since the samples have limited amount, and mercury porosimeter will make the sample useless after mercury porosity measurement, therefore most of the porosity are tested with conventional Helium porosimeter. Helium has extremely small gas molecule size: 280pm, which equals 0.28nm. Compare with the pore size of tight sand and shale (analyzed in the next section), the Helium molecule size is hundred to thousand time smaller, where the Helium porosimeter would be applicable to measure that of tight sand and shale.

Tight sand porosity data is presented in Table 3.2. The 3 bulk tight sand samples are all sliced from the same 4 in bulk core. The Helium porosity measurement gives their effective porosity is from 11.72% to 13.33%, and the 3 time measurement for each sample is very close to each other. The effective porosity for this tight sand indicates they are relatively uniform in effective porosity.

Table 3.2. Tight sand porosity

Sample No.	Porosity, %			
	1st	2nd	3rd	Average
BS1	13.104	13.436	13.446	13.33
BS2	11.72	12.052	12.402	12.06

Table 3.2. Tight sand porosity (cont.)

Sample No.	Porosity, %			
BS3	11.518	11.636	12.002	11.72

Table 3.3 demonstrates the effective porosity of gas shale. 4 bulk shale samples are also sliced from a 4 inch bulk core. Their porosity data could be as high as 5.39% to as low as 1.39%, which is lies in the same range with current publication (Nelson 2009). This shale sample has some heterogeneity from these porosity data.

Table 3.3. Shale rock porosity

Sample No.	Porosity, %			
	1st	2nd	3rd	average
MB1	5.30	5.49		5.39
MB2	4.330	5.163	5.953	5.15
MB3	2.056	1.656	1.673	1.80
MB4	1.573	1.226	1.368	1.39

3.1.4. Pore Size Distribution. The pore size distribution is measured with PoreMaster 60 (Quantachrome, Boynton Beach, FL), as shown in Figure 3.8. PoreMaster 60 porosimeter will generate pressure up to 60,000 psia by mercury injection. The pore size could be analyzed from over 950 micron to 0.0036 micron pore diameter.

Figure 3.8. PoreMaster 60
(Source: Quantachrome)

The tight sand sample is analyzed with this instrument. 1 cm diameter and 2 cm long cylindrical sample was firstly drilled from the bulk core, and its surface was polished with 60 grit sandpaper. Then use oven to vaporize the water at temperature over 212°F. After sample cell was loaded with the dry cylindrical tight sand sample, put it into PoreMaster instrument, the system will inject mercury into rock sample and measure how much mercury is injected with corresponding pressure. The injection pressure is increasing from a few hundred psi to 60,000 psi. The injected mercury is considered as the pore volume in the rock sample, which is then converted to sample pore size as shown in Figure 3.9.

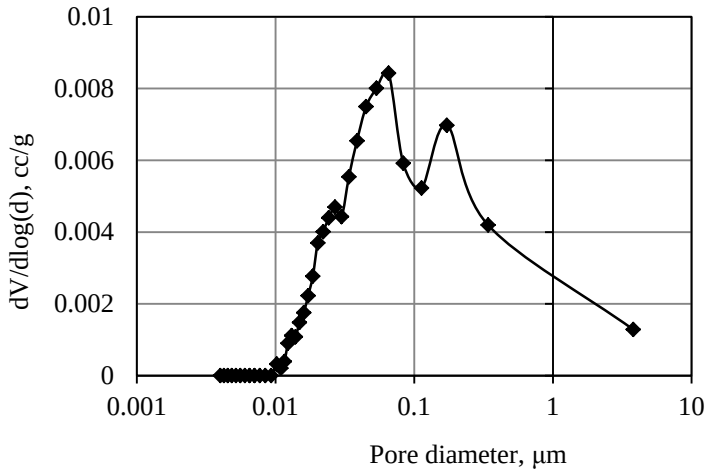

Figure 3.9. Tight sand sample pore size distribution

The pore size distribution of this sample is ranging from 0.01 micron to over 2 micron. The majority of pores lie in 0.02 micron to 0.5 micron. And it has two peaks at 0.15 and 0.065 micron. The red line is the intrusion process, where mercury is injected into the rock sample and the blue line the extrusion process, where system is decreasing pressure and mercury is extruded from the core sample.

The pore size of Marcellus shale is estimated from current publication (Nelson 2009), as shown in Figure 3.10. Since Marcellus shale is in the Devonian age, and extends throughout much of the Appalachian Basin. The pore size of this shale is suspected to from 0.019 micron to 0.024 micron.

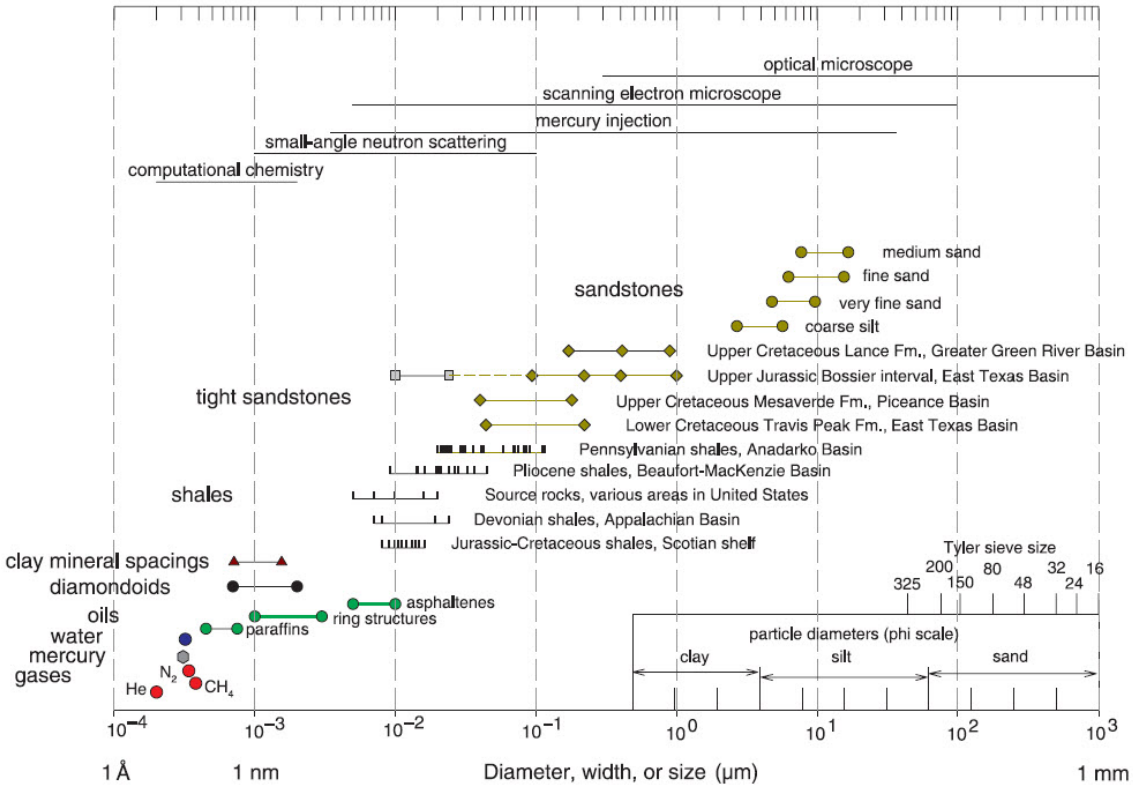

Figure 3.10. Pore throats sizes of different porous media (Nelson 2009)

3.1.5. Permeability. Core samples are placed in a thick walled Viton sleeve with end-plugs designed to facilitate the introduction of completion acid mixes and to allow insertion of ring spacers for accumulation of filter cake at the upstream end of the sample.

The absolute permeability of tight sand samples were measured with Ultra-Perm 600 Permeameter (CoreLab, Houston, TX), as shown in Figure 3.11.

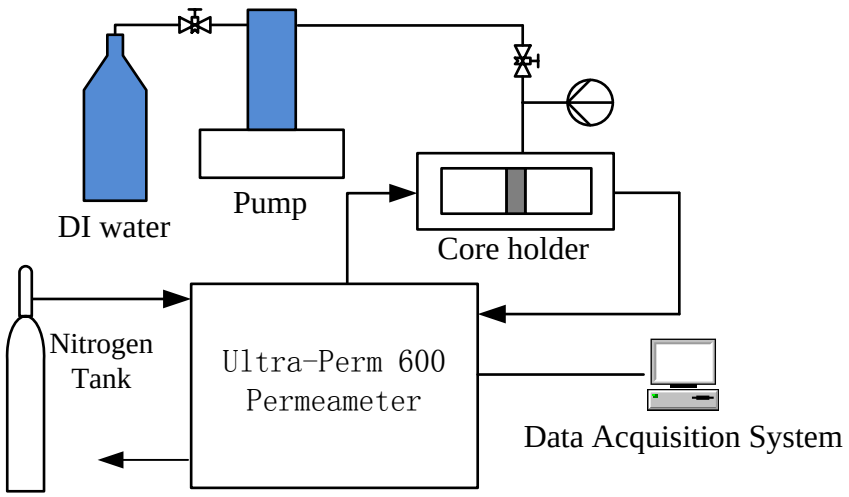

Figure 3.11. Schematic diagram of absolute gas permeability measurement

After sliced tight sand samples were dried with oven, put the sample in coreholder and injection gas from the Nitrogen tank. Apply different gas pressure by adjusting the knobs on permeameter to provide several upstream pressures on the core sample. Generally, 4 to 7 pressure was applied for each slice of the core sample. Absolute gas permeability of tight sand sample: TS11, TS12, TS14 were measured initially, as shown in Figure 3.12–Figure 3.14.

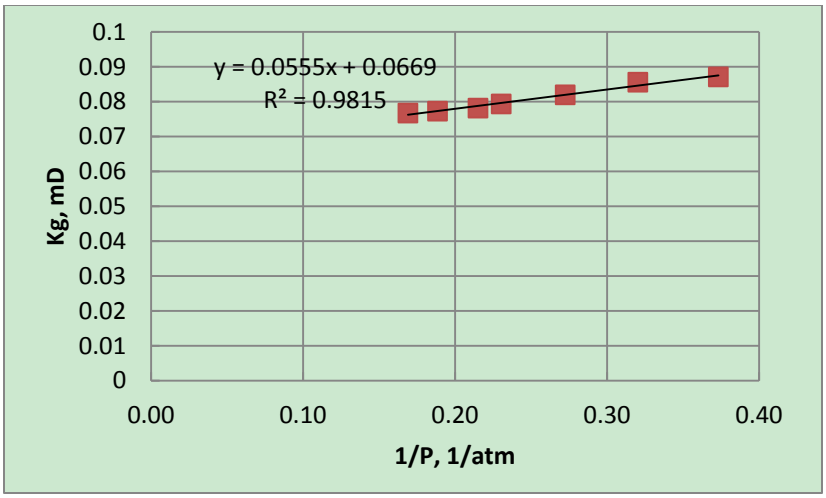

Figure 3.12. Absolute gas permeability of TS11

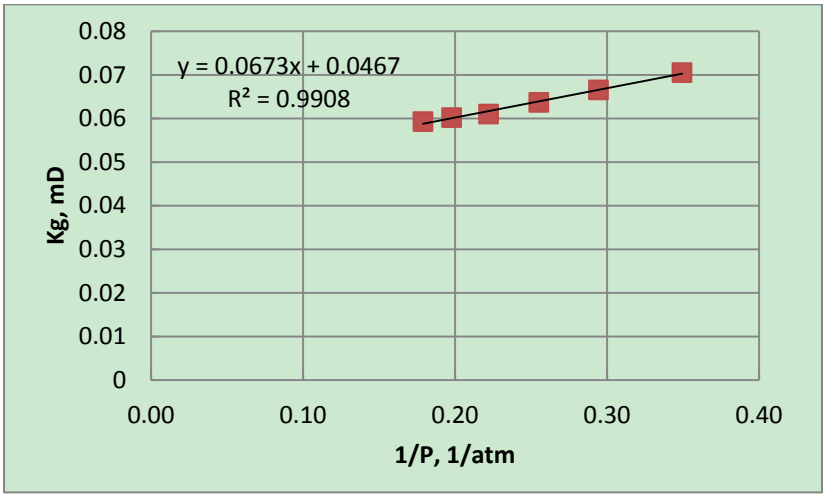

Figure 3.13. Absolute gas permeability of TS12

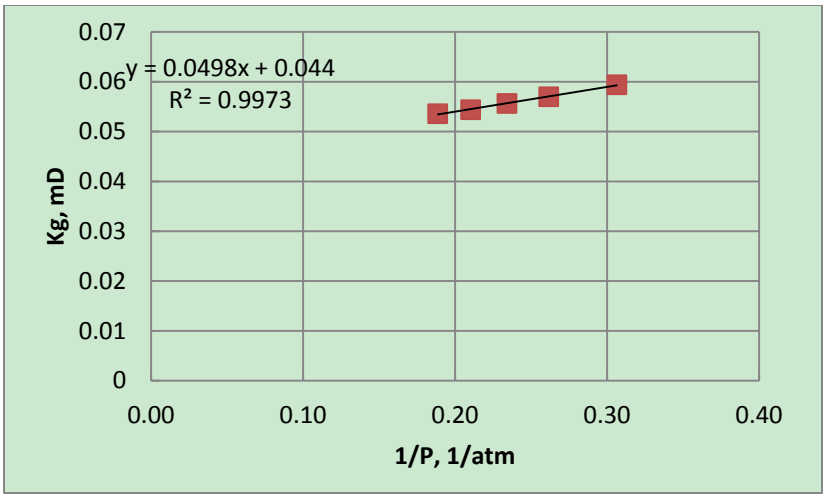

Figure 3.14. Absolute gas permeability of TS14

Then initial water saturation was created in these tight sand samples by injecting 1000PV of 2% KCl solution into each sample, respectively. Then each sample was flooded by humidified Nitrogen, where Nitrogen was going through brine accumulator before flooding the water in each sample in order to carry some moisture during flooding. Sample weight was measured at certain time intervals. Once their weight was changing at a rate smaller than 0.5% in an hour, initial water was considered to be created in samples. Then humidified Nitrogen was flooding the sample again at several pressure drops to measure the gas phase permeability with initial water. Experimental setup was shown in Figure 1.15. Gas phase permeability with initial water saturation of sample TS11, TS 12, TS14 were shown in Figure 3.16 – Figure 3.18.

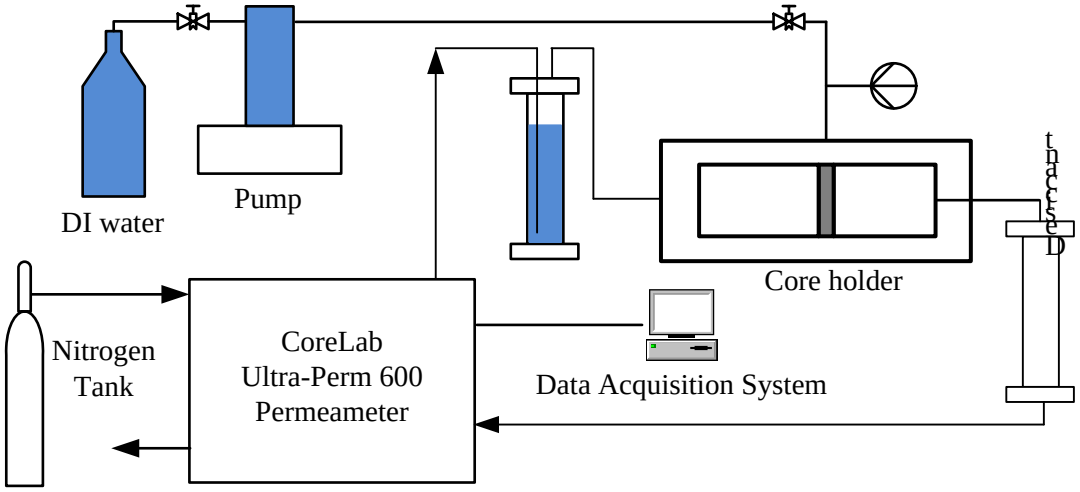

Figure 3.15. Schematic diagram of gas phase permeability measurement

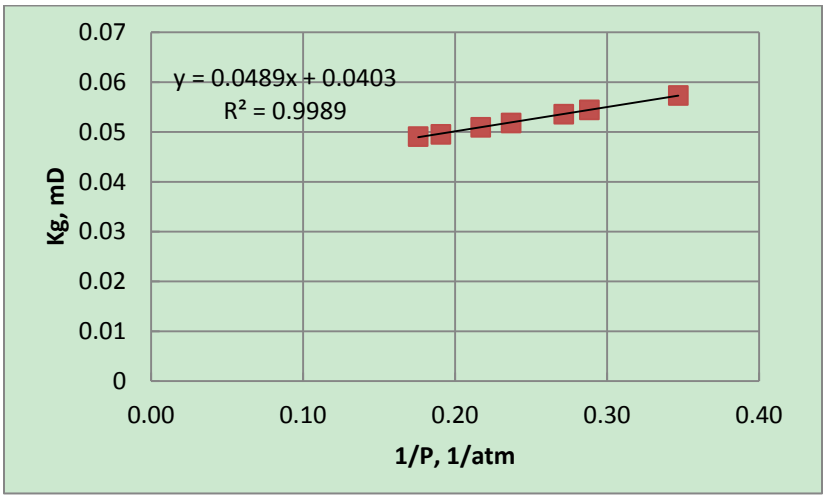

Figure 3.16. Gas phase permeability of TS11

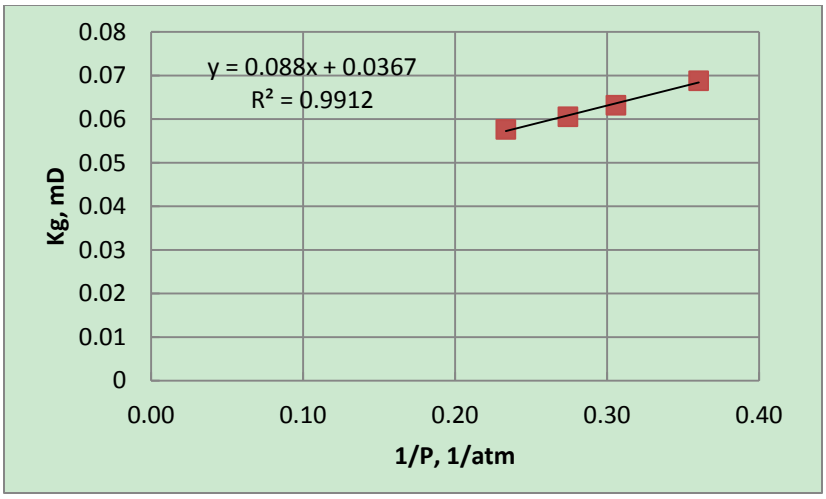

Figure 3.17. Gas phase permeability of TS12

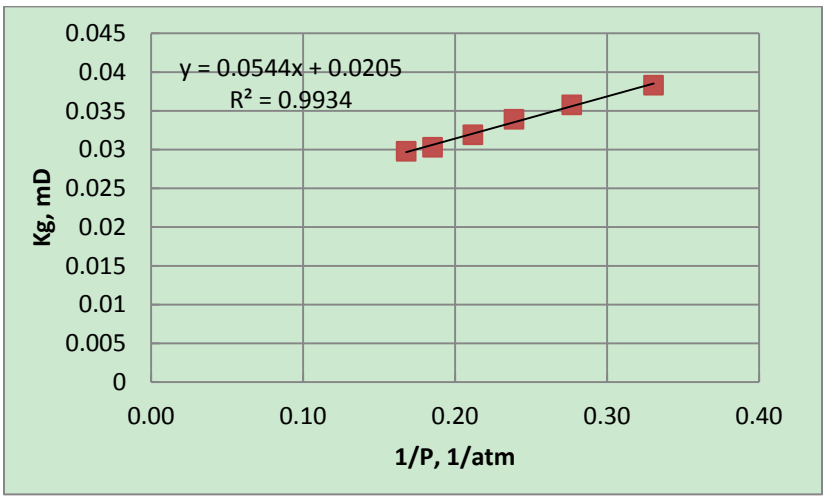

Figure 3.18. Gas phase permeability of TS14

Absolute gas permeability and gas phase permeability data are summarized in Table 3.4. Although the samples were sliced from one bulk rock and sample seems homogenous with the naked eyes, but its absolute permeability still have some variation. And their relative gas permeability: K_{rg}, which is calculated by gas phase permeability divided by the absolute gas permeability, also demonstrates their heterogeneity in permeability.

Table 3.4. Tight sand absolute gas permeability and gas phase permeability

Sample	K_a	K_g with S_{wi}	K_{rg}	S_{wi}
	mD	mD		%
TS11	0.0609	0.0403	0.662	6.3
TS12	0.0467	0.0367	0.786	9.1
TS14	0.044	0.0205	0.466	24.1

3.1.6. SEM Imaging. The tight sand samples were examined with Helios NanoLab 660 DualBeam SEM/FIB (FEI, Hillsboro, OR) for its surface structure and mineralogy.

The surface structure could be observed in Figure 19 with 350 magnitudes. With this SEM picture, it is very clear the sample is not homogeneous, and different from the relatively homogeneous condition observed by the naked eyes. The pores majorly exist in clay materials. Few intergranular pores can be found, as in Figure 3.20 with back scattered SEM. This pore has a tenth of micrometer height and few micrometer widths.

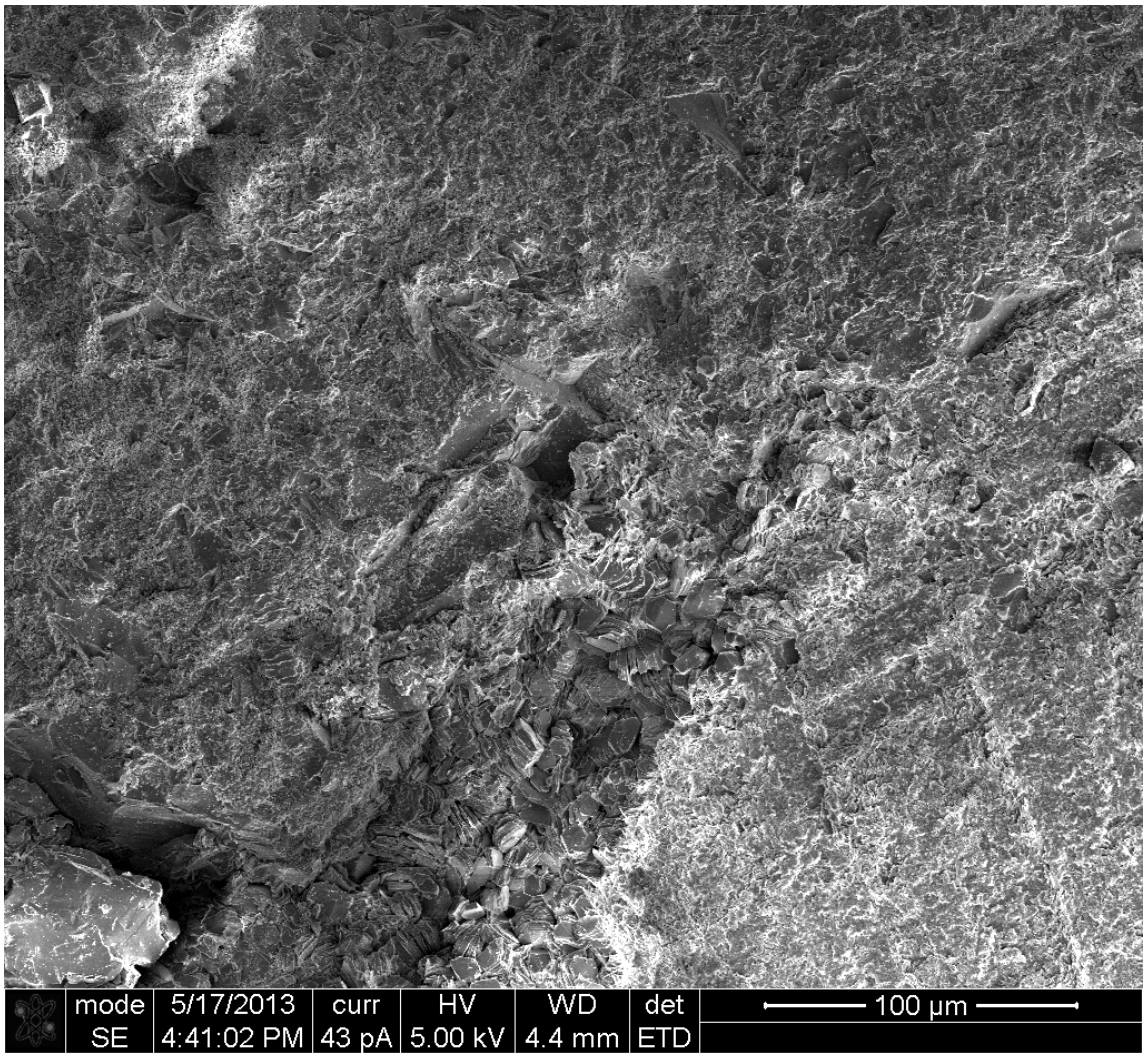

Figure 3.19. Surface structure of tight sand at 350 magnitudes

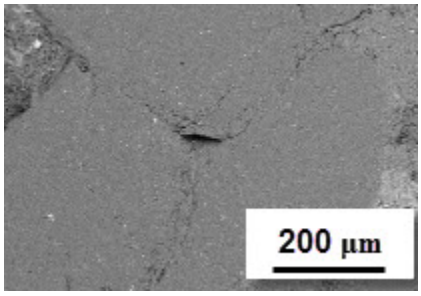

Figure 3.20. Intergranular pore in tight sand with backscatter SEM examination

Kaolinite is frequently seen in the center of Figure 3.19. Quartz is located in the left bottom corner. With 1500 magnitudes on the clay, as shown in Figure 3.21, kaolinite is piled in various directions around the pore, as in Figure 3.22. Micrometer size corrosion on quartz was also observed, as in Figure 3.23. This corrosion was suspected to be the candidate of pores (Wang, He et al. 2013)

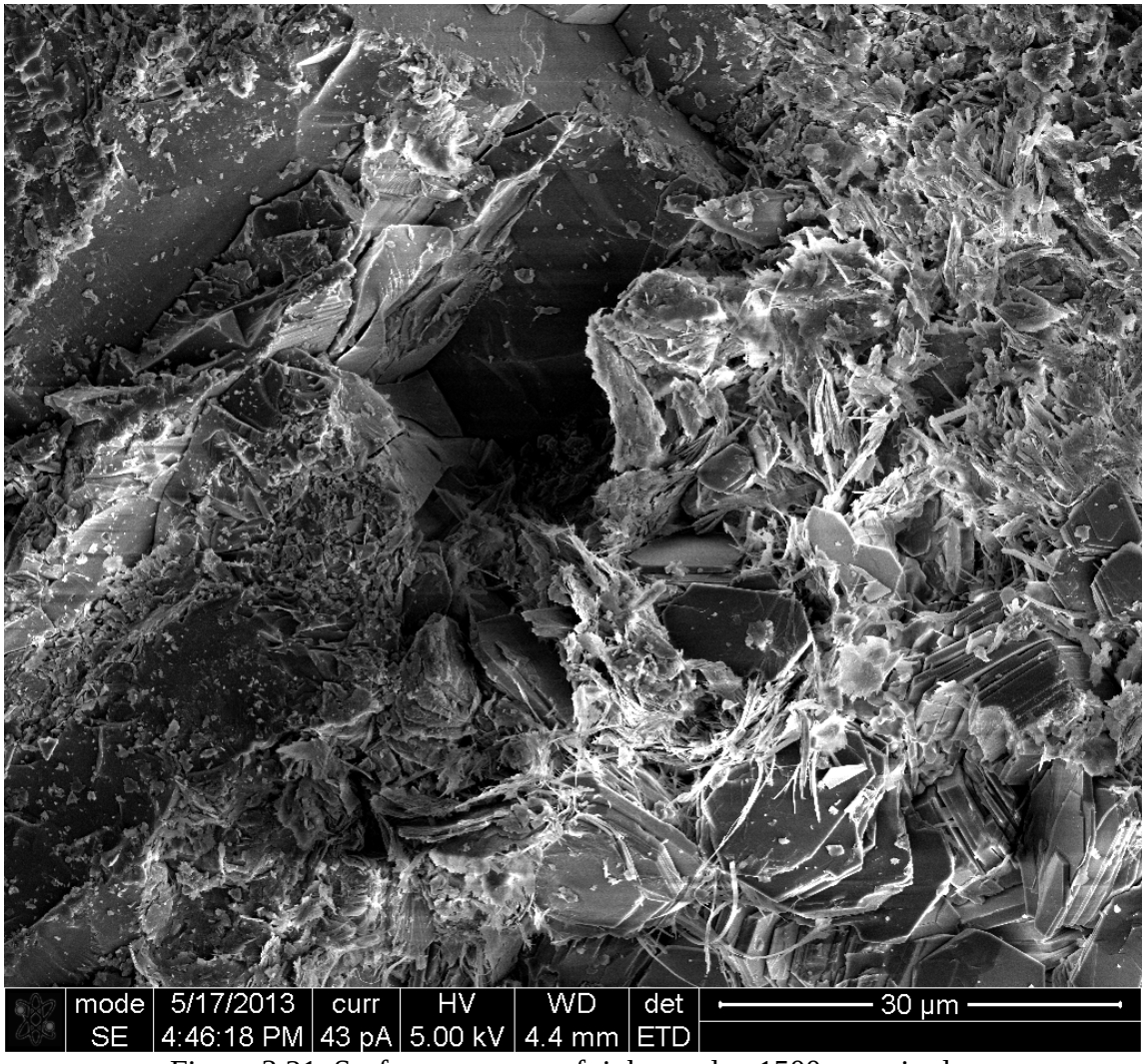

Figure 3.21. Surface structure of tight sand at 1500 magnitudes

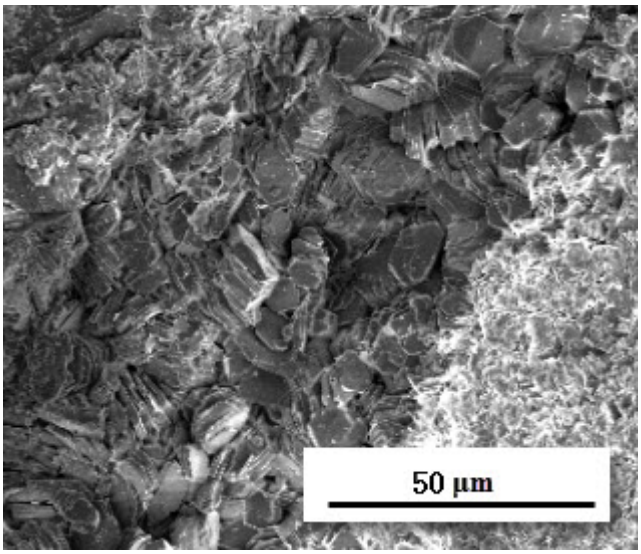

Figure 3.22. Kaolinite in tight sand

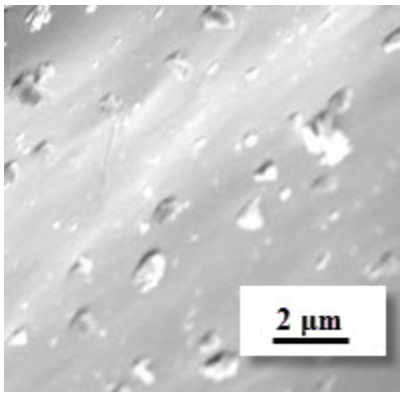

Figure 3.23. Corrosion on quartz in tight sand

3.1.7. Sample Parameters. After samples are sliced into thin pieces, the basic parameters of tight gas sandstone and shale samples were measured and summarized in Table 3.5 and Table 3.6. However, some sliced samples were broken or failed during experiment due to various reasons. These considerable amounts of samples are not reported here.

Table 3.5. Tight gas sandstone basic parameter

Sample No.	Thickness	Area	Porosity	PV	S_{wi}
	mm	cm^2	%	cm^3	%
TS11	4.015	2.34	11.72	0.110	6.3
TS12	3.5875	2.32	11.72	0.097	9.1
TS13	3.5975	2.29	11.72	0.097	
TS14	3.3075	2.26	11.72	0.087	24.1
TS20	5.39	2.13	12.95	0.149	
TS21	4.80	2.01	12.95	0.125	
TS22	5.42	2.00	12.95	0.140	
TS23	5.14	1.97	12.95	0.131	
TS24	4.28	2.02	12.95	0.112	
TS25	13.08	1.89	12.95	0.320	
TS26	5.00	1.98	12.76	0.126	
TS27	4.77	1.85	12.76	0.113	
TS28	4.62	1.92	12.76	0.113	
TS29	4.61	2.03	12.76	0.120	
TS30	4.97	2.07	12.76	0.131	
TS31	9.86	2.11	12.76	0.266	
TS32	9.28	1.96	13.17	0.239	
TS33	10.27	1.95	13.17	0.264	
TS34	13.94	1.93	13.17	0.354	
TS35	9.34	1.90	13.33	0.236	
TS36	14.79	2.16	11.77	0.376	
TS37	15.06	2.09	11.77	0.371	

Table 3.6. Shale rock sample basic parameters

Sample No.	Thickness	Area
	mm	cm^2
SH21	14.73	1.07
SH22	10.64	0.99
SH23	4.49	0.99
SH24	4.96	1.00
SH25	5.49	0.95
SH26	4.59	0.98
SH27	4.84	0.96
SH28	4.96	1.02
SH31	9.16	1.059
SH32	9.44	1.034
SH33	13.6	1.086

3.2. BASIC PARAMETERS OF FLUID ADDITIVES

Based on previous review and analysis of the fracturing fluid additives during unconventional gas hydraulic stimulation, brine, friction reducer, breaker, and surfactant are the major compositions of fracturing fluid. They were extensively studied in the following sections. Potassium Chloride (KCl) is from Fisher Scientific, friction reducer: FRW-20 (FR) and surfactant Gasflo G (GG) are from Baker Hughes, breaker: Ammonium persulfate (AP) is from Sigma-Aldrich.

FRW-20 is a polyacrylamide-based anionic polymer. It is manufactured as water-in-oil emulsions and added to the fracturing fluids (hydration) “on the fly”. During the pumping process, it changed to oil-in-water emulsion. It has a molecular weight around 20 million Da. It also features to be easily breakable, which causes little or no formation damage in fracture (Sun, Wood et al. 2011).

Gasflo-G is a non-ionic surfactant, which reduces surface and interfacial tension, enhancing cleanup and reducing flowback time while preventing water blocks and

emulsions. This surfactant is specifically designed for gas well fracturing, replacing micro-emulsion products.

Ammonium persulfate had proved to be working well with this FR. Under a temperature of 100°F, it will take 22 hr for the relative viscosity to reach down to 1cP. And 150 °F heating only costs it 75 min to be close to 1cP.

In the experiments involve with the real tight rocks, such as tight sand and shale, FR, GG, and AP were prepared with 2% KCl solution. In the microchannel and microfracture experiments, FR was prepared without KCl, because no rock was used in these experiments. Each solution was stirred at 700 RPM for 6-72 hrs on the stir plate (Fisher Science, MA).

The basic properties of these additives were measured. They would help to explain the phenomenon observed in the other experiments.

3.2.1. Surface Tension. The surface tension is one of the most important properties of a surfactant. For surfactant GG, its surface tension is measured with QC6000 Surface Tensiometer (SensaDyne, Milwaukee, WI), as shown in Figure 3.24. It is working by blowing a bubble through a liquid and measuring the maximum pressure of the bubble. During measurement, the SensaDyne unit uses an inert gas (Nitrogen), which slowly bubbled through two probes of different radii (r_1 and r_2) that are immersed in the test fluid. The bubbling of Nitrogen through the probes produces a differential pressure signal (Δp) which is directly related to the surface tension of the fluid. The pressure signal is detected by a stainless steel rod, and computer connected with it would directly tell the surface tension by the build-in software.

Figure 3.24. SensaDyne QC6000 Surface Tensiometer

Several concentrations of GG solution were measured, as shown in Figure 3.25. These four concentrations are commonly used in the field. It shows the decreasing of surface tension compares with DI water (72 mN/m).

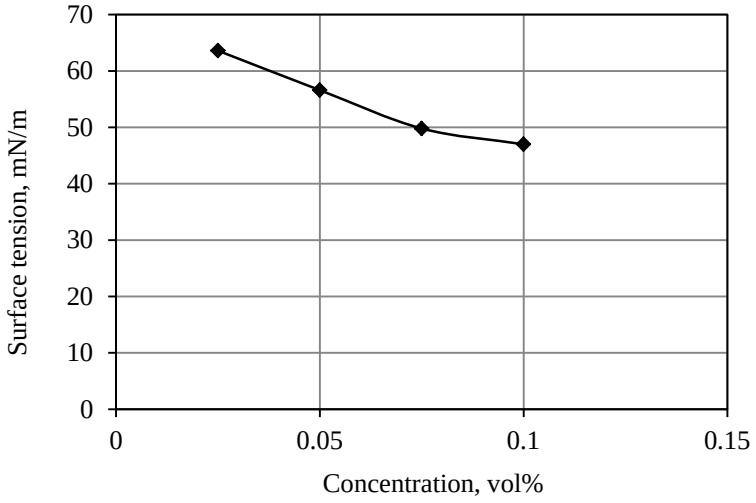

Figure 3.25. Surface tension V.S. Concentration

3.2.2. Particle Size Distribution. Since FR is a polyacrylamide emulsion polymer and widely used in unconventional gas reservoir, where the reservoir rock is featured with nanometer pore size, the emulsion particle size in FR solution would be critical compared with the pore size.

A dynamic light-scattering particle size analyzer Nanotrac 250 (Microtrac, Montgomeryville, PA) was used to characterize the FR solution particle size, as shown in Figure 3.26. It has a laser diode of 780nm wavelength, and 180° measuring angle. In order to give a more accurate result, the solution viscosity is firstly estimated by DV-III Ultra Viscometer (Brookfield, Middleboro, MA) as shown in Figure 3.27. Its viscosities at two different temperatures are listed in Table 3.7. Then this viscosity data was utilized for the solution particle size analyzer by input it in its software.

Figure 3.26. Nanotrac 250 particle size analyzer

Figure 3.27. Brookfield DV-III Ultra Viscometer

Table 3.7. Viscosity of 0.05vol% FR solution

Temperature	Viscosity
°C	cP
16.9	1.29
22	1.17

0.05vol% FR solution prepared with a stir plate at the highest shear rate (~1200 RPM) was measured. The average results based on five measurements are presented in Figure 3.28. The diameter of emulsion particles is from 0.0723 to1.944 μm, and the peak diameter is 0.818 μm.

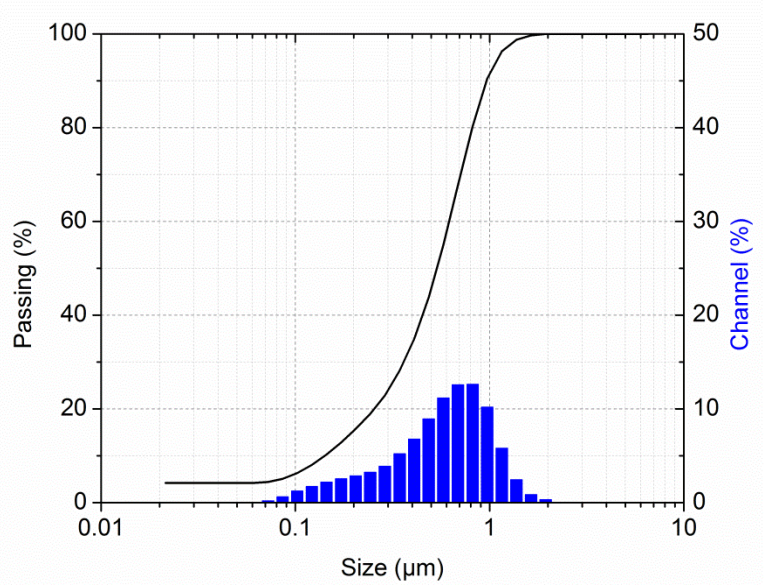

Figure 3.28. FR emulsion particle size distribution prepared with stir plate

The FR solution is also prepared under high shear rate to simulate its condition of field operation. The solution was firstly prepared on a stir plate at the highest shear rate (~1200 RPM), then it was sheared in Farberware 4-Speed digital blender model 103742 (Meyer, Vallejo, CA) for 10 minutes. The average results based on five measurements are shown in Figure 3.29. The emulsion particles are from 0.02343 to 0.0663 μm, and the peak diameter is 0.0331 μm.

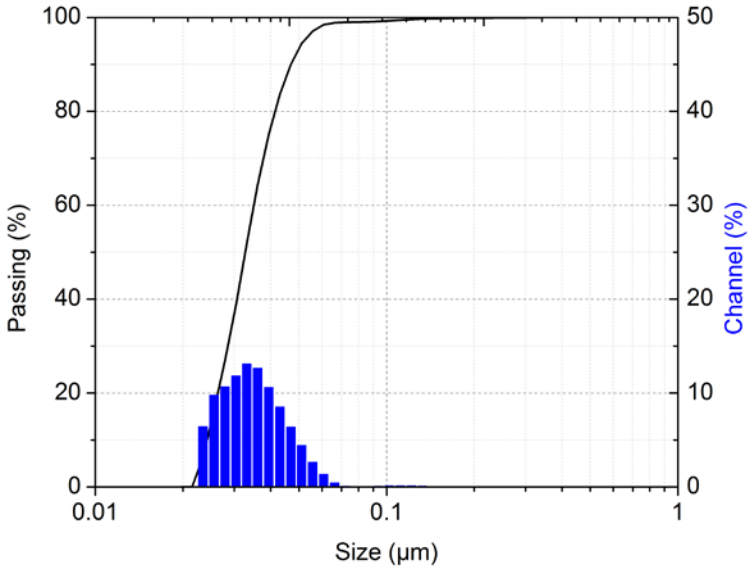

Figure 3.29. FR emulsion particle size distribution prepared with blender

3.3. CONCLUSION

1) A new sample preparation method is successfully developed by coating and slicing. It features to be faster permeability measurement and less rock consumption;
2) From the porosity data measured, this tight sand is relatively homogenous , while the shale samples indicate more heterogeneity properties;
3) The pore size distribution of this tight sand is measured to be ranging from 0.01 micron to over 2 micron. Shale rock pore size is suspected to be from 0.019 micron to 0.024 micron, based on previous researchers;
4) Absolute permeability test with tight sand shows it has some variation, even it is relatively homogeneous from its porosity. The initial water saturation in these tight sand has a big impact on the gas phase permeability;
5) SEM imaging of the tight sand demonstrates the sample is not homogeneous. The pores majorly exist in clay materials, even though few intergranular pores can be found. Kaolinite is extensively developed in this tight sand;

6) Particle size distribution in 0.05 vol% FR solution is measured to be from 0.1022 to1.156 μm when solution is prepared with stir plate. It changed to 0.02343 to 0.0663 μm when the solution is prepared with a blender at high shear rate.

4. FRICTION REDUCER TRANSPORTS IN MICROCHANNEL AND MICROFRACTURE

PART I - FRICTION REDUCER TRANSPORTS IN MICROCHANNEL

4.1. SUMMARY

Hydraulic fracturing can generate a fracture network in shale gas reservoir. The micro-sized fractures in the network have much more contact area with the matrix and therefore hold the majority of the productivity potential of shale gas. Slickwater fracturing has been proved to be an effective method to increase the recovery of shale gas reservoirs. Friction reducer, the primary component of this fluid, can decrease the flowing friction in the pipeline. Lab flow loop tests and field applications have addressed this issue thoroughly. However, the flow characteristics of this friction reducer solution in microfractures are not clear. This study used capillary tubes to represent microfractures and the flow behavior of friction reducer solution in capillary tubes was systematically studied. It is found that the friction reducer increased water flow resistance in microfractures by 20% rather than reduced flow friction as it acted in wellbore tubings. It is not sensitive to the surface wettability at high velocities, but this sensitivity increases in smaller microchannels and lower velocities. The existence of friction reducer in microfractures resisted water flow by up to a factor of 1.38. The solution is a shear thinning fluid. At the same shear rate, the apparent viscosity is higher in larger microchannels.

4.2. INTRODUCTION

Tight formations with extremely low matrix permeabilities can produce at economical rates primarily because of inborn fissures and hydraulic fractures created in formation during hydraulic stimulation. Hydraulic fracturing treatments in gas shale can connect/generate the inborn and introduced microfractures, causing them to become much more complex fracture networks than a pair of main fractures. Fracture networks will expose more matrix as the number of micro-sized fractures increases (Wang 2008, King 2010, Apaydin, Ozkan et al. 2012, Ding, Li et al. 2012, Tinni, Fathi et al. 2012).

Among the various fracturing methods, slickwater fracturing has been proved to be an effective method by which to increase the recovery of shale gas reservoirs (Grieser,

Hobbs et al. 2003, Palisch, Vincent et al. 2010). By adding a very small amount of chemical to the fluid (<1 vol% of the liquid volume) (Arthur, Bohm et al. 2009, Paktinat, O'Neil et al. 2011), slickwater fracturing fluid can lower the surface pumping pressure below that achieved with the traditional cross-linked fracturing fluid. This fluid also demonstrates a relatively low viscosity, which significantly reduces the gel damage during hydraulic stimulation.

Friction reducer is the primary component of this fluid. Most of the common friction reducers are polyacrylamide-based polymer, usually manufactured as water-in-oil emulsions and added to the fracturing fluids (hydration) “on the fly”. Polymers disrupt the near-wall turbulence regeneration cycle and reduce the turbulent friction drag by directly interacting with the vortex, thereby decreasing the flow friction in the pipeline (Ram, Finkelstein et al. 1967, White and Mungal 2008). Flow loop tests in laboratory (Kaufman, Penny et al. 2008, Rimassa, Howard et al. 2009, Rimassa, Howard et al. 2009, Zelenev, Gilzow et al. 2009, Baser, Shenoy et al. 2010, Shah and Kamel 2010) and field applications (Sun, Stevens et al. 2010, Lindsay, Mcneil et al. 2011, Paktinat, O'Neil et al. 2011, Sun, Wood et al. 2011, Zhou, Sun et al. 2011) have addressed this phenomenon well, showing 10% to 82% friction reductions in the lab, compared with that of fresh water.

During slickwater fracturing treatment, a pair of main fractures firstly is generated perpendicular to the wellbore direction. As the fluids continue to pump, more micro-sized fractures are generated near the main fractures. These microfractures have much more contact area with the matrix, therefore hold the majority of the productivity potential of shale gas (King 2010, Odusina, Sondergeld et al. 2011, Apaydin, Ozkan et al. 2012). However, when this fluid comes into the microfractures, its flow characteristics there are not clear.

The present study attempts to represent how this fluid flows in microfractures by considering how it flows in long circular microchannels. A commercial friction reducer was used and prepared with deionized water at various concentrations. The friction reducer solution fluxed the microchannels with various velocities. The effects of solution concentrations, microchannel size and wettabilities on injection pressure were

investigated in details. The residual resistance factor to water also was studied. Experiments data were then discussed with that in flow loop experiment.

4.3. EXPERIMENTAL

4.3.1. Materials. Friction reducer (FR): A commercial polyacrylamide-based anionic polymer, FRW-20, with a molecular weight around 20 million Da, was used for the study. Deionized (DI) water was used to prepare the FR solutions with four concentrations: 0.025, 0.05, 0.075, and 0.1 vol%, according to standard industry practice. Microchannels (Polymicro, Phoenix, AZ) are circular, made of fused silica. Their product labels indicate their nominal inner diameters as 25, 48.6and 102 μm. However, in order to achieve more reliable data, the inner diameters of these microchannels were examined with a Helios Nano Lab 600 Scanning Electron Microscope (SEM) (FEI, Hillsboro, OR). Figure 4.1 depicts a microchannel with a nominal diameter of 102 μm. A circle was drawn to fit into the actual inner wall, and then the diameter was generated automatically. This technique indicated that the inner diameter is 103.43 μm, different than the nominal size of 102 μm. This difference between the nominal and actual diameter is frequently seen in microchannel studies (Celata, Cumo et al. 2006, Krishnamoorthy and Ghajar 2007).

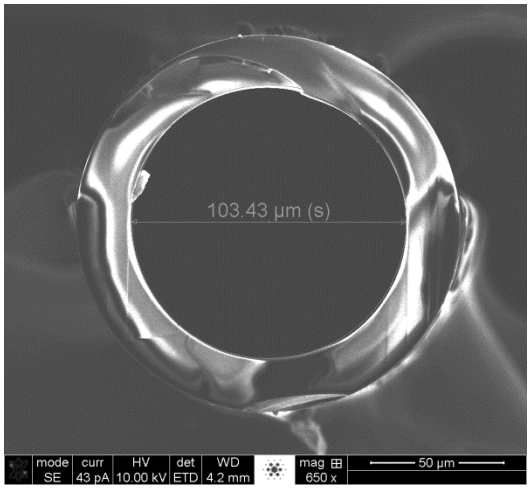

Figure 4.1. Microchannel cross-sectional diameter examined with SEM

The microchannels come with hydrophilic inner surfaces (Henares, Mizutani et al. 2008, Wang, Yue et al. 2009, Song, Wang et al. 2010). In order to study the wettability effect, the insides of some microchannels were coated with a thin (preferably monomolecular) layer of a hydrophobic, non-ionic polymer using the following coating procedures (Hjertén and Kiessling-Johansson 1991):

1) Rinse the microchannels with 1M HCl, 1M NaOH and methanol for 5 minutes;
2) Fill the microchannels with methanol and 3-(trimethoxysilyl)propyl methacrylate mixture (1:1), and incubate at room temperature for 15 hours;
3) Flush the microchannels with methanol and DI water;
4) Fill the microchannels with acrylamide reaction reagent, and keep the reagent in the microchannels for 2.5 hours;
5) Flush the microchannels with DI water and Nitrogen for 10 minutes.

The diameters of all microchannels were examined by SEM, resulting in the parameters listed in Table 4.1.

Table 4.1. Microchannel Parameters

Nominal ID (Hydrophilic)	Actual ID (Hydrophilic)	Actual ID (Hydrophobic)	Length
μm	μm	μm	ft
25	26.29	26.22	0.246
48.6	52.25	51.56	0.478
102	104.06	103.43	1

4.3.2. Equipment. The apparatus used in the experiment consisted of a pump, a digital pressure gauge, two non-piston accumulators, microchannel inlet assemblies, and a data acquisition system, as shown in Figure 4.2. A high-pressure ISCO 500D syringe pump (Teledyne Technologies, Thousand Oaks, CA) provided the fluid driving power, with a flow rate ranging from 0.001-204 mL/min. The digital pressure gauge (Keller,

Winterthur, Switzerland) measured the microchannel inlet pressure over a pressure range of 0-4350 psi with an accuracy of ± 0.1%. To provide continues flow in the flow lines, two non-piston accumulators (Swagelok, Solon, OH) were used. Decane (Fisher Science, Waltham, MA), a nonpolar liquid that will not dissolve in water, was employed to fill the pump so that it could work as a driving fluid to push the DI water and FR solution from the accumulators into the microchannels, respectively. The microchannel inlet was checked to ensure that it was tight enough to hold the maximum inlet pressure before each experiment. The data acquisition system was connected to the digital pressure gauge to collect pressure data over time. All experiments were carried out at room temperature.

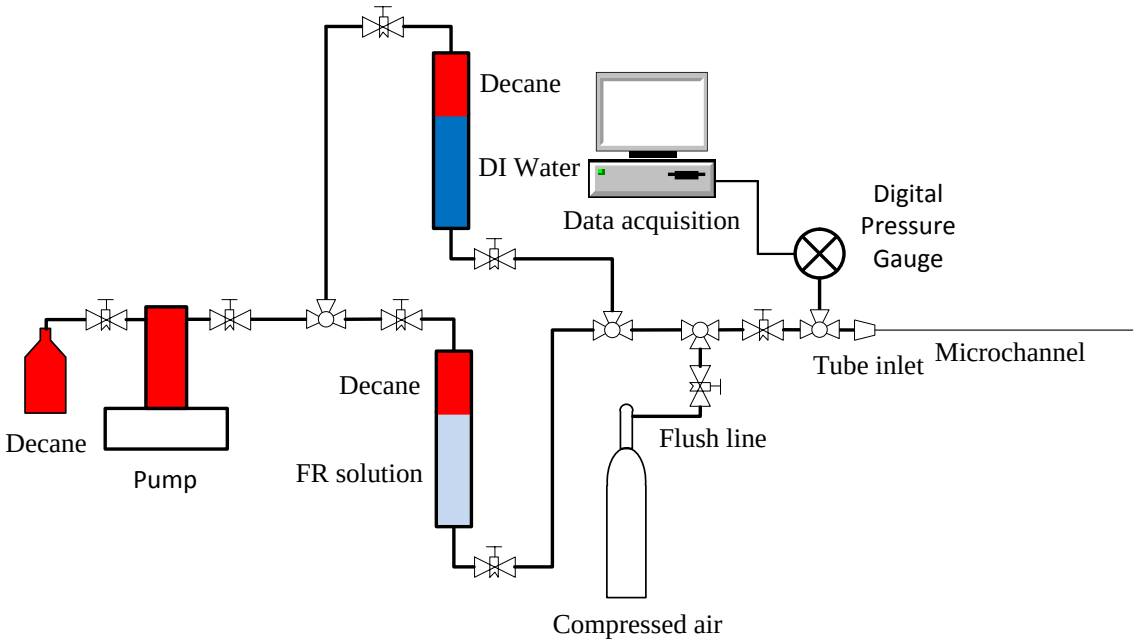

Figure 4.2. Schematic diagram of experiment

4.3.3 Procedure. The pump cylinder was filled with Decane first and allowed to sit for two hours. Then, Decane was pumped into the infill line at a low flow rate until no gas bubbles come out. The infill line valve then was closed, and the accumulators were filled with DI water and FR solution with a syringe, respectively. To ensure that no gas

bubbles existed in the accumulators, the fluids were stirred with a clean glass stick. The entire flow line was checked before running experiments to prevent any future gas bubbles or leaking. Each experiment used a new microchannel. Their length was measured by a vernier caliper. Due to the fragility of the fused silica, equal lengths during cutting cannot be guaranteed each time. A difference of a few millimeters may exist. Therefore, the pressure gradient is used in the Results and Discussion sections.

Based on the flow rate and the inner diameter of the microchannel, the fluid velocity was calculated by:

$$v = \frac{4q}{\pi \times D^2} \tag{2}$$

where v is the fluid velocity in ft/s; q is the fluid flow rate in ft^3/s; and D is the inner diameter of the microchannel in ft.

During one experimental run, the following five fluid velocities were implemented in the microchannels: 11.4-12.6, 5.7-6.3, 2.8-3.2, 1.4-1.6, and 0.3 ft/s, respectively. The pump was set to maintain the highest flow rate initially. Pressure vs time was measured. When the pressure was constant remained within 0.3% of the current reading over a 5-minute period, the flow was considered reaching stable condition. Then, the next lower flow rate was employed, continuing in this manner until all velocities were tested. The data presented in this paper were all at the steady state. For each experiment, time, pressure and flow rate were recorded by the data acquisition system.

4.4. RESULTS

Eighteen experiments were conducted to study the impact of the FR concentration, microchannel size, and wettability on the flow behavior of the FR solution and its residual resistance factor to water was also tested at different velocities. Experiments data were then discussed with that in flow loop experiment. Shear rate impact on apparent viscosity was studied.

4.4.1. Concentration Effect on Pressure Gradient and Apparent Viscosity.

The following four concentrations of FR solution were studied: 0.025, 0.05, 0.075, and 0.1 vol%. Each sample was injected into a new 52.25 μm microchannel, respectively.

Figure 4.3 (a) depicts the effect of the different FR solution concentrations: pressure gradient as a function of velocity. Higher concentration solutions display a larger pressure gradient. And the pressure gradient decreases as the fluid velocity decreases.

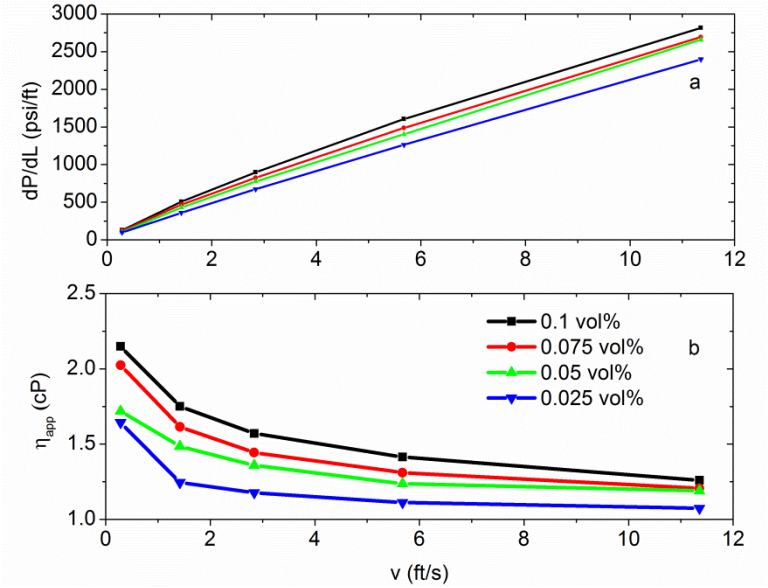

Figure 4.3. Effect of FR solution concentration

Equation 3 can be used to calculate its apparent viscosity, η_{app}:

$$\eta_{app} = c_1 \times k \frac{AdP}{qdL} \tag{3}$$

where η_{app} is the apparent viscosity in cP; c_1 is the conversion factor, c_1=7.32×10^{-7}; k represents the permeability in mD; A is the cross-sectional area in ft^2; dP is the pressure drop in psi; and dL is the microchannel length in ft.

Each concentration of FR solution was used to flux a new, same diameter microchannel, respectively. At the same velocity, in Equation 3, k, A, and q will not change. From Darcy's equation, apparent viscosity then can be simplified to:

$$\eta_{app} = \frac{(dP/dL)_{FR}}{(dP/dL)_{DI\ Water}} \quad (4)$$

As illustrated in Figure 4.3 (b), the apparent viscosity of the FR solution decreases with the fluid velocity increases, and it is always higher than that of DI water (1cP). But its apparent viscosity change is not significant. Therefore, Newtonian equation was used to calculate viscosity, Reynolds number, and Shear Rate.

This FR fluid becomes more viscous at lower velocity. When it flows in microchannel at high velocity, it could display an apparent viscosity as low as 1.07 cp, which is a little bit larger than that of water. When it slows down, it could exhibit an apparent viscosity as high as 2.15 cp.

4.4.2. Microchannel Size Effect on Pressure Gradient and Apparent Viscosity. A 0.05 vol% FR solution was used to flux the 104.06, 52.25, and 26.29 μm microchannels at five velocities, respectively. It took a longer time for the microchannels with small diameters than those with large diameters to reach a steady state, as shown in Table 4.2.

Table 4.2. Time to reach equilibrium

ID ↓ (10^{-6} m)	Time (min)				
26.29	150	120	160	150	170
52.25	23	15	18	17	23
104.06	6	3	3	4	5
Velocity → (ft/sec)	11.4 -12.6	5.7 -6.3	2.8 -3.2	1.4-1.6	0.3

Figure 4.4 (a) illustrates that at the same velocity, the pressure gradient in small microchannels is larger than that in big ones. When comparing this behavior of the FR solution with DI water, as shown in Figure 4.4 (b), the apparent viscosity increases as the velocity decreases. The fluid in large microchannels has a higher apparent viscosity than that in small ones at the same velocity. But it is not very significant. For the friction reducer solution flow in these microchannels at low velocity, the apparent viscosity is still below 2 cp.

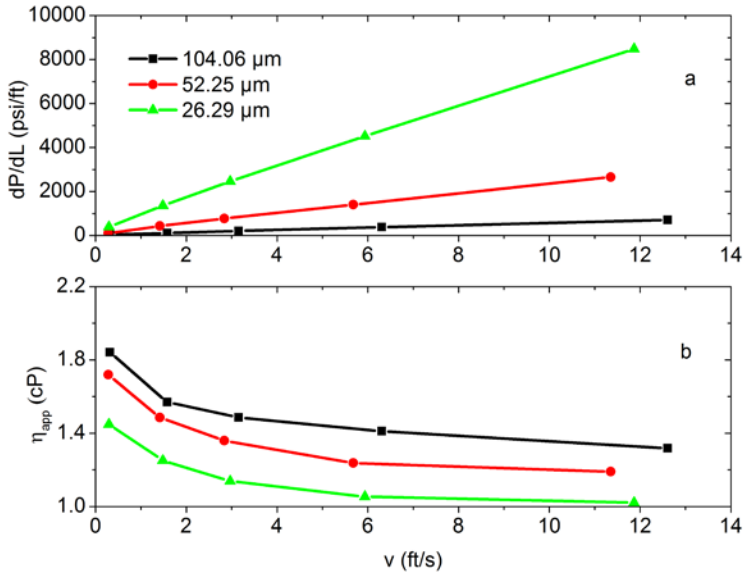

Figure 4.4. Effect of microchannel size

4.4.3. Wettability Effect on Pressure Gradient and Apparent Viscosity.

With a 0.05 vol% FR solution, experiments were conducted in bare (52.25 μm, 104.06 μm) and coated (51.56 μm, 103.43 μm) microchannels, respectively. As shown in Figure 4.5, the effect is very similar between bare and coated microchannels of the same size. However, with Equation 5, the difference between the hydrophilic and hydrophobic microchannels still exists, as shown in Figure 4.6. The pressure gradient of the FR solution in microchannels with hydrophilic surfaces is always higher than in those with

hydrophobic surfaces. At high velocities, the difference is small (< 3%), but it increases to 20% as the velocity decreases.

$$\Delta dP/dL = \frac{(dP/dL)_{Hydrophilic} - (dP/dL)_{Hydrophobic}}{(dP/dL)_{Hydrophobic}} \times 100\% \quad (5)$$

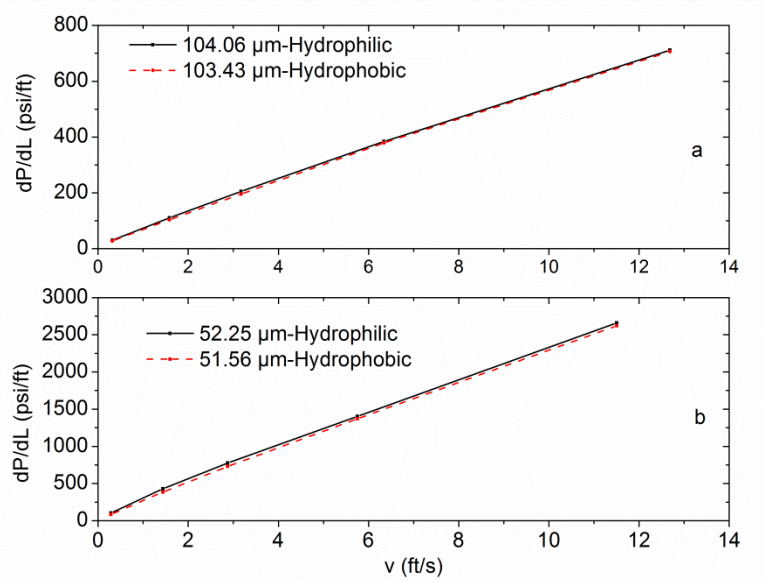

Figure 4.5. Wettability effect

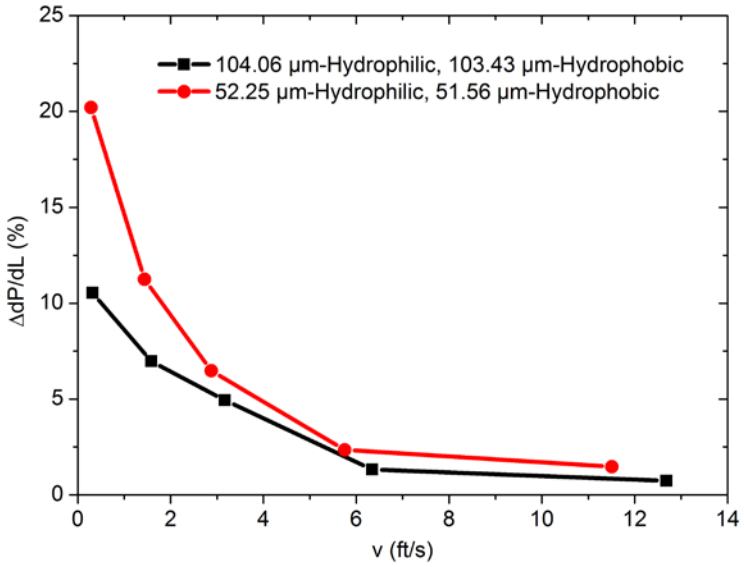

Figure 4.6. Pressure gradient difference vs. velocity under different wettabilities

The sensitivity to velocity can be explained by the changing boundary layer thickness, where the boundary layer is caused by a shear migration of the polymer chains from the channel center to the wall. Its thickness is affected by the fluid velocity in the channel and the surface wettability condition. Due to the interaction between the shear force provided by the driving fluid and the fluid's internal resistance, the boundary layer would be thicker at low fluid velocities and thinner at high fluid velocities. At low velocities, a thick boundary layer would result in a relatively smaller flow path diameter and would require higher pressure for fluid to pass through, and vice versa for a thin boundary layer.

Small microchannels display a bigger difference than that seen in large microchannels, especially at low velocities. This reveals that the FR solution is not very sensitive to the surface wettability at high velocities, but this sensitivity increases in smaller microchannels and at lower velocities. The sensitivity of FR solution to the microchannel size could be interpreted as follows. When the fluid is flowing in large channels, the boundary layer occupies less portion of the cross-sectional area, thus having less impact on the flowing pressure. In small channels, however, it occupies a relatively

large portion of the cross-sectional area. Therefore, the boundary layer in a small channel has a larger impact on flowing pressure at the same fluid injection velocity.

4.4.4. Residual Resistance Factor to Water. The chemical residual condition after stimulation is closely related to the fracturing fluid flowback, gas production rate, etc. The residual resistance factor, F_{rr}, is often used to describe how rock permeability is changed after a chemical treatment. F_{rr} can be defined by Equation 6:

$$F_{rr} = \frac{M_b}{M_a} = \frac{(k/u)_b}{(k/u)_a} \tag{6}$$

where M is the water mobility in mD/(cP); b and a represent DI water flux the microchannel before and after FR solution, respectively.

If F_{rr} equals 1, then the fluid flow after polymer injection will not be affected by the introduced fluid.

In this study, DI water was injected into 52.25(bare), 51.56(coated), 104.06(bare), 103.43(coated) μm capillary first, then flux them with 0.05vol% FR solution, respectively, and then inject DI water to each capillary again. Each experiment was conducted at 5 velocities, pressure was recorded with a computer. Stable pressure at each velocity was used. The water injection pressure is used to give the F_{rr}, as in Equation 7, which is simplified from Equation 6 and combined with Darcy's equation.

$$F_{rr} = \frac{\Delta P_a}{\Delta P_b} \tag{7}$$

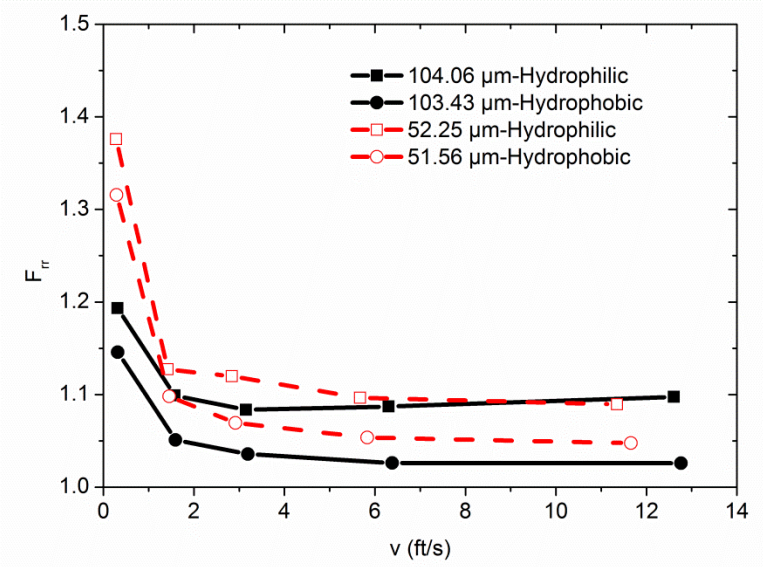

Figure 4.7. Residual resistance factor in different microchannels

Figure 4.7 gives the residual resistance factor as a function of velocity. The residual resistance factor is low (1.02) at high velocity and high (1.38) at low velocity. This is due to the FR solution viscous property and its polymer adsorption condition on the wall. As a viscous polymer solution, once it goes into the microchannel, there will be some polymer adsorbed on the wall. For microchannels of the same size, at a high velocity, this adsorbed polymer could be flushed out easier than that at low velocity. Furthermore, if a flowback additive is considered for slickwater fracturing, its performance at low velocity would be critical.

Smaller microchannels have larger residual resistance factors at the same velocity and surface wettability. At the same velocity, the boundary layer occupies a large portion of the cross-sectional area in small microchannels and a small portion in large ones. If the fluid is flowing at the same velocity, when using DI water to push FR solution out, higher pressure is required for small microchannels.

The residual resistance factor at the hydrophobic surface is always approximately 0.05 higher than that at the hydrophilic surface. Because the FR solution has a hydrophilic property, the boundary layer in hydrophilic microchannels would be thicker than that in hydrophobic ones. Then it would occupy more portions of the cross-sectional

area in hydrophilic microchannels than that in the hydrophobic ones. Therefore, the relatively small flow path diameter in hydrophilic surface would require a higher pressure at the same velocity.

4.5. DISCUSSION

4.5.1. Data Comparison with Flow Loop Experiment. Zhou et al (2011) used the tubings with the diameters of 0.677, 0.9, and 1.162 in to conduct flow loop experiments using the same friction reducer with the concentration of 0.075 vol%. At fluid velocity around 10 ft/s, the injection pressure decreased around 40% compared with water. However, in our experiments, when the FR solution was injected into a 52.25 μm microchannel at the velocity of 11.5 ft/s, which is similar with the FR fluid flow velocity in flow loop experiment, its injection pressure did not decrease but rather increased 20% comparing to DI water, as shown in Figure 4.3.

To explain the difference, we calculate the Reynolds number which is the ratio of inertial forces to viscous forces and is used to characterize different flow regimes, such as laminar or turbulent flow, using the following equation:

$$\mathrm{Re} = c_2 \times \frac{\rho v D}{\mu} \tag{8}$$

where c_2 is the conversion factor, c_2=1489.6; ρ is the fluid density in lb/ft^3; and μ is the fluid dynamic viscosity in cP.

Figure 4.8 gives the Reynolds number at different velocity for different sizes of microchannels that were used in our experiments. It can be seen that large microchannels have a larger Re at the same velocity. The maximum Re is 300, which is much smaller than the transitional Re of 2300, indicating that the flows in our experiments were under laminar flow regime. However, Re values calculated from Jia's experiments indicates the flow was turbulent under the similar velocities because their tubing sizes are much larger than ours.

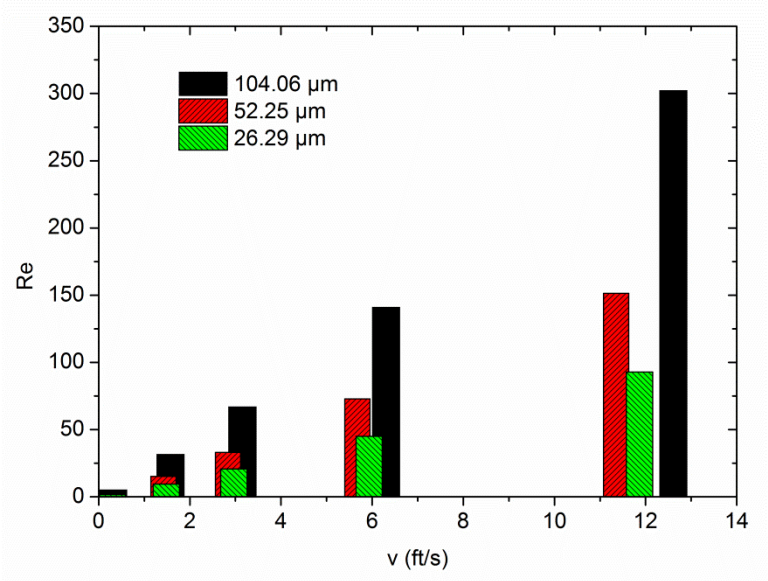

Figure 4.8. Reynolds number vs. velocity

This above comparison indicates that the friction reducer can reduce the flowing friction when FR solution flows in wellbore due to the high Reynolds number. However, the friction reducer will increase flow resistance when it enters the microfracture because the flow regime change from turbulent to laminar flow due to reduced Reynolds number.

4.5.2. Shear Rate Impacts on Apparent Viscosity. In this industry, most people are familiar to express the viscosity as a function of shear rate. Therefore, we converted the velocities in Figure 4.4 to the shear rates using the following equation, which is used to calculate the maximum shear rate on the wall (Bird, Stewart et al. 2007).

$$\dot{\gamma}_w = \frac{4Q}{\pi R^3} = \frac{4 \times vA}{\pi R^3} = \frac{4 \times v \times \pi \times D^2 / 4}{\pi \times D^3 / 8} = \frac{8v}{D} \tag{9}$$

We expected that all data would be in the same line after we converted the velocities in Figure 4.4 to shear rate. However, the converted results shown in Figure 4.9 show that the apparent viscosity has a good linear relationship with the shear rate in log-log scale for different size of microchannels and their relationship can be expressed using

power law equations as shown in Table 4.3. However, the data from different microchannels are not in the same line. At the same shear rate, larger microchannel displays a higher apparent viscosity. For most of the shear rate in Figure 4.9, the apparent viscosities in 104.06 and 52.25 μm microchannels are around 20% higher than that in 26.29 μm microchannels. This indicates the apparent viscosity is the function of both shear rate and microchannel size.

$$\eta_{app} = K \dot{\gamma}_w^{n-1} \tag{10}$$

Table 4.3. Power law index of FR in microchannels

Microchannel size (μm)	K	n	R^2
26.29	4.034	0.900	0.986
52.25	4.610	0.897	0.988
104.06	4.094	0.910	0.996

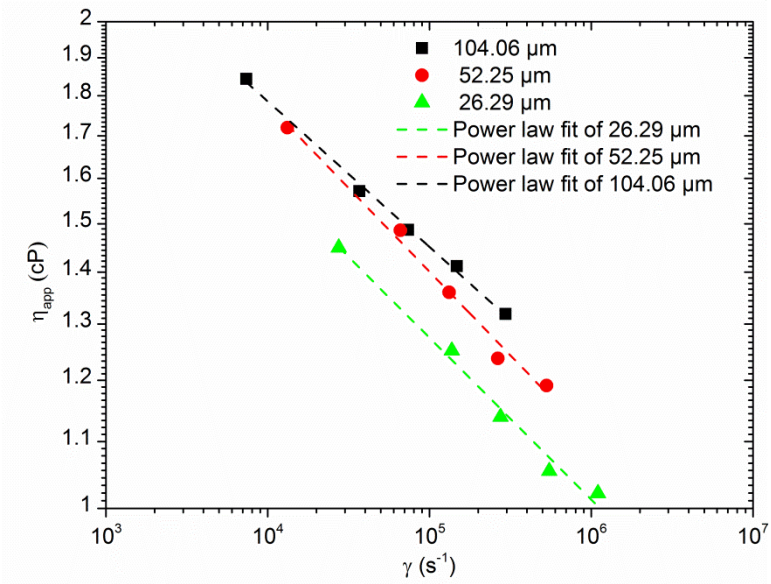

Figure 4.9. Shear rate effect

Generally, for the same fluid, ideally its shear rate and apparent viscosity curve should be always on a same line. At the same shear rate, its apparent viscosity should be the same, no matter what size of channel it is flowing through. However, similar phenomenon was observed by Seright, Fan et al. (2011). They used Xanthan, which is also a shear thinning polymer, fluxed in 55 mD, 269 mD, and 5120 mD rocks. Under the assumption that the rock is homogeneous, the pore size of each sample was converted to circular capillary diameters from permeability and porosity data, as shown in Table B.1. Then, the velocity was converted to shear rate. Figure 4.11 shows the relationship between the shear rate and the resistance factor. It can be seen that their data were not in the same line either for different permeability rocks. The resistance factor in the high permeability sample is larger than that in the low permeability one.

One reason for this phenomenon can be attributed to a low viscosity boundary layer (e.g. water). It can be present without any FR polymer chains near the wall. This low viscosity boundary layer is created through a shear migration of the polymer chains away from the wall and it will have a higher influence at small diameter capillaries and high shear rates. Another reason may be due to the configuration restriction of the polyacrylamide inside small capillaries where basically chains are in elongated configurations that can render different flow dynamics and different viscosity than in bulk. This would be more evident at small capillaries especially when using high molecular weight polymers (as this is normally the case in FR).

PART II - FRICTION REDUCER TRANSPORTS IN MICROFRACTURE

4.6. SUMMERY

Tight formations with extremely low matrix permeabilities, such as gas shale, can produce at economic rates is due to the inborn fissures and fractures introduced during hydraulic stimulation. These microfractures have much more contact area with the matrix and therefore hold the majority of the productivity potential of shale gas. Slickwater fracturing has been proved to be an effective method by which to increase the recovery of shale gas reservoirs. And friction reducer is the primary component of this fluid. However, the flow characteristics of this solution in microfractures are not clear.

Micro-sized fluidic chip was used to represent the microfracture. Friction reducer solution is a shear thinning fluid. Rather than reducing flowing friction, with 0.075 vol%

of this fluid flowing in a 1000 μm height, 50 width μm and 4.14 cm length microfracture, the injection pressure increased more than 50%. The impact of the solution concentration was found to be more obvious at low velocities. If a flowback additive is considered for slickwater fracturing, its performance at low velocity or low shear rate would be critical. At the same shear rate, the apparent viscosity is higher in large microfractures. At the same velocity, large microfractures display higher residual resistance factors. Through the analysis of fluid emulsion particle size and gas shale matrix pore size, this friction reducer solution will not go into the matrix pores easily, but can block the pore entrance on fracture face to prevent the fluid from leak off and help pressure build up during slickwater fracturing.

4.7. INTRODUCTION

Shale gas reservoir with extremely low matrix permeabilities is producing at economical rates. This can be attributed to the inborn fissures and introduced fractures. Due to the rock mechanical properties of gas shale, hydraulic fracturing can connect and generate these fractures, causing them to be a fracture network than a pair of main fractures. The fracture network will expose more matrix as the number of micro-sized fractures increases (Wang 2008, King 2010, Apaydin, Ozkan et al. 2012, Ding, Li et al. 2012).

Among the various fracturing methods, slickwater fracturing has been proved to be an effective method by which to increase the recovery of shale gas reservoirs (Grieser, Hobbs et al. 2003, Palisch, Vincent et al. 2010). By adding a very small amount of chemical to the fluid (<1 vol% of the liquid volume), slickwater fracturing fluid can lower the surface pumping pressure below that achieved with the traditional cross-linked fracturing fluid. This fluid also demonstrates a relatively low viscosity, which significantly reduces the gel damage during hydraulic stimulation. In order to carry proppant in this low-viscosity fluid, high pump rates usually are required. Therefore, the friction along the pipeline could be significant.

Friction reducer (FR) is one of the primary components of this fluid. Most of the common FRs are polyacrylamide-based polymer, usually manufactured as water-in-oil emulsions and added to the fracturing fluids (hydration) “on the fly”. Polymers disrupt the near-wall turbulence regeneration cycle and reduce the turbulent friction drag by

directly interacting with the vortex, thereby decreasing the flow friction in the pipeline (Ram, Finkelstein et al. 1967, White and Mungal 2008). Flow loop tests in the laboratory (Kaufman, Penny et al. 2008, Rimassa, Howard et al. 2009, Rimassa, Howard et al. 2009, Zelenev, Gilzow et al. 2009, Baser, Shenoy et al. 2010, Shah and Kamel 2010, Paktinat, O'Neil et al. 2011) and field applications (Sun, Stevens et al. 2010, Lindsay, Mcneil et al. 2011, Paktinat, O'Neil et al. 2011, Sun, Wood et al. 2011, Zhou, Sun et al. 2011) have addressed this phenomenon well, showing 10% to 85% friction reductions in the lab and 30% to 90% in the field, respectively, compared with fresh water.

During slickwater fracturing treatment, a pair of main fractures firstly is generated perpendicular to the wellbore direction. As the fluids continue to pump, more microfractures are generated near the main fractures. These microfractures have much more contact area with the shale matrix and therefore hold the majority of the productivity potential of shale gas (King 2010, Odusina, Sondergeld et al. 2011, Apaydin, Ozkan et al. 2012). However, the flow characteristics of FR solution in these microfractures are not clear.

Microfluidic chips have been widely used in the area of chemistry, biology, microelectromechanical systems, and etc. The flowing channel in the micro fluidic chip could be manufactured from micrometer to nanometer depth. Therefore, a single straight channel in microfluidic chip with micrometer width and height would act like a microfracture.

The present study investigates how the friction reducer solution flows in microfractures by employing the microfluidic chip model. The fluid flow in microfracture had been extensively examined. A commercial FR was prepared with deionized water at various concentrations. FR solution concentration effect, microfracture size effects, and residual resistance factor to water was investigated in detail. Fluid shear rates and Reynolds number in microfractures also were studied. Then the microfracture experimental results were compared with that in macro tubing. FR solution impact on fracture face, which is shale matrix, also was analyzed. The emulsion particle size in FR solution was analyzed from micrometer to nanometer scale. Then it was compared with the pore size of typical gas shale.

4.8. EXPERIMENTAL

4.8.1. Materials. A commercial friction reducer, FR, a polyacrylamide-based polymer, was used in experiment. Four concentrations, 0.025, 0.05, 0.075, and 0.1 vol% were prepared according to industry practice. Deionized (DI) water was used to prepare the FR solution. Microfluidic chip (Micronit, The Netherlands) was bonded with two pieces of glass of 145 µm and 1.1 mm thick, respectively. The channel was etched in the later one with a quarter circles of 50 µm radius on top and bottom of the fracture. Each chip contains 3 separated microfractures with 50 µm width, 1500 µm, 1000 µm, and 500 µm heights, respectively. Figure 4.10 shows the microfluidic chip with micro-sized fractures (a) and cross-sectional view of a single fracture (b).

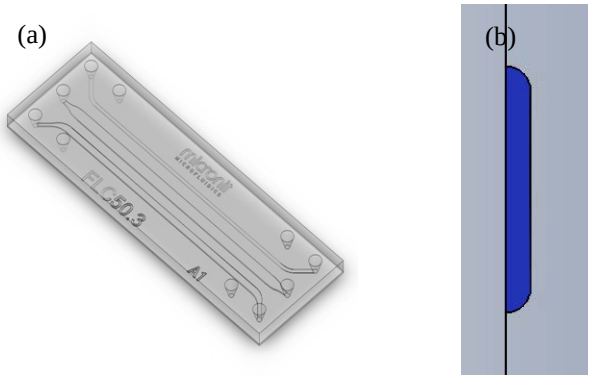

Figure 4.10. Microfluidic chip with microfractures (a) and cross-sectional view of a single fracture (b)

In order to calculate Reynolds no. and shear rate, equivalent diameter was introduced. The area of equivalent circle is the same with the microfracture cross-sectional flowing profile. Equivalent diameter is the diameter of this circle, as listed in Table 4.4. Since microfractures were not of equal length, pressure gradient is used in the Results and Discussion part.

Table 4.4. Microfracture parameters

Height (μm)	Width (μm)	Length (cm)	Equivalent diameter (μm)
1500	50	3.94	306.8
1000	50	4.14	249.59
500	50	4.14	174.54

4.8.2. Equipment. The apparatus used in the experiment consisted of a pump, a digital pressure gauge, two non-piston accumulators, microfluidic chip inlet assemblies, and a data acquisition system, as shown in Figure 4.11. A high-pressure ISCO 500D syringe pump (Teledyne Technologies, Thousand Oaks, CA) provided the fluid driving power, at a flow rate ranging from 0.001-204 mL/min. The digital pressure gauge (Keller, Winterthur, Switzerland) measured the microfracture inlet pressure over a pressure range of 0-3.1 MPa with an accuracy of ± 0.1 %. To minimize the friction in the flow line, two non-piston accumulators (Swagelok, Solon, OH) were used. Decane (Fisher Science, Waltham, MA), a nonpolar liquid that will not dissolve in water, was employed to fill the pump so that it could work as a driving fluid to push the DI water and FR solution, respectively, from the accumulators into the microfractures. A 250 μm inner diameter capillary was used to connect the 1/8’’ stainless steel tubing and the microfluidic chip. The data acquisition system was connected to the digital pressure gauge to collect pressure data over time. A dynamic light-scattering particle size analyzer U1732 (Nanotrac, Montgomeryville, PA) was used to characterize the FR solution emulsion particle size. All experiments were carried out at room temperature.

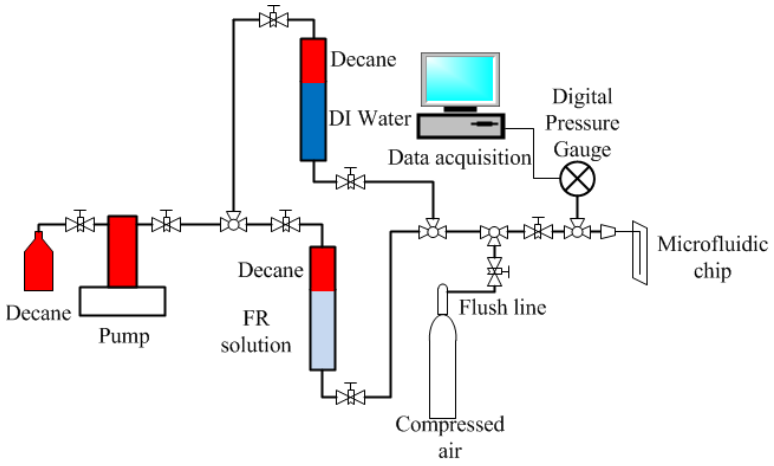

Figure 4.11. Schematic diagram of the experiment

4.8.3. Procedure. The pump cylinder was filled with Decane first and allowed to sit for two hours. Then, the Decane was pumped into the infill line at a low flow rate until no more gas bubbles come out. The infill line valve then was closed, and the accumulators were filled with DI water and FR solution with a syringe, respectively. To ensure that no more gas bubbles existed, the fluids were stirred with a clean glass stick. The entire flow line was checked before running the experiments to prevent any future gas bubbles or leaking. The microchannel inlet was checked to ensure that it was tight enough to hold the maximum pressure before each experiment.

Based on the flow rate and the cross-sectional area of the microfracture, the fluid velocity was calculated by:

$$v = \frac{q}{A} = \frac{q}{\pi \times r^2 / 2 + 50 \times (h - 2 \times r)} \tag{11}$$

Where v is the fluid velocity in m/s; q is the fluid flow rate in m^3/s; A is the cross-sectional area of the microfracture in m^2; and h is the microfracture height in m.

DI water was firstly injected into the microfracture at various velocities. FR solution was fluxed at the same velocities. Then DI water was injected again. During one experimental run, the following five fluid velocities were implemented in the

microfractures: 4.2-4.6, 2.1-2.3, 1.04-1.14, 0.52-0.57, and 0.01-0.011 m/s. The pump was set to flux at the lowest velocity initially. Pressure vs. time was recorded. When the pressure was remained within 0.3% of the current reading over a 1 minute period, the flow was considered reaching stable condition. Then, the next higher velocity was employed. Repeat the measurement until all velocities were tested.

The pressure gauge was seated before the capillary connection. The capillary connection, which has a smaller diameter compare with that of the stainless steel tubing, would generate an additional pressure drop. Therefore, experiments were conducted with two conditions respectively: capillary only and microfractures with the same capillary connected. The pressure drop in microfracture was acquired by subtracting the pressure drop in capillary only from that in microfracture with the same capillary connected. For each experiment, time, pressure and flow rate were recorded. The data presented in this paper were all at the steady state.

To clean the inner surface after each experiment, microfluidic chip was flushed with the following steps:

1) 1 mole/L Nitric acid for 15 min with 25 ml;
2) DI water for 15 min with 25 ml;
3) Repeat 1) and 2) one time, and use methanol and DI water (1:1) for 15 min with 25 ml;
4) DI water for 15 min with 25 ml.

4.9. RESULTS AND DISCUSSION

4.9.1. Concentration Effect. The following four concentrations of FR solution were studied: 0.025, 0.05, 0.075, and 0.1 vol%. Each sample was injected into a 1000 μm height microfracture, respectively. Figure 4.12 illustrates the effect of the different FR solution concentrations vs. pressure gradient. High-concentration solutions display a larger pressure gradient that decreases as the fluid velocity decreases. The four lines are closing to each other at lower velocities. At the velocity of 0.1 m/s, they are almost identical.

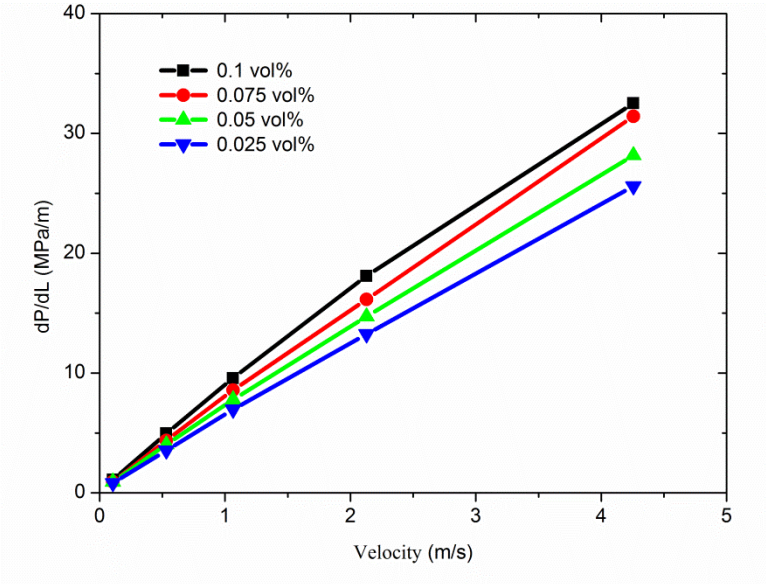

Figure 4.12. Effect of FR solution concentration

This FR solution is polyacrylamide-based polymer, so it is a non-Newtonian fluid. Equation 12 can be used to calculate its apparent viscosity, η_{app}:

$$\eta_{app} = k\frac{AdP}{qdL} \tag{12}$$

where k represents the permeability in m^2; A is the cross-sectional area in m^2; dP is the pressure drop in MPa; and dL is the microfracture length in m.

Each concentration of FR solution, respectively, was used to flux the same sized microfractures. At the same velocity, in Equation 13, K, A, and q will not change. With Darcy's equation, apparent viscosity can be simplified to:

$$\eta_{app} = \frac{\left(dP/dL\right)_{FR}}{\left(dP/dL\right)_{DI\ Water}} \tag{13}$$

As displayed in Figure 4.13, the apparent viscosity of FR solution is always higher than that of DI water (1×10^{-3} Pa·s). This viscosity is small at high velocity (4.3 m/s) and large at low velocity (0.1 m/s). This is because FR is polyacrylamide-based polymer, and its solution usually behaviors as non-Newtonian fluid. It also indicated that the FR solution had a higher resistance in microfracture than that with water. This resistance could reduce FR penetration intro microfracture during hydraulic stimulation and thus would minimize its damage to formation.

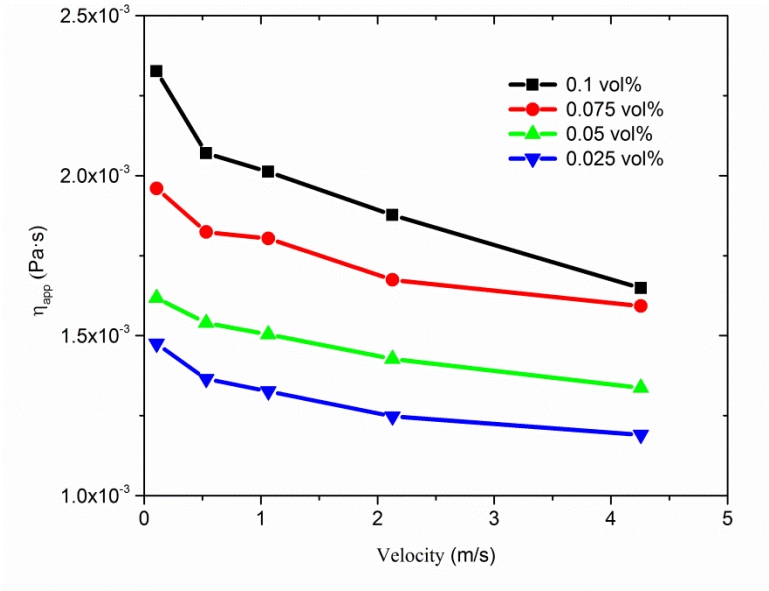

Figure 4.13. Apparent viscosity of FR solution

4.9.2. Microfracture Size Effect. A 0.05 vol% FR solution was used to flux the 1500 μm, 1000 μm, and 500 μm height microfractures at five velocities, respectively. It takes microfractures with small height longer to reach a steady state than that in large height.

When comparing the flow behavior of FR solution with DI water, as shown in Figure 4.14, the apparent viscosity increases as the fluid velocity decreases. Large microfractures have a higher apparent viscosity than that in small ones.

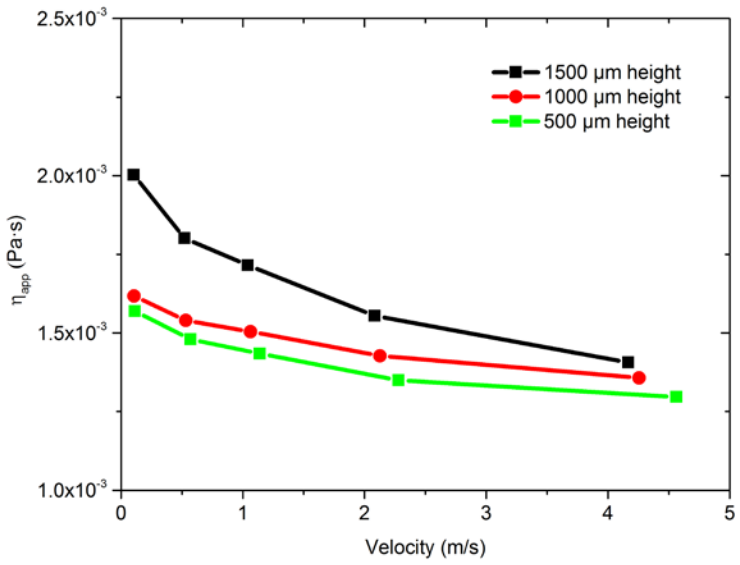

Figure 4.14. Effect of microfracture size

Xanthan, a shear thinning polymer was found to behave in a similar way (Seright, Fan et al. 2011), as shown in Appendix A. Resistance factor (F_r) is defined as the mobility ratio of water to the mobility of polymer. For the same experiment, resistance factor equals to the apparent viscosity. With the 55 mD, 269 mD, and 5120 mD cores, at the same fluid velocity, the resistance factor is higher in high-permeability rocks than that in low-permeability ones, as shown in Figure A.1.

Reynolds number gives a measure of the ratio of inertial forces to viscous forces and is used to characterize different flow regimes. It can be calculated using Equation 14:

$$\mathrm{Re} = \frac{\rho V D}{\mu} \tag{14}$$

where Re is the Reynolds number; ρ is the fluid density in kg/m^3; D is the equivalent diameter of the microfracture cross-sectional area in m; and μ is the fluid dynamic viscosity in Pa·s.

Re is presented vs. velocity with different sized microfracture in Figure 4.15. Large microfractures have a larger Re at similar velocities. In this study, Re can reach to 890, much smaller than the transitional Re of 2300, which indicates that the experiments were under the laminar flow regime.

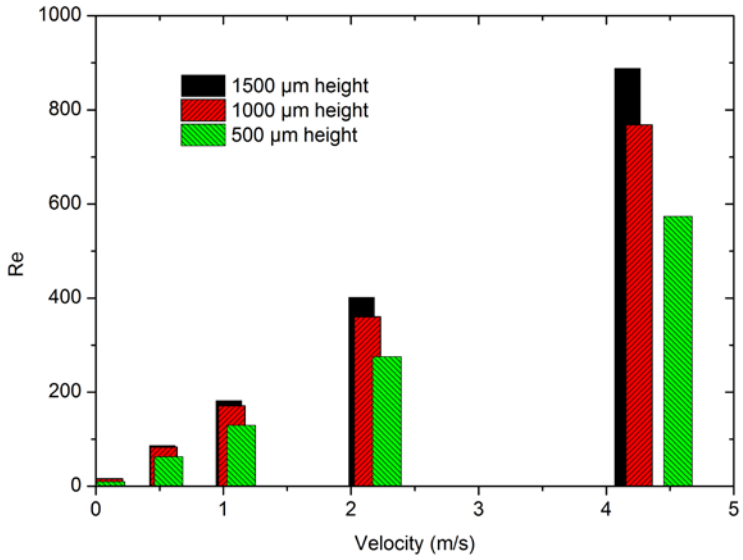

Figure 4.15. Reynolds number as a function of velocity

4.9.3. Shear Rate Effect. Shear rate is the velocity gradient measured across the diameter of a fluid flow channel. It is the rate change of velocity at which one layer of fluid passes over an adjacent layer. 0.05 vol% of FR solution was used to flux the 1500 μm, 1000 μm and 500 μm height microfractures, respectively. As shown in Figure 4.16 in log-log scale, with the shear rate increases, the apparent viscosity of the FR solution decreases. This indicates that FR solution is a shear thinning fluid.

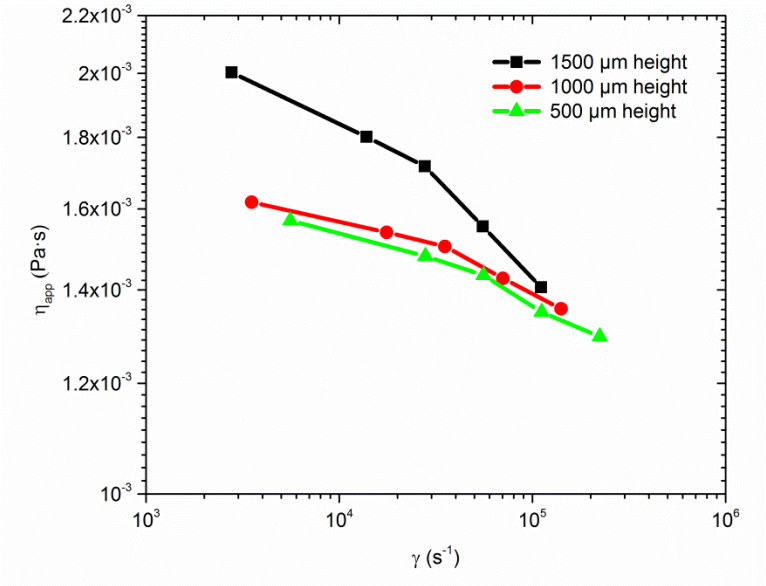

Figure 4.16. Shear rate effect

At the same shear rate, the fluid in larger microfracture displayed a higher apparent viscosity. However, for the same fluid, ideally the apparent viscosity should be the same at the same shear rate, where the three curves here should be on the same line. The difference may partially explain by the boundary layer theory. Based on the laminar flow, two dimensional boundary layer theory (Schlichting and Gersten 2004), the boundary layer thickness can be estimated with Equation 15,

$$\delta \approx 5\sqrt{\frac{\upsilon x}{v}} = 5\sqrt{\frac{\mu x}{\rho \gamma D}} \tag{15}$$

where δ is the boundary layer thickness in m, υ is the kinematic viscosity in m^2/s, x represents the boundary layer development length; and γ is the shear rate in s^{-1}.

Consider the boundary layer development length equals the microfracture length, and then the boundary layer thickness was in $D^{-1/2}$ relations with the microfracture equivalent diameter. The boundary layer area occupied the cross-sectional area would be in $D^{-2.5}$ relation with the microfracture equivalent diameter. This indicated that at the

same shear rate, when the fluid is flowing in small channels, the boundary layer occupied more portion of the cross-sectional area than that in large channels, which would result in smaller flow path diameter in small channels than that in large channels. Therefore, the actual shear rate in small microfracture would be higher than calculated. For this shear thinning fluid, at the same shear rate, the apparent viscosity was lower in small microfractures, and vice versa in large ones. Xanthan flooding experiment in porous media also confirmed this phenomenon. Assuming a homogeneous rock property, porous media was simplified to capillary bundle model. Based on their permeability and porosity, capillary diameter was calculated as in Appendix B, Table B.1. Figure B.1 shows the shear rate vs. resistance factor, indicating that the large porous media has a larger resistance factor at the same shear rate, which is consistent with this study in Figure 4.16.

4.9.4. Residual Resistance Factor to Water. The chemical residual condition after stimulation is closely related to the residual fluid flowing resistance, fracturing fluid flowback, gas production rate, and etc. This phenomenon can be described by the residual resistance factor, F_{rr}, as in Equation 16:

$$F_{rr} = \frac{M_b}{M_a} = \frac{\left(k/u\right)_b}{\left(k/u\right)_a} \tag{16}$$

where M is the fluid mobility in $m^3/(Pa \cdot s)$; b and a represent DI water flows before and after the FR solution, respectively.

If F_{rr} equals 1, then residual FR solution in microfracture will not be affected by the introduced fluid during hydraulic fracturing.

In this study, DI water was used to flux the microfracture before and after 0.05 vol% FR solution. Hence, the viscosity is the same in Equation 16. With Darcy's equation, Equation 16 can be converted into Equation 17:

$$\mathrm{F_{rr}} = \frac{\Delta P_a}{\Delta P_b} \tag{17}$$

Figure 4.17 gives the residual resistance factor as a function of velocity in various sized microfractures. The residual resistance factor is low at high velocity and high at low velocity. This is due to the viscous property of FR solution. As a polymer solution, it may leave some amount of fluid behind after flooding. For the same sized microfractures, at a high velocity or high shear rate, the fluid had high mobility and low apparent viscosity (Figure 4.16); therefore, it could be flushed out easily. The exact opposite is true under the condition of low velocity or low shear rate. Furthermore, if a flowback additive is considered for slickwater fracturing, its performance at low velocity or low shear rate would be critical.

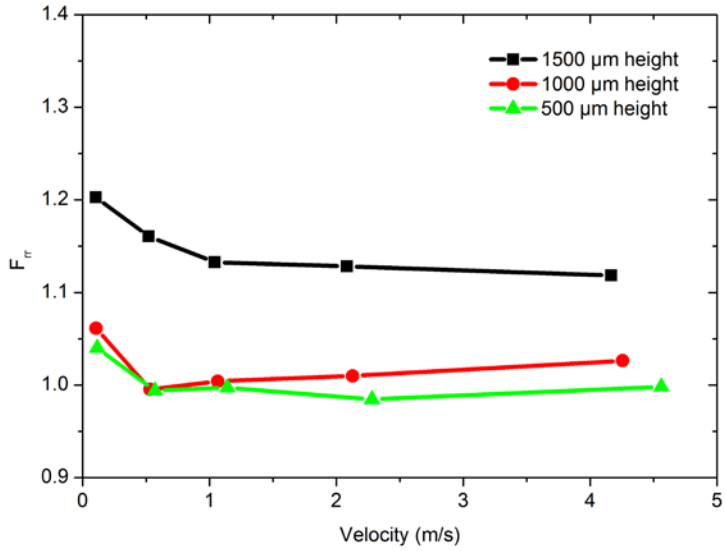

Figure 4.17. Residual resistance factor in different microfractures

Large microfractures display larger residual resistance factor at the same velocity. This could be explained in this way. Assume the fluid can achieve a same velocity at both large and small microfractures, respectively. The shear rate in small ones would be higher than that in large ones. The sweep efficiency in small ones would be larger than that in

large ones. Therefore at the same fluid velocity, the residual resistance in small microfractures is smaller than that in larger ones.

4.9.5. Data Comparison with Flow Loop Experiment. With 0.677 in, 0.9 in, and 1.162 in macro tubing, flow loop experiment was conducted with the 0.075 vol% FR solution (Zhou, Sun et al. 2011). At fluid velocity around 4 m/sec, the injection pressure decreased more than 40% compared with that of water. However, with the same fluid flowing at the velocity of 4.3 m/s in a 1000 μm height, 50 μm width and 4.14 cm length microfracture, the injection pressure did not decrease but rather increased more than 50%, as shown in Fig 4.13. This means that when FR solution flows in pipeline, it can reduce the flowing friction. When it comes to the microfracture with the size mentioned, it cannot achieve turbulent flow regime. The flowing friction increased. The fluid will not easily penetrate into the microfractures compare with DI water.

4.9.6. Analysis of FR Solution Emulsion Particle Size. FR was produced as water-in-oil emulsion. When pumped into the pipeline with a very high pump rate, the emulsion was reversed and the polymer was released, which swelled (hydrates). The oil phase of the FR will form diluted oil-in-water emulsion. The emulsion particle size distribution in 0.05 vol% FR solution was analyzed by a Nanotrac U1732 Particle Size Analyzer. The average results over five tests are shown in Figure 18. The solution has two peaks. The left peak indicates that there are particles with a 0.00093 μm diameter of 3.7 vol%. The majority of the particles lie in the right peak. Their diameters are 0.0723-1.635 μm of 96.3vol%, and the peak diameter is 0.555 μm.

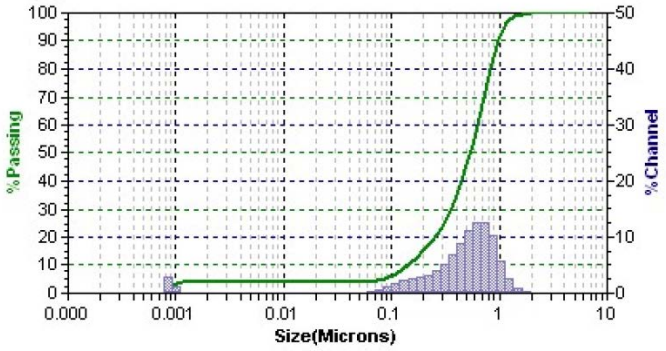

Figure 4.18. Emulsion particle size distribution of 0.05 vol% FR solution

4.9.7. Potential Impact of FR Fluid on Shale Matrix. Shale gas is stored in shale. It is composed of "free" compressed gas in pores and fractures (Ross and Marc Bustin 2007) and adsorbed gas in organic kerogen in shale matrix (Bai, Elgmati et al. 2012, Gasparik, Ghanizadeh et al. 2012). Due to the extremely tight properties of gas shale, the oil-in-water emulsion particles in slickwater fracturing fluid may impact on the flow of fracturing fluid into the micropore, microfracture and matrix.

During hydraulic fracturing, once the gas rich pores, fracture or organic kerogen were reached by fracture networks, compared with the original reservoir pressure, there would be a pressure drop. If this pressure drop is big enough, gas would be desorbed from the kerogen and start to flow through microfractures to wellbore (Leahy-Dios, Das et al. 2011). However, at the same time, if the matrix pore throat is blocked by the emulsion particles from the introduced fluid, which will form a filter cake on the fracture face, an additional pressure drop would be required. If this pressure drop required is too high, the gas production would be impaired. Further formation damage recovery methods need to consider.

The pore throat size of typical gas shale usually ranges from 0.005 to 0.1 μm (Nelson 2009, Clarkson, Solano et al. 2012), as shown in Figure 4.19. When compared with the emulsion particle size distribution of the FR solution (Figure 4.18), there is only a small overlap, less than 5%. From Figure 4.19, only Pennsylvanian shales can reach up to 0.1 μm. Pliocene shales, source rocks, Devonian shales, and Jurassic-Cretaceous shales are ranging from 0.008-0.07 μm, which pore throat size hardly overlaps with emulsion particle size of FR solution. Therefore, such FR solution will not easily go into the shale matrix pores, but it may block the matrix pore entrance to build a filter cake, prevent the fluid from leak off. This filter cake on the fracture face would also help to build up pressure, once the pressure gradient is high enough, more fractures would generate.

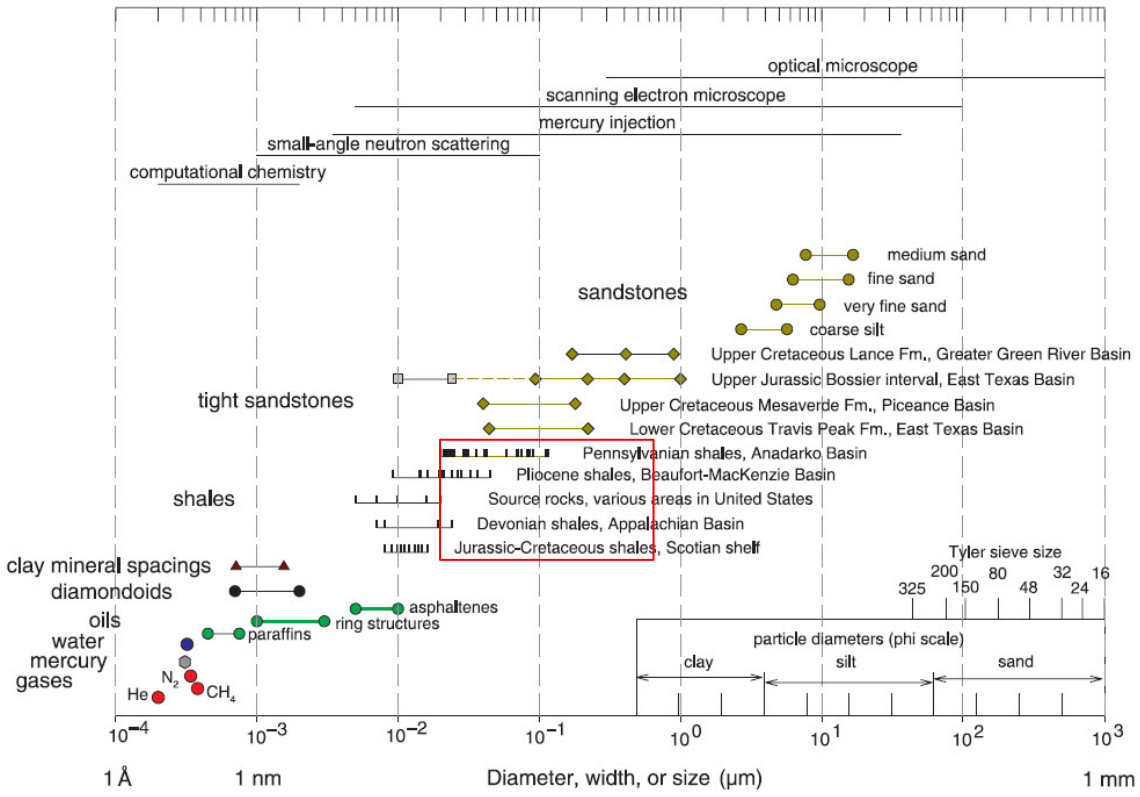

Figure 4.19. Pore throats sizes of different porous media (Nelson 2009)

4.10. CONCLUSIONS

Microfracture experiments were conducted to study the effects of concentration, microfracture size, Reynolds number, shear rate and residual resistance factor on the flow behavior of FR solution. Experimental results were then compared with that in macro tubing. FR solution emulsion particle size was analyzed and its impact on fracture face was discussed.

The following can be concluded from this study:

1) FR solution is a shear thinning fluid, with power law dimensionless flow behavior index n: 0.89-0.91. At the same shear rate, the apparent viscosity is about 20% higher in large microchannels than that in small ones;

2) The impact of FR solution concentration was more obvious at low velocities. Higher concentrations of FR solution displayed a larger pressure gradient than lower concentration;
3) With similar velocity in the flow loop experiment, the fluid flow in microfracture experiments was under laminar flow regime, instead of turbulent in flow loop. The same friction reducer did not decrease the injection pressure, but increased more than 50%;
4) The residual resistance factor to water is relatively low for this friction reducer;
5) This FR solution is not sensitive to the surface wettability at high velocities, but this sensitivity increases in smaller microchannels and lower velocities;
6) Based on the analyzes of emulsion particle size and the typical gas shale pore size, this FR solution will not go into the matrix pores easily, but can block the pore entrance on fracture face to prevent the fluid from leak off, and help pressure build up during slickwater fracturing;
7) If the flow is already laminar, as in microchannel here, there is no turbulence for the friction reducer to suppress. Consequently, the addition of a polymer under these conditions can only increase flow resistance and pressure drop (given a fixed flow rate), but its impact is not very significant;

5. PETROPHYSICAL PROPERTIES IMPACT OF MULTIPLE ADDITIVES CONSECUTIVELY TREATING ON TIGHT SAND

5.1. INTRODUCTION

The Gas Technology Institute (GTI) estimates that the gas in place in the U.S. tight gas basins is over 5,500 Tcf (Gas 2001). The tight sand is characterized with micro-Darcy (μD) permeability and nanometer sized pore throats (Wells and Amaefule 1985). These microscopic features result in some macroscopic characteristic features such as high capillary pressures, low porosities, high irreducible wetting phase saturation and low permeability. Therefore, in order to obtain commercial production from these reservoirs, after the well is completed, hydraulic fracturing is generally required to enhance the production rate.

Among the various additives in hydraulic fracturing fluid, clay stabilizer, friction reducer, breaker, and surfactant are widely used in unconventional gas stimulation. Each of them has its own purpose. Clay stabilizer is working against the clay from swelling. Friction reducer is usually added in fracturing fluid to reduce the flowing friction and increase the pump rate. The emulsion friction reducer may also form a filter cake on the fracture face and block the pore throat in the near fracture matrix, which would help the pressure build up in fracture and reduce the fluid leak off. After proppant is placed, friction reducer require breaker to dissolve so the gas could transport through the adjacent fracture face. Ammonium persulfate, an oxidization breaker is usually used to degrade the polymer, such as friction reducer, therefore release the gas flowing pores and channels. It is working by creating highly reactive free radicals in solution that it reacts with the polymer backbone and break it (Sarwar, Cawiezel et al. 2011, Kelland 2012). Surfactant could reduce surface tension between the injected fluids, reservoir fluids and rocks (Paktinat, O'Neil et al. 2011). It contributes to increase the fluid flow back.

These additives may impair the adjacent fracture matrix permeability, and alter the rock wettability, which influences the gas flow ability. The petrophysical impact of such additives on the tight sand matrix is still not clear. In this study, sample surface contact angle, spontaneous cocurrent imbibition, gas transportation, and gas phase permeability with the remaining liquid will be measured, before and after the sample is

treated with each additive. And the data before and after each additive introduced will be compared and analyzed in detail.

The research will contribute to understanding of introduced fluid petrophysical impact on low-permeability gas reservoir, which will be major importance for success well completion, stimulation, production planning, and reservoir management for tight gas reservoir.

5.2. EXPERIMENTAL

5.2.1. Materials. Previous tight gas sandstone sample and fluids were used in this study, including: clay stabilizer: 2% KCl, friction reducer: 0.05 vol% FRW-20, breaker: 0.012% ammonium persulfate, and surfactant: 0.05 vol% Gasflo-G.

5.2.2. Equipment

1) Coreflooding system

Core flooding system mainly consists of an ISCO pump, an intermediate accumulator, a coreholder, and a data acquisition system, as shown in Figure 5.1. It is used to inject the additives into the tight sand samples, respectively.

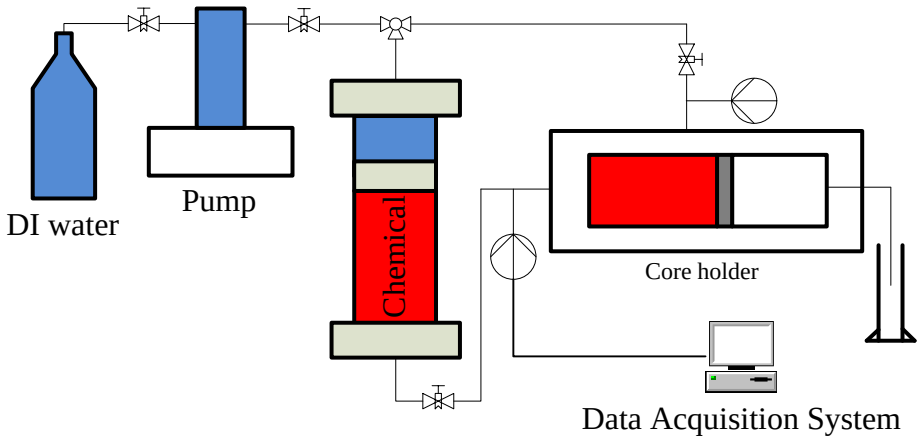

Figure 5.1. Coreflooding system

2) Goniometer

Contact angle measurement is a direct method to estimate the rock wettability. The Rame Hart Model 500 Advanced Goniometer (Rame Hart, Succasunna, NJ) presented in Figure 5.2 is exploited to measure the surface contact angle before and after sample treated with additives.

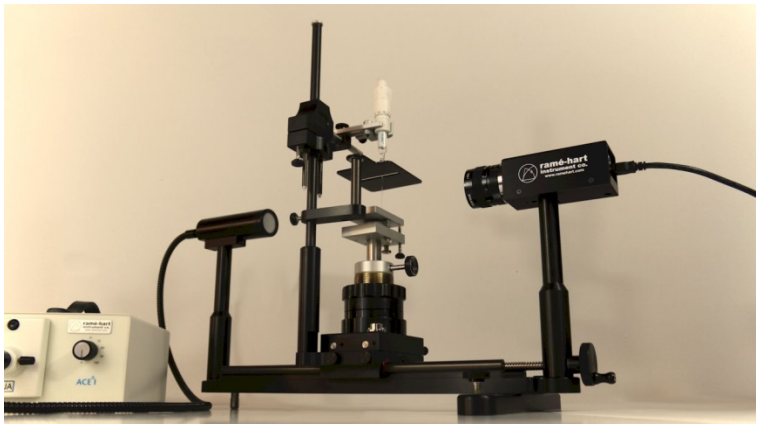

Figure 5.2. Contact Angle Goniometer Instrument

The contact angle measurement uses sessile drop technique, which is defined by the following equation:

$$\theta = 2\tan^{-1}\frac{2h}{d} \tag{18}$$

where θ is the contact angle, h is the drop height and d is the drop diameter or width.

2% KCl was used to test the contact angle on tight sand surface after each additive flooding. Each sample was tested at 5 evenly distributed points, as shown in Figure 5.3. After liquid drop placed, contact angle was measured each 5 seconds, and a total of 60 measurements (For 5 minutes). Each point was repeated for 3+ times, until 3 results were very close to each other, then the result with middle value was plotted here.

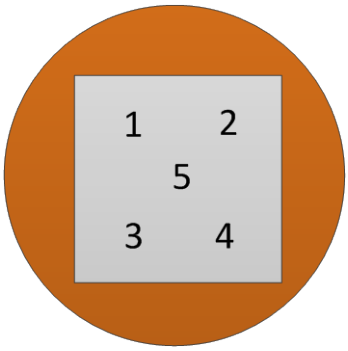

Figure 5.3. The five points where the contact angle were tested

3) Humidified Nitrogen flooding

The liquid in the sample could be flooded out by Nitrogen. Since dry N_2 flooding will have some impact on the remaining liquid saturation (Kewen and Abbas 2000), we used humidified N_2 instead of dry N_2. Humidified N_2 is prepared by forcing N_2 through a 2% KCl accumulator before entering the core sample, as shown in Figure 5.4.

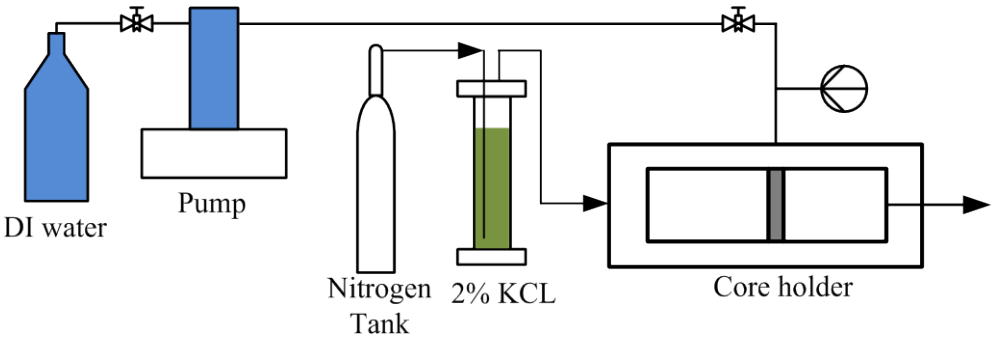

Figure 5.4. Humidified N_2 core flooding setup

4) Gas phase permeability measurement

Sample is considered to reach irreducible liquid saturation after flooded with humidified Nitrogen. The gas phase permeability is then measured with core flooding setup hooked with permeameter and a desiccant tube, as shown in Fig 5.5.

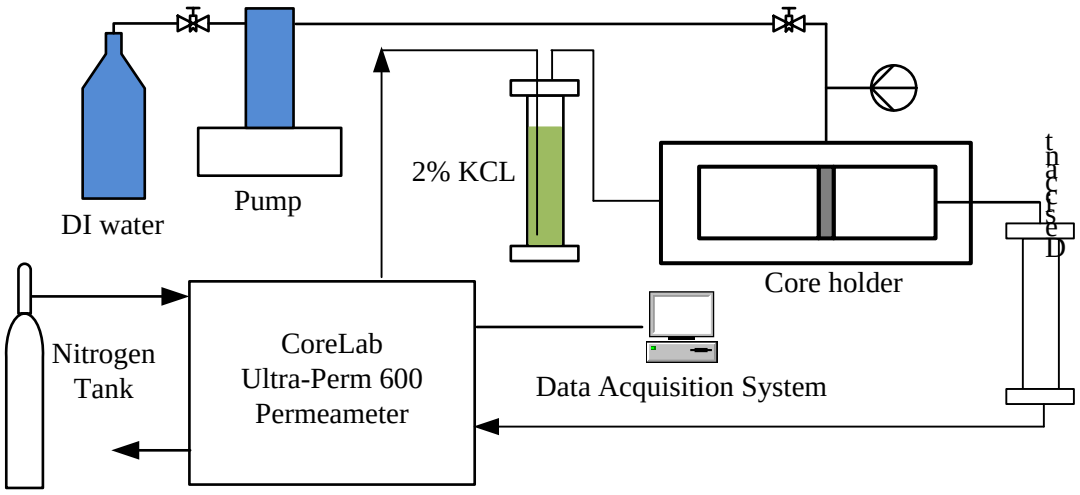

Figure 5.5. Gas phase permeability measurement with humidified N_2

5) Spontaneous imbibition

Spontaneous imbibition experiments were used to evaluate the fluid intake condition after each fracturing fluid component was injected into the rock sample, respectively. A liquid spontaneous imbibition system, built in house, was used to conduct the fluid imbibition, as shown in Figure 5.6. Sample was placed horizontally and gripped by a customized holder. The sample had one side facing air, with the other side contact with liquid, to simulate the frac fluid transport from the fracture face into matrix in gas reservoir. During the experiment, liquid, sample, and holder were sitting in a sealed box. Holder was connected to a digital balanced Adam PW184 (Adam, Danbury, CT), which has a resolution of 0.0001g. The reading in digital balance was acquired through the data acquisition software from the connected PC.

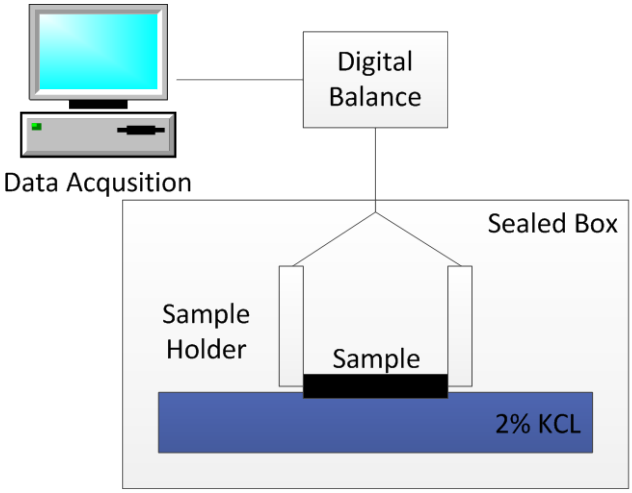

Figure 5.6. Spontaneous cocurrent imbibition system

5.2.3 Evaluation Procedure. In order to simulate the additives enter the formation through fracture face to matrix during stimulation, core flooding system is used to inject brine, friction reducer, breaker, and surfactant, respectively. After sample surface contact angle was measured, Humidified Nitrogen (Nitrogen through brine accumulator) was used to flood the free liquid out, and leave the irreducible in the sample. Experiment was performed at ambient condition.

Due to the extremely small pore throat, the emulsion in friction reducer solution would be able to block or partially block the pore throat, and form filter cake during hydraulic fracturing process. Breaker would work to remove the filter cake and recovery the permeability at this time. In the real tight gas stimulation process downhole, due to the complexity of fracture geometry, the interaction of friction reducer and breaker at fracture face may exist 3 scenarios:

- 1st is balanced condition, where breaker pressure is similar to the formation pressure. The filter cake is soaking in breaker solution, the reaction happened at very small pressure drop (soak);
- 2nd is over-balanced condition, where breaker in fracture has higher pressure than FR filtration in fracture matrix. The solution with breakdown of FR will enter the matrix;

- 3rd is under-balanced condition, where FR will first be flooded out by reservoir gas then encountered with breaker. The solution with breakdown of FR will not enter the matrix.

In order to study the petrophysical impact of these additives on tight sand samples, the whole study was carried out based on the following flow chart: Figure 5.7.

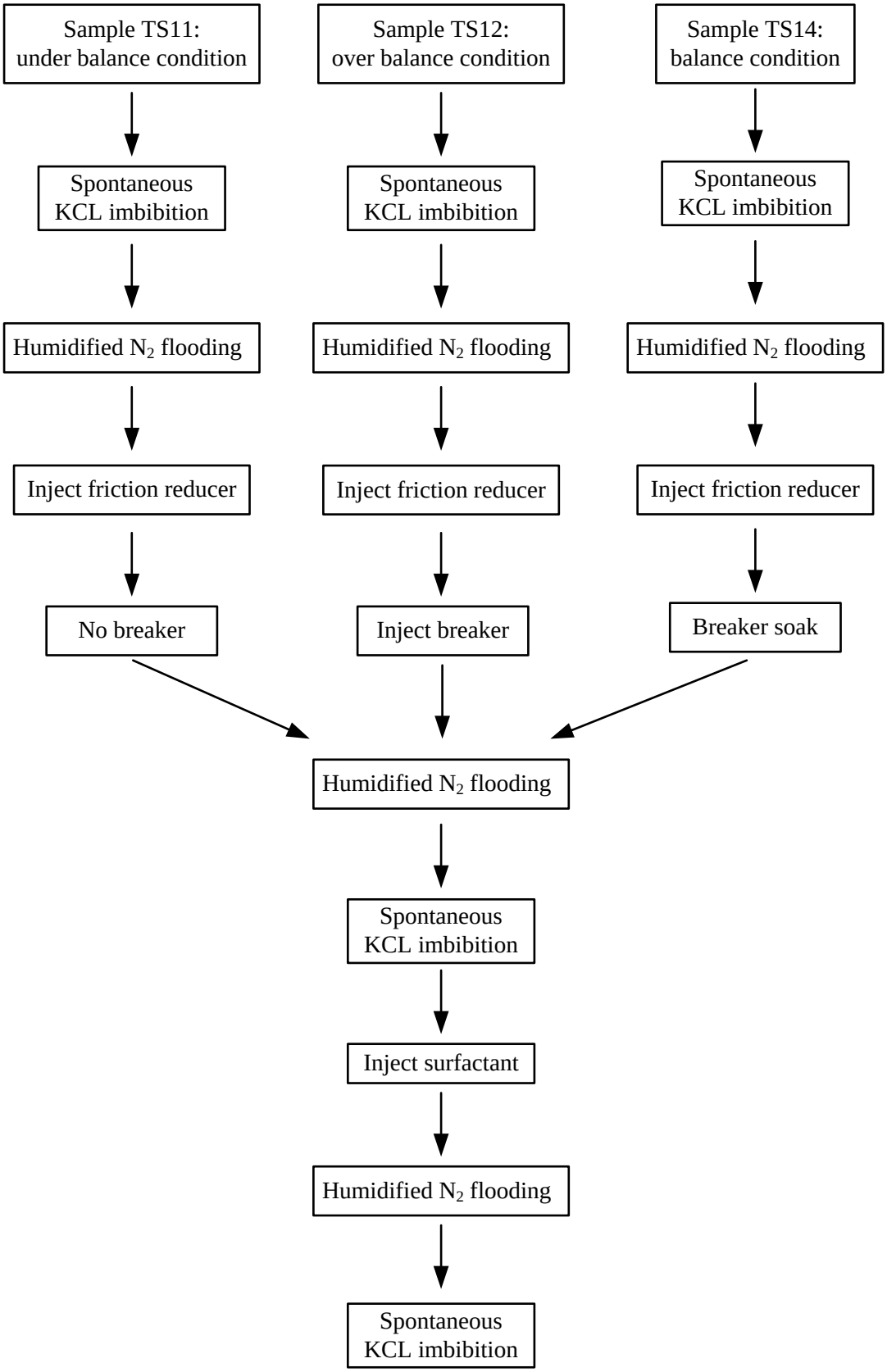

Figure 5.7. Flowchart of experimental procedure

In the spontaneous imbibition test, the dry core was immersed 2 mm deep into the brine solution such that only the lower face of the core touches the liquid face. When the bottom of the rock touched the liquid, the liquid was spontaneously imbibed into the rock. Brine imbibes into the core at a rapid rate because of the strong capillary force. The amount of brine imbibed into the core was reflected and recorded as a function of time using the digital balance. Since the slice is very thin, gravity effect is neglected here. It is a process where only capillary forces drive imbibition.

The fluid injection test is to force the hydraulic fluid additives into the rock matrix to simulate that enter the fracture matrix during hydraulic stimulation. 100 PV of KCl, FR, breaker, and surfactant were flooding into the sample, respectively. Constant flow rate was used initially, once the pressure built up to 300 psi, constant pressure was used. A confining pressure of 400 psi was applied all the time.

In order to study the introduced fluid impact on fracture face, sample was put in a coreholder perpendicular to the fluid flow direction.

In the Humidified N_2 flooding test, Humidified N_2 flood the free liquid out of the rock sample at a pressure gradient of 700 psi/in, the sample weight was measured each hour, until its weight remains 0.5% of current weight for 5 hrs.

5.3. RESULT AND DISCUSSION

5.3.1. Contact Angle Measurement. Sample was flooded or treated in the order of brine, friction reducer, breaker, and surfactant, respectively. In between each treatment, the sample surface contact angle was measured at five pts. The impact of each additive is shown and discussed separately.

1) Brine impact on tight sand wettability

After saturated with 2% KCl, sample TS12 and TS14 were placed in Rame Hart 500 Goniometer sample chamber for contact angle measurement, respectively. The test results indicate both sample surface is water wet, as shown in Figure 5.8 and Figure 5.9. The initial contact angle of five points on sample TS12 is from 23.2° to 27.2°, while sample TS14 is from 17.8° to 31.4°. This could be attributed to the high clay and quartz content in the tight sand.

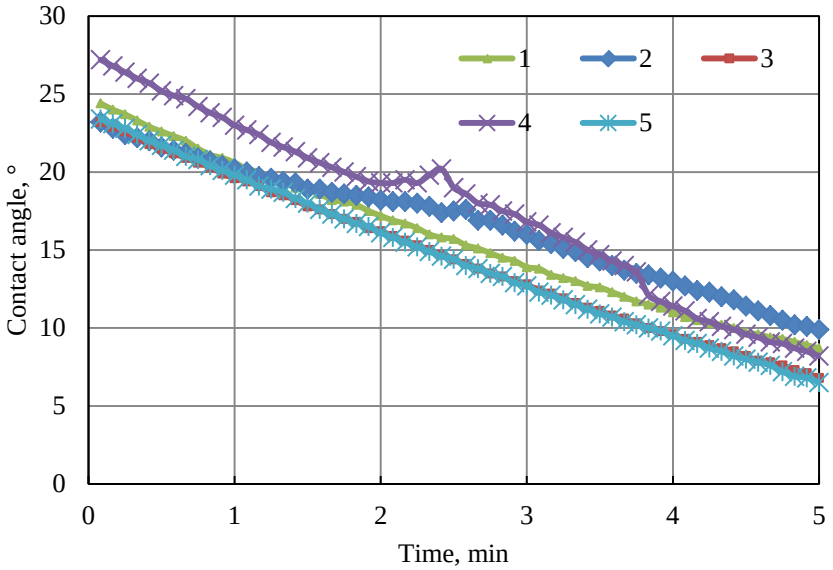

Figure 5.8. Contact angle of TS12

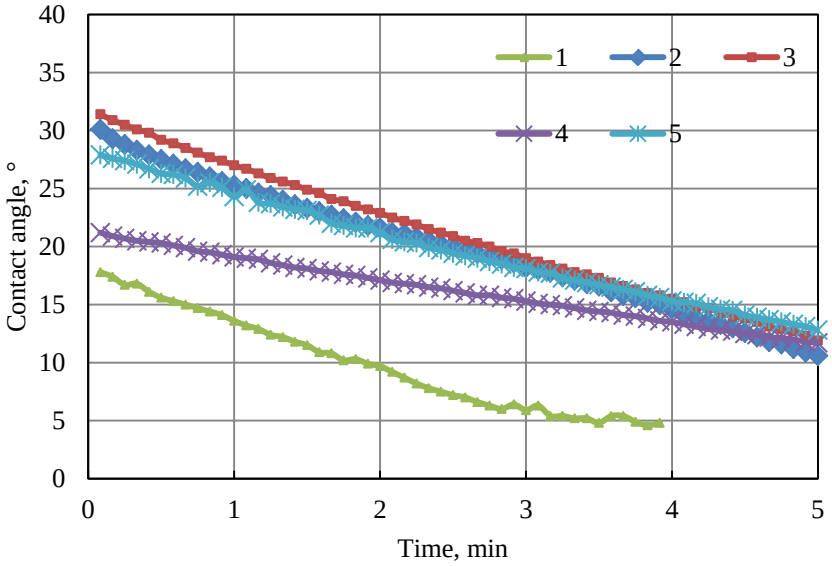

Figure 5.9. Contact angle of TS14

For both samples, the contact angles were all decreasing with time. In the period of 5 min, the contact angle of sample TS12 decreased to 6.5°-9.9°, while sample TS14

decreased to 10.6°-12.8°, and the pt. 1 of sample TS14 reach to 5° at 4 min, and then it became smaller and cannot be detected. The solid-liquid interfacial tension, solid surface tension, liquid surface tension combined with gravity force would account for the decreasing angle with time. Liquid evaporation, even the sample and liquid drop was settled in the sealed chamber, is another factor. In contact angle measurement, the general method to avoid these is to place the sample in oil filled chamber, and then place the water drop. However, it if not applicable here. The tight sand samples are from gas reservoir, oil in chamber may change the rock properties. Moreover, the same sample will be used for further test, oil is not allowed to contact with the sample at this step. Therefore, the contact angle did not employ oil filling to prevent these. But it is supposed the contact angle should still be comparable at the same time frame and the same environment.

2) Friction reducer impact on tight sand wettability

100 PV of FR was then injected into sample TS12 and TS14 for 6 hrs, respectively. Since the pore throat size of tight sand is smaller than the FR emulsion size, a filter cake is formed at the sample face. The contact angle test on filter cake displayed the liquid drop was gone within 2 seconds, which meant it is strongly water wet. This is consistent with the oil-in-water emulsion when this FR is hydrated. After the filter cake was gently removed, the pore throat of sample TS12 and TS14 was supposed still blocked by the emulsion particles in FR, and the contact angle is shown in Figure 5.10 and Figure 5.11.

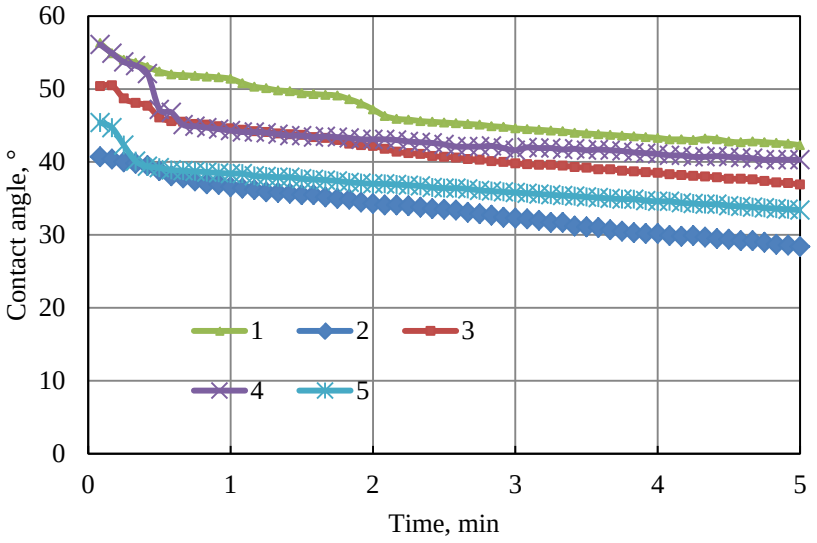

Figure 5.10. (After FR injection) Contact angle of sample TS12

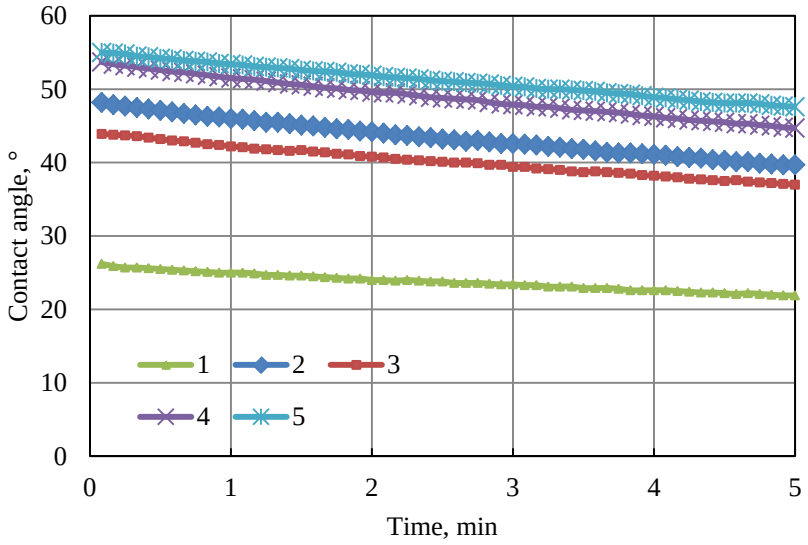

Figure 5.11. (After FR injection) Contact angle of sample TS14

When the FR is presenting and blocking the surface pore throat of tight sand, the tight sand surface became less water wet. 5 test points on sample TS12 exhibit the initial

contact angle is from 40.7°to 56.3°, and sample TS14 is from 43.9° to 55°. While pt. 1 point of sample TS14 changed less compare with other points. It is only 26.2°. This may attribute to the tight gas sandstone heterogeneity.

3) Breaker impact on tight sand wettability

Breaker injection after FR injection: Breaker was injected into sample TS12 from the same side where FR was injected, as shown in Figure 5.12. 100 PV of liquid was injected for 6 hrs. The contact angle test shows the initial contact angle of pt. 2-5 increased to 82.2° to 86.2°, while point No. 1 enlarged to 67.8°, as shown in Figure 5.13.

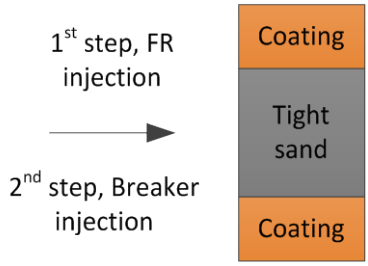

Figure 5.12. The flow direction of FR and breaker injection

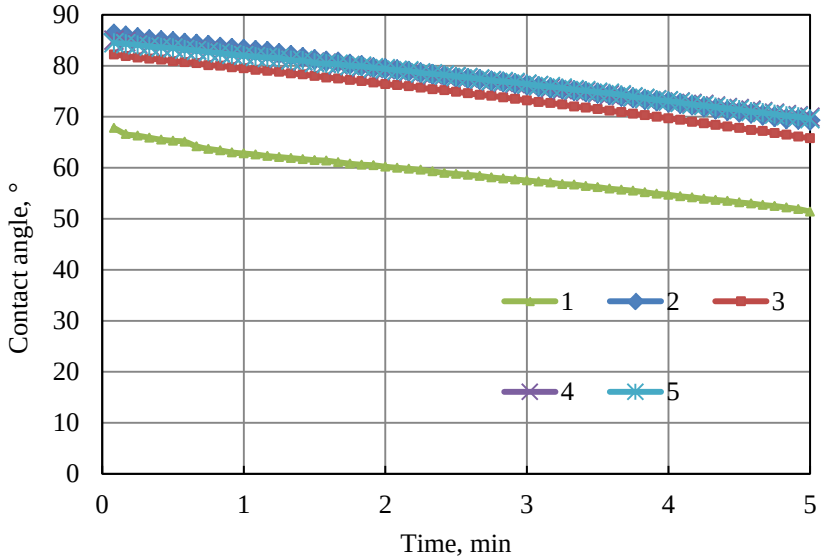

Figure 5.13. (After breaker injection) Contact angle of TS12

Breaker soak after FR injection: Sample TS14 was firstly flooded by FR, and then soaked with breaker, as shown in Figure 5.14. Breaker would be able to react with filter cake first, and then react with the emulsions blocked at the pore throat. Compare with breaker injection in sample TS12, the pressure drop of breaker along the sample would be insignificant. After soaking for 6 hrs, the initial contact angle of sample TS14 increased to 67°-77.8° for pt. 2-5, and it increased to 54.8° for pt. 1, as shown in Figure 5.15.

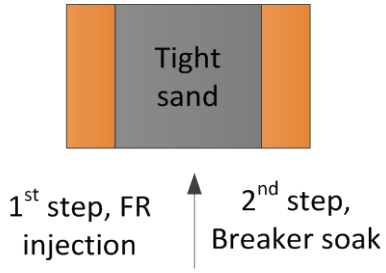

Figure 5.14. The flow direction of FR injection and breaker soaking

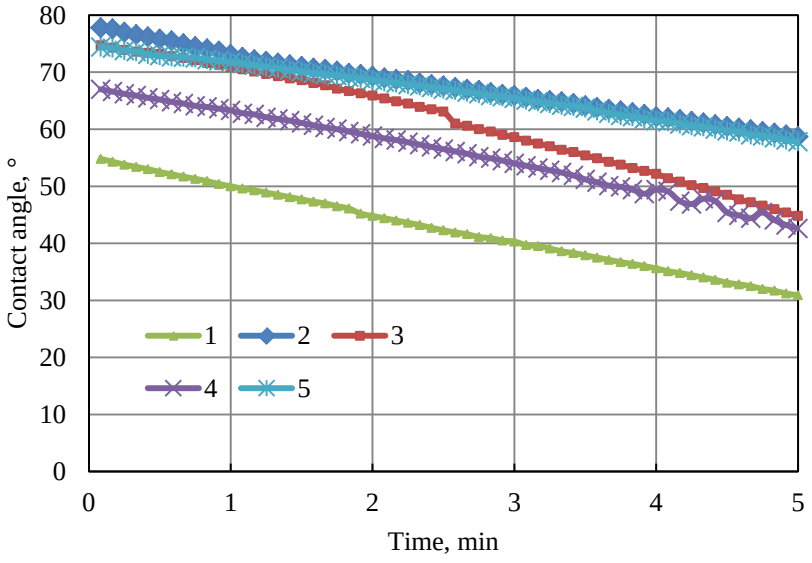

Figure 5.15. (After breaker soaking) Contact angle of TS12

The initial contact angle is smaller when the sample was soaking with the breaker than flooded with breaker. And for the balanced and over-balanced scenarios, the initial contact angle for most the 10 points measured changes to intermediate wet or becomes less water wet.

4) Surfactant impact on tight sand wettability

Surfactant was injected after breaker injection and soaking to TS12 and TS14, respectively. When the extra liquid on the sample surface was gently wiped out, for the 10 measuring point of two samples, the brine drop disappeared or spread within 2 seconds on the wet sample. This is caused by the lower surface tension provided by surfactant. However, when the samples were dried at ambient condition for 2 hrs, the wetting on the sample surface was gone. The contact angle measurement was successfully conducted, as shown in Figure 5.16 and Figure 5.17.

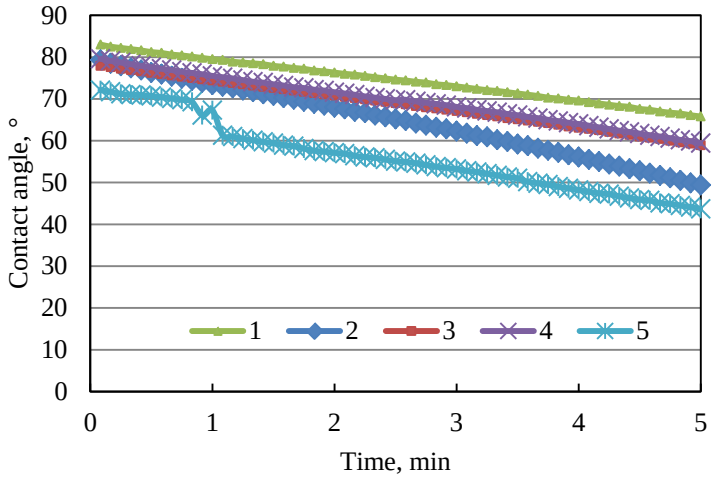

Figure 5.16. Contact angle of TS12 with brine drop

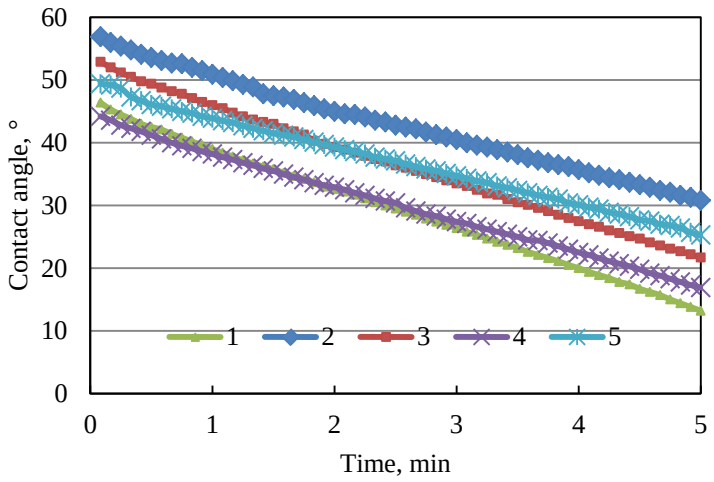

Figure 5.17. Contact angle of TS14 with brine drop

For TS12, where the breaker was injected into the sample, its initial contact angle after flooded with surfactant is 68°-86°. This is virtually the same as when it was flooding with breaker (Figure 5.13). For TS14, where the breaker was soaking the friction reducer at no pressure drop, its initial contact angle after flooded with surfactant is 46°-57°. And this is almost the same at when it was flooding with friction reducer only (Figure 3.11).

These two figures indicate this surfactant did not change the surface wettability on this tight sand. The contact angle will remain the same after the sample treated with FR or FR and breaker, respectively.

5.3.2. Liquid Saturation by Gas Flooding

1) Humidified N_2 flooding after FR and breaker injection

After the sample was treated with additives, humidified Nitrogen was used to displace the liquid in the sample. The free liquid was flooded out, and left the remaining liquid in the sample. Sample was weighted at certain time intervals. Then its liquid saturation is defined as weight difference of the wet sample and dry sample over the dry sample filled with brine, as shown below:

$$S_l = \frac{w_L - w_{dry}}{PV} \times 100\% \quad (19)$$

where S_L=liquid saturation, %; w_L=sample weight at certain time, g; w_{dry}=sample dry weight, g; PV= sample pore volume, cm^3;

Sample TS12 was flooded by brine, friction reducer, breaker and surfactant, respectively, in between of each flooding, sample was flooded by humidified N_2, and sample weight was measured each hour, until remaining liquid in the sample was attained. Liquid saturation vs. time was shown in Figure 5.18.

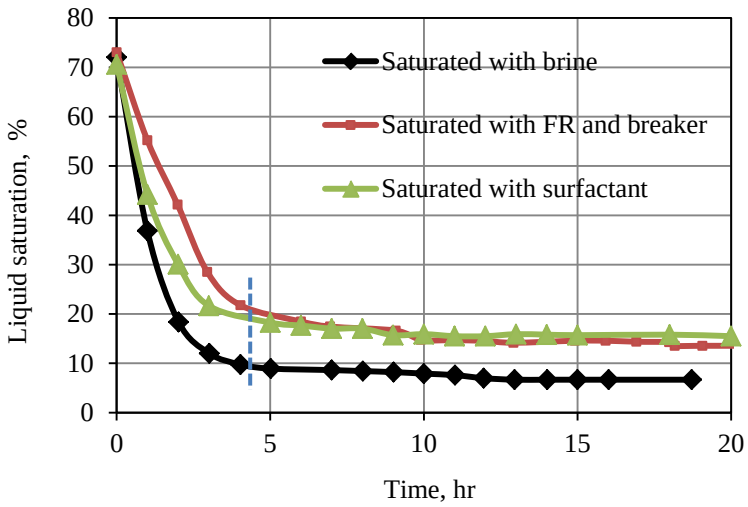

Figure 5.18. Gas flooding in liquid saturated tight sand (breaker injected)

As shown in Figure 5.18, the liquid saturation has a sharp decrease from 72%to 10-20% in the first 4 hrs, and then it changes much slower, and decreased less than 5% in 15 hrs.

After FR and breaker injected, the humidified N_2 was flowing slower than that with only brine saturated. After FR was injected, the emulsion particle larger than pore throat size would block the pore throat and form a filter cake at the sample surface. The

injected breaker after this would release the block by degrading the polymer and breaking the emulsion. But the smaller sized emulsion would still fill the small pore throat. Since the smaller pore throat requires larger pressure gradient to flow through, this would make the jam at small pore throat and hard to wash out. For the humidified N_2 flooding of 20 hrs, the liquid saturation after FR and breaker saturated is 8% higher than that saturated with brine.

With the adding of surfactant, the liquid saturation decrease slowest in the early time. However, over 20 hrs flooding, it shows 2% higher of liquid saturation than FR and breaker saturated condition. This indicates once the friction reducer, breaker, and surfactant enter tight sand matrix, certain contamination, such as water block or chemical residual will exist, and it is hard to remove by post frac gas production. The surfactant will not help to recover more fluid in porous media blocked with emulsion particles.

2) Humidified N_2 flooding after FR injection and breaker soaking

Sample TS14 was flooded by brine, friction reducer first, then soaked with breaker, then inject surfactant, in between each flooding, sample was flooded by humidified N_2. Sample weight was measured each hour, until remaining liquid in the sample was attained. Liquid saturation vs. time was shown in Figure 5.19.

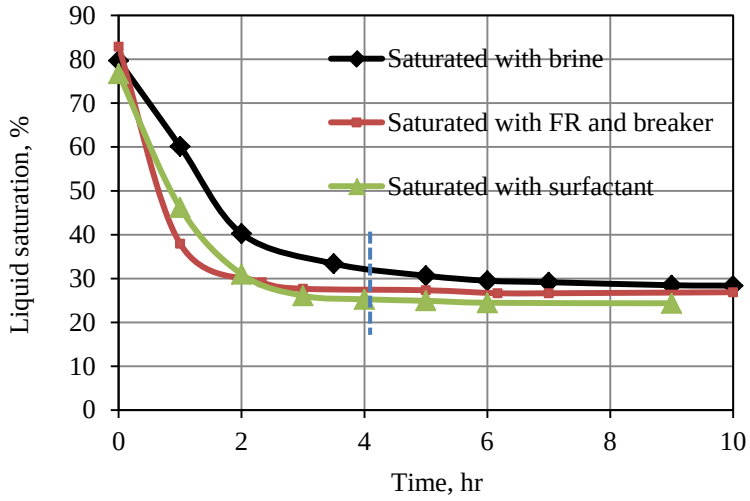

Figure 5.19. Gas flooding in liquid saturated tight sand (breaker soaked)

As shown in Figure 5.19, the liquid saturation also decreases sharply initially and then slowed down. For 10 hrs flooding, the liquid saturation in sample which initially saturated with FR and breaker is very close to when it was saturated with brine. The injected FR blocked the pore throat near injection face in the tight sand. The soaking of breaker at no pressure drop would degrade the polymer long chain and release the jam in pore throat. The degraded FR will have very limited entrance to deep pore throat due to negligible pressure drop. Therefore, it is assumed only FR was in sample, with relatively large emulsion particle, it could be flushed out as easy as sample saturated with brine only.

The surfactant treatment makes the liquid saturation decrease 2% compare with when the sample was treated with FR and breaker. This indicates when the FR particles were flushed out. Surfactant could work to reduce the remaining water saturation. And these liquid saturations with FR, breaker, and surfactant treatment all lower than that saturated with brine.

5.3.3. Gas Phase Permeability

1) Initial brine saturation impact on gas phase permeability

After absolute permeability was measured, samples were vacuumed for 24 hrs, and then saturated with 2% KCl. After humidified Nitrogen flooded each one until initial water saturation achieved, permeability measurement was conducted with same humidified Nitrogen under distributed 4 to 7 pressures. The linear regression of these data gave the gas phase permeability, as shown in Figure 5.20.

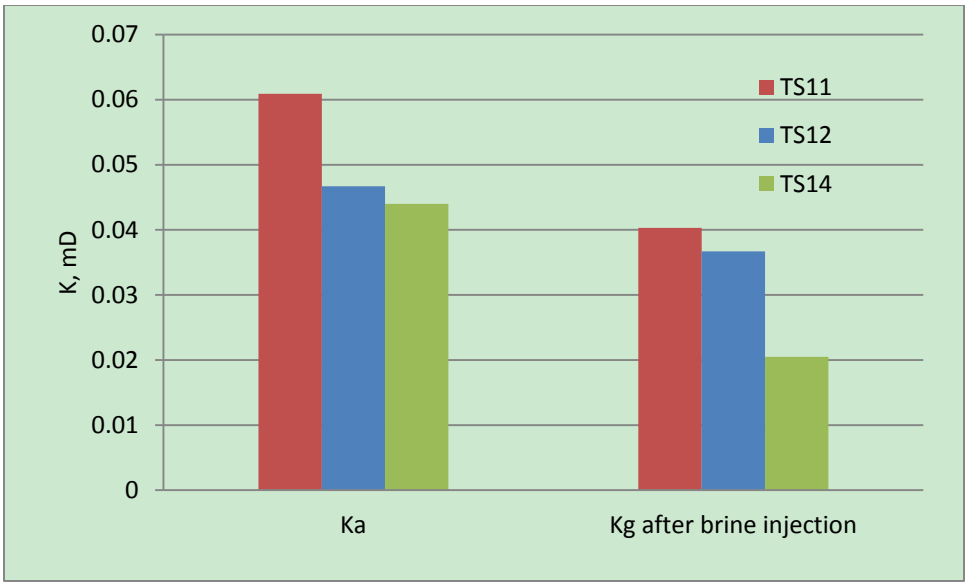

Figure 5.20. Gas phase permeability with initial water saturation

There is some difference in samples' absolute permeability. However, this difference is even more obvious in the gas phase permeability. Divided by absolute permeability, gas phase permeability change to relative gas permeability:

$$K_{rg} = \frac{K_g}{K_a} \tag{20}$$

where K_a is absolute permeability; K_g is gas phase permeability, K_{rg} is relative gas permeability.

As shown in Table 5.1, the relative gas permeability of three samples has relatively large range: 0.47-0.66. Sample initial water saturation has a very intimate relation with the relative gas permeability, ex. sample TS 14 has the highest initial water saturation and lowest relative gas permeability.

Table 5.1. Sample permeability after brine saturated

Sample No.	K_a	K_g	K_{rg}	S_{wi}
	mD	mD		%
TS11	0.061	0.040	0.66	6.3
TS12	0.047	0.037	0.79	9.1
TS14	0.044	0.021	0.47	24.1

2) FR and breaker impact on gas phase permeability

Sample TS11 was flooded with FR only, as under-balanced condition, then its gas phase permeability was measured. Sample TS12 was flooded with FR and breaker, respectively, as over-balanced condition, and then its gas phase permeability was tested. Gas phase permeability of both samples was shown in Figure 5.21. In under-balanced condition, the gas phase permeability of sample TS12 did not decrease, where breaker did not enter the matrix. In over-balanced condition breaker entered the fracture matrix and degraded the FR emulsion, caused the gas phase permeability decreased 12%, as shown in Table 5.2.

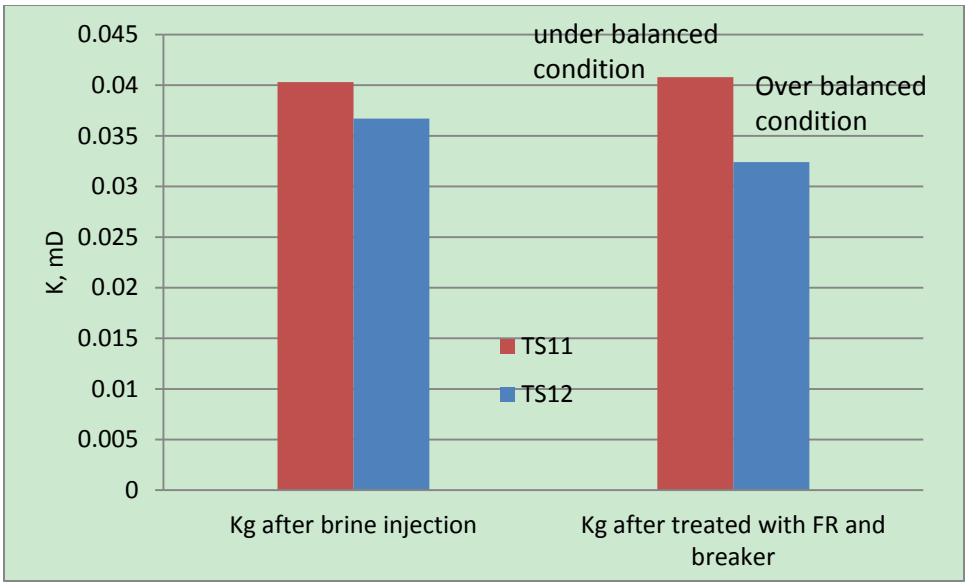

Figure 5.21. Gas phase permeability reduction due to the introduction of FR and breaker

Table 5.2. Gas phase relative permeability

Sample No.	$K_{g\text{-}swi}$	$K_{g\text{-}FR\ and\ breaker}$	Permeability regain
	mD		%
TS11	0.040	0.0408	101.2
TS12	0.037	0.0324	88.3

3) Surfactant impact on gas phase permeability

After sample TS 11 was treated with brine and FR, surfactant was injected to simulate the process happened in the reservoir during hydraulic stimulation. Gas phase permeability tested after surfactant injection was found to increase 20%, compare with sample treated with brine and FR, as shown in Figure 5.22. The injection of surfactant had the ability to increase the gas transportation capacity, which is reflected by the gas phase permeability.

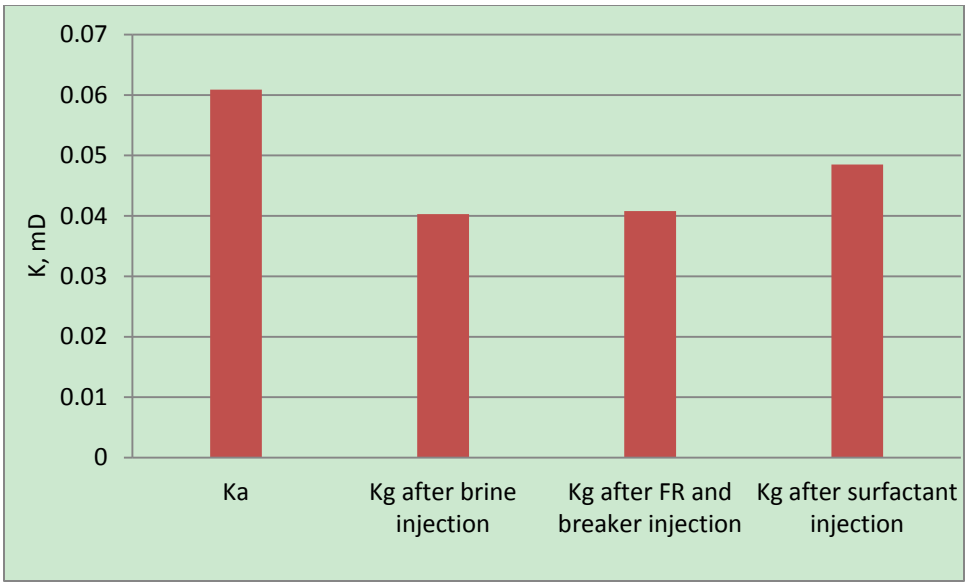

Figure 5.22. Gas phase permeability after each additive treated

5.3.4. Spontaneous KCl Imbibition. Brine, friction reducer, breaker, and surfactant were injected into tight gas sandstone samples, respectively, to simulate the hydraulic fracturing fluid entering the fracture matrix during stimulation. In order to study the wettability impact of each additive, spontaneous cocurrent imbibition were conducted with 2% KCl before and after each additive applied. The imbibition test can be illustrated with weight gain on sample with time.

1) Spontaneous imbibition at under-balanced condition

Spontaneous cocurrent imbibition in tight sand after brine, FR and surfactant (GG) treatment is shown in Figure 5.23. For each imbibition curve, the weight gain could be divided into two sections separated by the blue dotted line. On the left of the line (early time), the imbibition is very fast. However, on the right of the line (later time), the imbibition is very slow or becomes constant. The left of the blue line is related to the time it takes for the imbibition front to fill the large pores. The right of the blue line was when the imbibition was occurring in small pores and matrix. This phenomenon is also reported by other researchers (Roychaudhuri, Tsotsis et al. 2011).

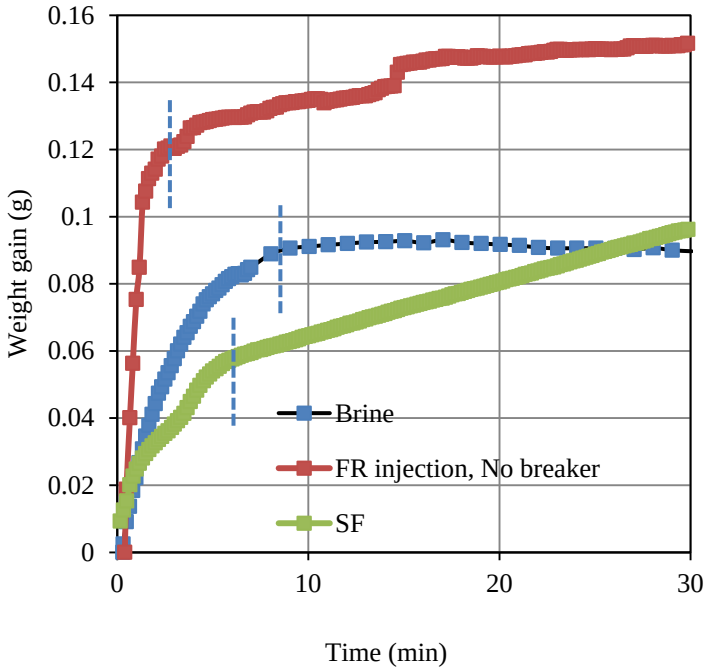

Figure 5.23. Brine imbibition with only FR injection

After FR injection, the imbibition rate at early time is faster than before. This could be explained by the capillary pressure as shown below:

$$P_c = \frac{2\sigma\cos\theta}{r} \tag{21}$$

where P_c is the capillary pressure, σ is the surface tension, θ is the contact angle, r is the diameter of capillary.

As reported in Section 2, this FR has emulsion particle diameter ranging from 0.0723 μm to 1.635 μm prepared with stir plate where it is used here. During FR injection, once this FR enters the large pores, they would be partially blocked. The blocked large pores would make the equivalent radius of tight sand decrease sharply. Since capillary pressure is inversely proportional to the size of pore throats in a water wet tight sand, therefore a smaller pore radius would result a higher capillary pressure. And since the Cos (θ) after FR treated did not change too much, as shown in Table 5.3. The surface

tension may have some impact on the capillary pressure, but it will not as big as the capillary radius. Therefore, the sharp increase in the early time would majorly attribute to the high capillary pressure resulted from pore radius decrease.

Table 5.3. The tight sand contact angle after additives treatment

Additive	Contact angle: θ (°)	Cos (θ)
Brine	25	0.91
FR	50	0.64
Breaker injection	85	0.09
Breaker soak	75	0.26
Surfactant	50-80	0.64-0.17

The surfactant injected displayed the capacity to change the rock wettability by smaller imbibition rate and less brine amount, and this is more obvious in Figure 5.24 and Figure 5.25. This could explained by the lower surface tension provided by surfactant. With the very close contact angle and Cos (θ), the surface tension is the major difference in capillary pressure after sample treated with breaker and surfactant. And surfactant could provide a much lower surface tension than FR and breaker. Therefore, a lower capillary pressure caused a lower liquid intake.

2) Spontaneous imbibition at balanced condition

The balanced condition is where FR was injected into the core sample, and then soaked in breaker solution to degrade the emulsion in FR filter cake at the fracture face and near fracture matrix. As shown in Figure 5.24, at this condition, the difference of early time and later time imbibition slopes still exists.

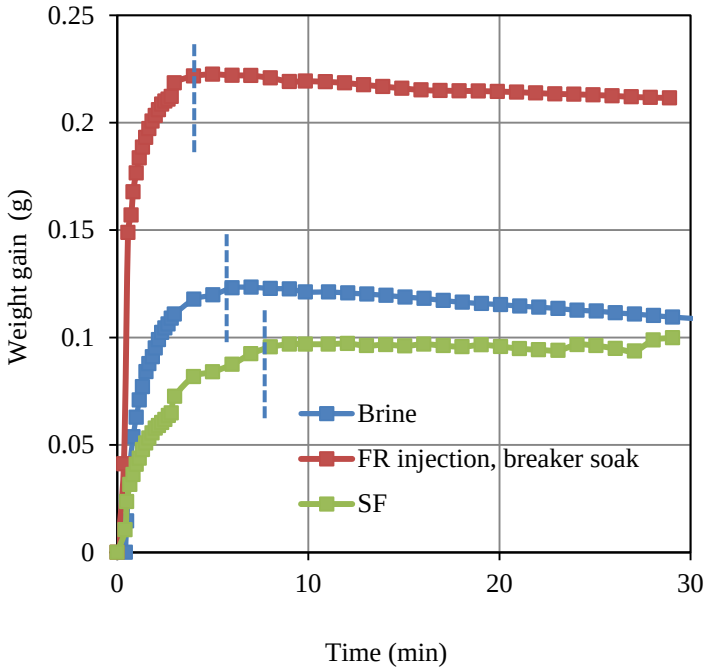

Figure 5.24. Brine imbibition with FR injection, breaker soak

FR was injected under a pressure drop, which is similar to the field application. The small emulsion particle would enter the tight sand matrix and jammed at the pore throat. The soaking of breaker under no pressure drop will have very limited entrance into deep pore throat and would leave the FR particle there. Therefore, the imbibition curves of FR and brine are very much the same to the under-balanced condition, where breaker was not used.

After surfactant injection, the fluid imbibition rate and amount is the smallest among the three, which indicate an alteration of the rock matrix wettability.

3) Spontaneous imbibition at over-balanced condition

At the over-balanced condition, the FR and breaker would inject into tight sand, respectively, and then inject surfactant. The imbibition curves are shown in Figure 5.25.

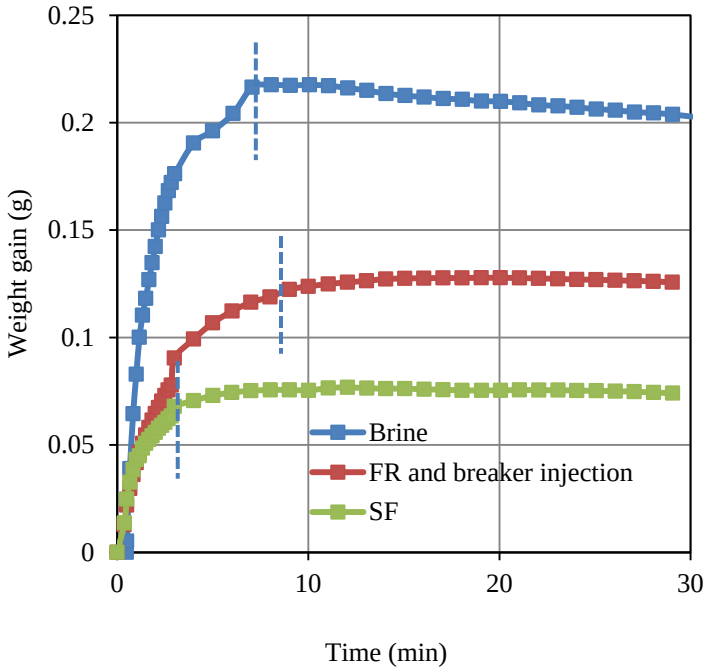

Figure 5.25. Brine imbibition with both FR and breaker injection, respectively

After FR injection, the injected breaker would be able to degrade the emulsion particle in FR in pore networks, and generated a lower imbibition rate and amount, compared with imbibition after brine treatment. For this phenomenon, the degradation of polymer in FR is one of the reasons. The break of oil in water emulsion is another reason. After emulsion break, oil phase exists in pore network, which makes the capillary pressure smaller by providing a contact angle of 85°, as shown in Table 5.3.

The imbibition behavior after surfactant injection still displayed the capacity to change the rock wettability by smaller imbibition rate and less brine amount.

5.4. CONCLUSIONS

1) Due to the high content of quartz and clay, the tight sand and shale surface displays water wet;
2) The introduction of friction reducer makes the tight sand become less water wet;
3) The injection and soaking of breaker all turn the tight sand surface to be intermediate wet, and the contact angle is little bit higher achieved by breaker injection;

4) This surfactant did not change the surface wettability on this tight sand. The contact angle will remain the same after the sample treated with FR or FR and breaker, respectively;
5) Fast imbibition at early time and slow imbibition at later time in tight sand exist for all conditions;
6) At under-balanced and balanced condition, the pore radius decrease in tight sand resulted in higher imbibition rate and amount than brine treated only.
7) During over-balanced condition, where FR, breaker were injected into tight sand, respectively, the imbibition rate and amount are opposite. However, in the latter condition, the degraded FR polymer would possibility goes deep into the matrix, and cause near fracture damage. An equilibrate policy needs to be considered between fluid imbibition and near fracture damage during hydraulic fracturing design;
8) Surfactant illustrated the lowest fluid imbibition capacity for all conditions, which indicate kind of wettability alteration in deep matrix;
9) At under-balanced condition, breaker did not enter the sample matrix, the gas phase permeability is not impacted;
10) At over-balanced condition, FR and breaker interacted with each other and enter the sample matrix, the gas phase permeability decreased a little;
11) For the humidified N_2 flooding, if FR and breaker enter the formation matrix first, the liquid saturation by gas flooding would be 8% higher than the initial water saturation. The adding of surfactant could only decrease the liquid saturation by 2%;
12) Once the friction reducer, breaker, and surfactant enter tight sand matrix, certain contamination, such as water block or chemical residual will exist, and it is hard to remove by gas flooding;
13) If friction reducer degraded with breaker soaking at no pressure drop, the degraded polymer and broken emulsion particle would be released from the blocked pore throat, the remaining liquid saturation would not be impacted. The humidified N_2 flooding displayed similar liquid saturation with the initial water saturation.

6. FORMATION DAMAGE OF FRICTION REDUCER AND BREAKER ON TIGHT SAND

6.1. INTRODUCTION

Hydraulic fracturing in tight gas reservoir will increase the production rate. Slickwater fracturing has been proved to be performed very well in this kind of reservoir. Slickwater fracturing fluid is not polymer or gel based. It contains water as main composition and many chemical additives by very small amount. Water could be up to 90% of the liquid, and additives are usually less than 1%, proppant occupies the other share. This fluid is featured to be low viscosity, and little formation damage. It can generate small spread-out micro-fractures in unconventional reservoir rather than the pair of large dominant fractures in conventional reservoir.

During fracture creation stage, friction reducer, brine, and breaker are the major composition. With the Bossier shale fracture model, after treated with friction reducer and breaker, it shows the permeability regain is 56 to 100% (Sun, Stevens et al. 2010). However, the most commonly used friction reducer is in emulsion condition, it has emulsion particle size comparable with the pore size of the unconventional reservoir, but the formation damage condition in the near fracture matrix is not clear.

The present study uses the coreflooding system to simulate the fluid enters the fracture matrix during hydraulic fracturing process. Three different conditions during FR and breaker interaction are investigated in detail. FR concentration effect, sample length effect, breaker concentration effect are all studied carefully. Permeability regain, the permeability after treated with additives above permeability before, is calculated based on the permeability data. After treatment of FR and/or breaker, gas transportation in sample is also examined.

6.2. EXPERIMENTAL

6.2.1. Materials. Rock sample: tight sand TS20 to TS37 were used in this part. Their parameters are shown in Table 6.1. The sample length around 5mm is defined as short samples, 10mm as medium samples, 15mm as long samples.

Fluid: 3 concentrations FRW-20: 0.025, 0.05, 0.1 vol%, 3 concentrations of ammonium persulfate breaker: 0.012, 0.024, 0.048 wt% were employed as treating fluid.

Table 6.1. Tight gas sandstone basic parameter

Sample length	Sample No.	Length	FR concentration	Breaker concentration
		mm	vol%	wt%
Short	TS11	4.02	0.05	No
	TS28	4.62	0.025	No
	TS20	5.39	0.025	No
	TS22	5.42	0.05	No
	TS21	4.80	0.1	No
	TS29	4.61	0.1	0.024, soak
	TS30	4.97	0.1	0.024
	TS26	5.00	0.1	0.012
	TS27	4.77	0.1	0.048
Medium	TS33	10.27	0.1	No
	TS35	9.34	0.1	0.024
Long	TS25	13.08	0.1	0.024
	TS34	13.94	0.1	No

6.2.2. Equipment. The liquid coreflooding system, humidified N_2 coreflooding system, Gas phase permeability measurement system were applied in this study, as shown in Figure 6.1 to Figure 6.3.

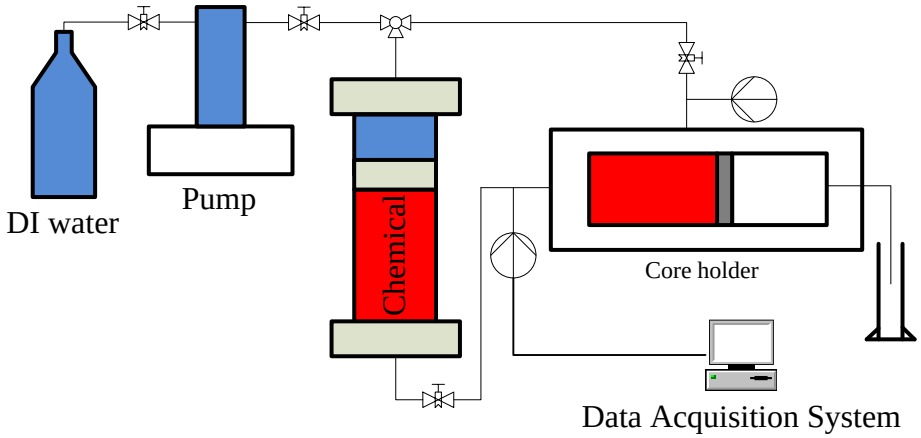

Figure 6.1. Liquid coreflooding system

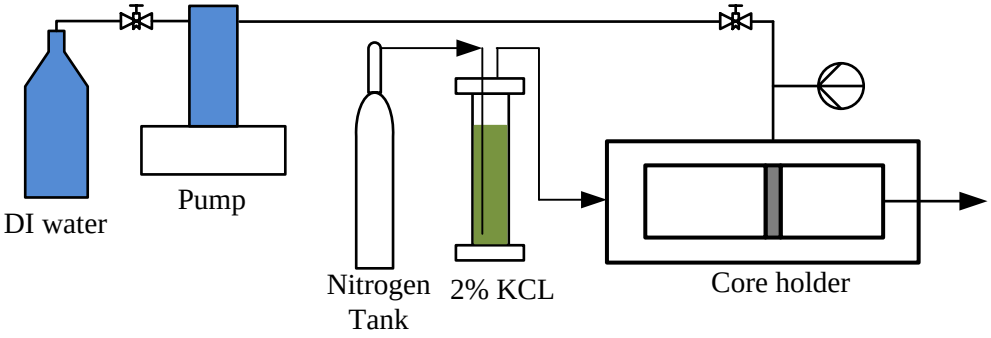

Figure 6.2. Humidified N_2 coreflooding system

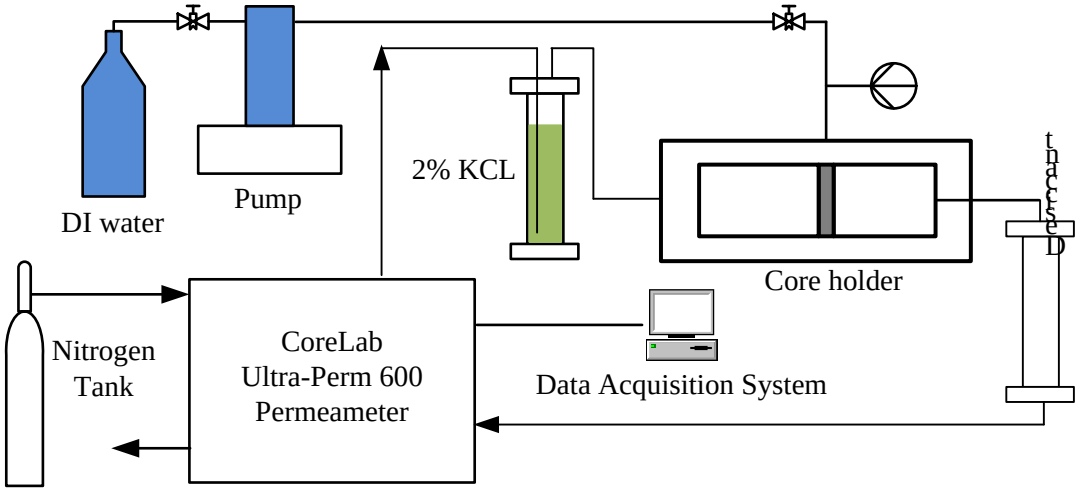

Figure 6.3. Gas phase permeability measurement with humidified Nitrogen

The liquid coreflooding system was used to simulate how the additives enter the formation matrix during hydraulic fracturing. Humidified N_2 coreflooding system was to push out the saturated liquid in the sample. And gas phase permeability measurement system was to measure the gas phase permeability in tight sand sample before and after they were treated with FR and breaker, with humidified Nitrogen.

6.2.3. Procedure. Three scenarios of breaker treatment were studied after FR treatment. For each scenario, after sample dried by oven, gas phase permeability was measured first with humidified Nitrogen, then flooded with 50 PV of FR solution. For the under-balanced condition, no breaker is used. For the balanced condition, breaker was used to soak the sample at no pressure drop. And for the over-balanced condition, breaker was flooded into the sample after FR treatment. Then all samples were dried with humidified Nitrogen under the same flooding strength (pressure gradient and time per unit length). Then gas phase permeability was measured on all samples with humidified Nitrogen, as shown in Figure 6.4.

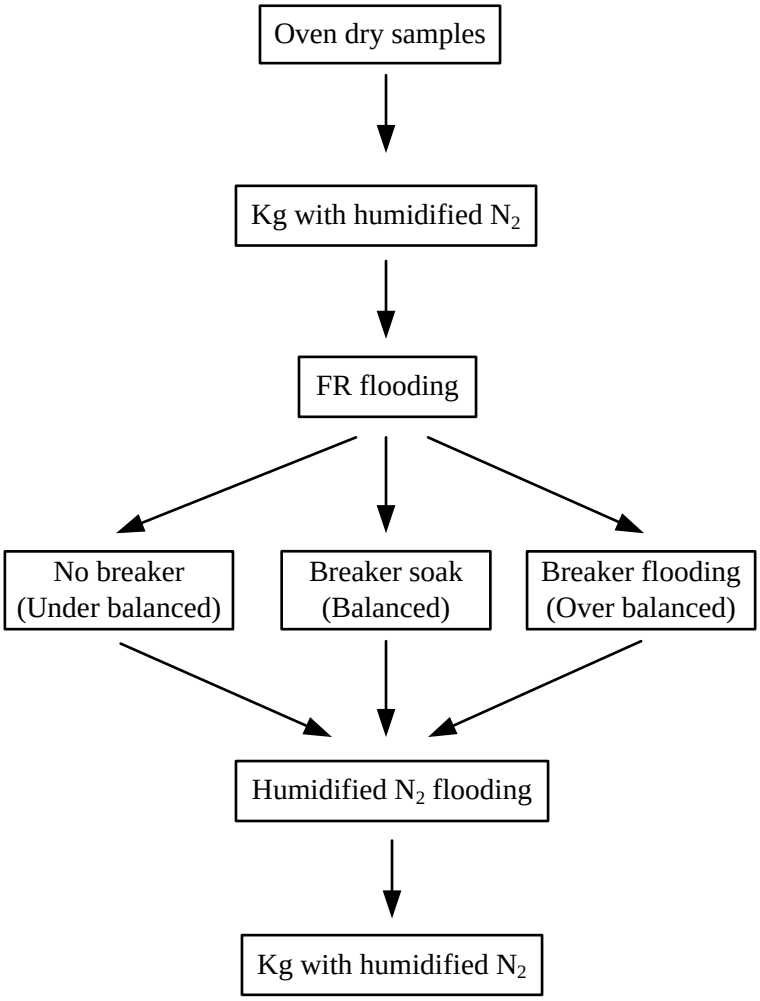

Figure 6.4. Experiment flow chart

The flooding is directional sensitive. To simulate the process in the reservoir during and after hydraulic fracturing, for each sample, the liquid flooding is always conducted at one face: the fracture side. The humidified Nitrogen flooding is carried out at the other face: the deep matrix side. When liquid flooding is applied, 50 PV of additive solution is injected each time. The humidified Nitrogen was flooding the sample saturated liquid at a pressure drop of 20 psi/mm and a time of 1.2 hr/mm, based on previous experimental experience. Therefore, samples were dried by humidified Nitrogen under the same flooding strength, the gas transportation after additive treatment is comparable.

6.3. RESULT AND DISCUSSION

All the gas phase permeability was measured with humidified Nitrogen before and after the sample was treated with FR and/or breaker, respectively. The permeability data is shown are Appendix C.

6.3.1. Different Breaker Treatment after FR Flooding. Three different breaker treatment methods after samples flooded by FR are studied in detail. Three short samples were flooded with 0.1 vol% FR first. Then one sample was soaking in 0.024 wt% of breaker solution at 150 °F for 1hr, with one side contacted with liquid, one sample was flooded by 0.024 wt% breaker and oven heated at 150 °F for 1hr, and one sample was not treated with breaker. Then after humidified Nitrogen flooding, their gas phase permeability regain was measured and calculated, as shown in Figure 6.5.

$$K_{re} = \frac{K_{ga}}{K_g} \times 100\% \tag{22}$$

where K_{re} is the permeability regain after sample treated with additives; K_g is the initial gas phase permeability, K_{ga} is the gas phase permeability after sample treated with additives;

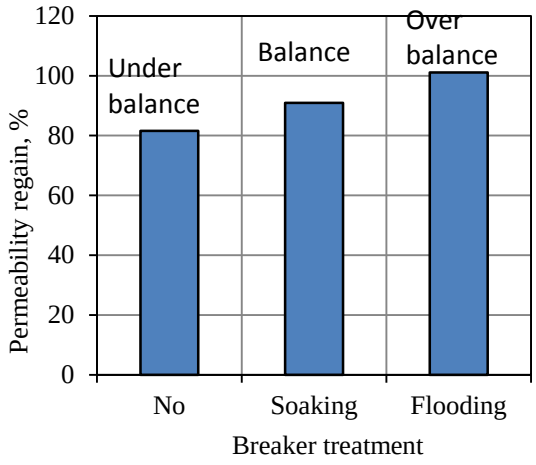

Figure 6.5. Permeability regain after three different breaker treatments

From Figure 6.5, the ammonium persulfate breaker does have a positive function with this FR. The permeability regain is 81.6% at under-balanced condition, where breaker will not enter the matrix. As analyzed in Section 3, this FR is prepared with stir plate and blender, to simulate the high shear rate condition in the field. Its emulsion particle is from 0.02343 to 0.0663 μm, ten times smaller than that prepared with stir plate only. It lies in the lower range of pore size of this tight sand. This FR prepared with blender has the capacity to enter the small pores and block the gas flowing path. Without the breaker introduction, permeability did not regain well.

The permeability regain is 101.1% at over-balanced condition, where breaker will interact with FR with pressure drop. Breaker was injected into the sample after it was flooded by FR, the injected breaker would be able to enter the sample in deep matrix, degrade the polymer and recover the damage. Therefore, the permeability is totally recovered after breaker injection.

The permeability regain at balanced condition is 91.0%, where breaker will interact with FR at no pressure drop. Because FR was injected into the sample under pressure, and the breaker was soaking on the side where FR was injected at no pressure drop, the interaction of breaker with FR in sample deep matrix is very hard. Therefore, the permeability regain lies in the middle of the three.

6.3.2. FR Concentration Effect on Permeability Regain without Breaker. Three samples were flooded with different concentration of FR, respectively. Their permeability regain is shown in Figure 6.6.

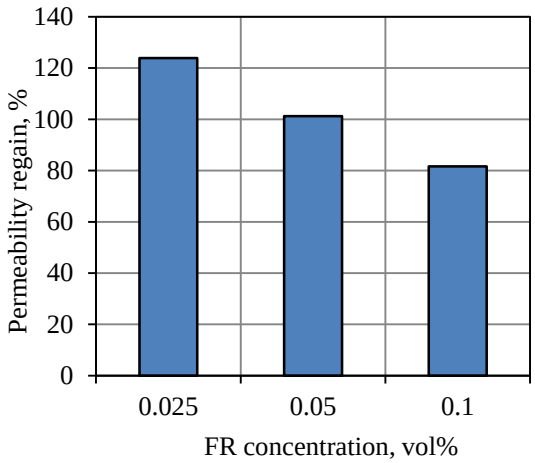

Figure 6.6. Permeability regain after treated with FR only

The concentration has a large impact on the permeability regain on the short samples, without the introduction of breaker. Lower concentration FR achieved a higher permeability regain. The 0.05 vol% FR can achieve a 101.2% permeability regain. However, 0.1 vol% FR shows some damage, it K_{re} is 81.6%. The 0.025 vol% FR indicates a permeability increasing after sample treated with FR, its K_{re} is 123.9%. With the sample PV of FR injected into the short samples, the lower concentration of FR solution contains less emulsion particle than the high concentration FR solution. This means the low concentration FR has smaller formation damage to the rock than high concentration FR. And based on previous contact angle measurement, this FR changed the surface to be more like intermediate wet. This intermediate wet surface would contribute to the gas transportation and enable a high permeability regain.

6.3.3. Length Effect of FR Injection on Permeability Regain without Breaker. With the short, medium, and long samples, 0.1 vol% FR was injected into each one, respectively. After humidified nitrogen flooding, gas phase permeability was measured and permeability regain was drawn as in Figure 6.7.

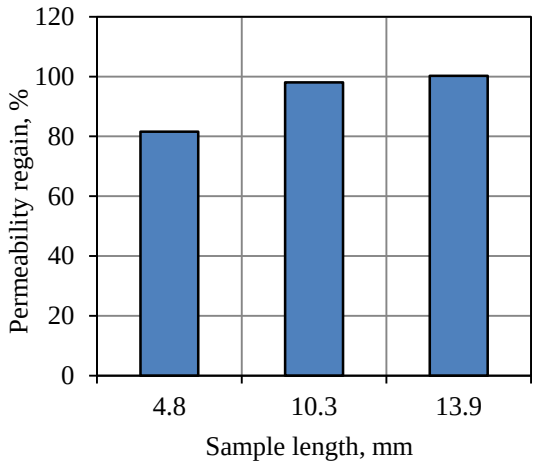

Figure 6.7. Length effect of FR injection on permeability regain

Formation damage is mostly happened in the near fracture matrix. The short sample shows 81.6% permeability regain, however, it is 98.0% and 100.3% for the medium and long core. For this emulsion FR solution, with the comparable pore size, it formed a filter cake on the inlet face. Then the pressure was built up very fast, and filtration process happened. With the coreflooding continues, the filtrated liquid would push the emulsion particle from inlet to outlet (from near fracture to deep matrix). Then a concentration gradient would generate, it is high at the inlet and low at the outlet. As observed in 6.3.2, the lower concentration of FR will result in a higher permeability regain due to the wettability alteration. If the sample is simplified to be two parts, one part has a high FR concentration and a low K_{re}, one part has a low FR concentration and a high K_{re}, as illustrated in Figure 6.8. Therefore, the recovery of permeability in medium and long core is reasonable.

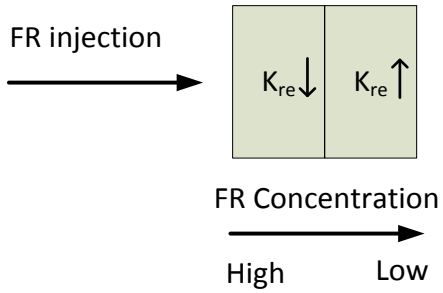

Figure 6.8. Simplified model for permeability regain with FR in long core

6.3.4. Breaker Concentration Effect on Permeability Regain. According to a previous study (Sun, Stevens et al. 2010), for 1 gpt FR, 2 pptg breaker is usually used, where 1 gpt equals 0.1 vol% FR, 2 pptg equals 0.024 wt% breaker. A lower and higher concentration of breaker is applied in this part. For three short samples, 0.1 vol% (1gpt) FR was injected into each one, then the samples were flooded by 0.012 (1pptg), 0.024 (2pptg) and 0.048 (4pptg) wt% of breaker, respectively. After oven heated for 1hr at 150 °F, each sample was flooded by humidified Nitrogen, and then gas phase permeability was measured, as shown in Figure 6.9.

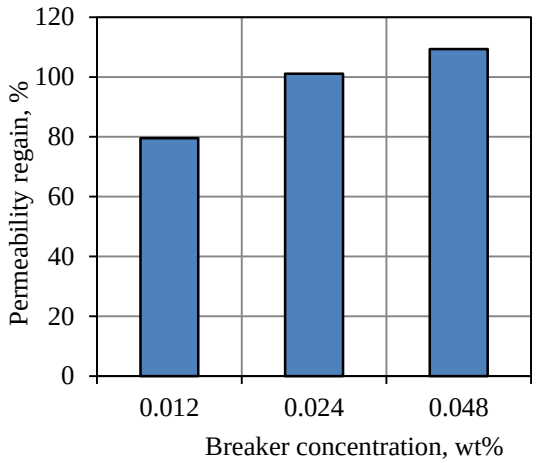

Figure 6.9. Breaker concentration effect on permeability regain

The permeability regain increases with the breaker concentration. For 0.1 vol% FR, 0.024 wt% breaker will recover 101.1% of permeability. The lower concentration breaker: 0.012 wt% is not enough to release the formation damage. Its K_{re} is 79.5%. And the higher concentration breaker will increase the gas transport capability with K_{re} of 109.3%. With the same PV of FR and breaker injected for each sample, low concentration breaker does not fully degrade the FR polymer, but high concentration breaker does. However, for this tight sand sample, 1 gpt FR with 2 pptg breaker is good enough, same as previous publication (Sun, Stevens et al. 2010).

6.3.5. Length Effect of Breaker Injection on Permeability Regain. For three lengths of tight sand samples, 0.1 vol% of FR was injected first, and then 0.024 wt% breaker was flooding each one, respectively. After dried with humidified Nitrogen, their gas phase permeability was measured, and permeability regain was calculated, as shown in Figure 6.10.

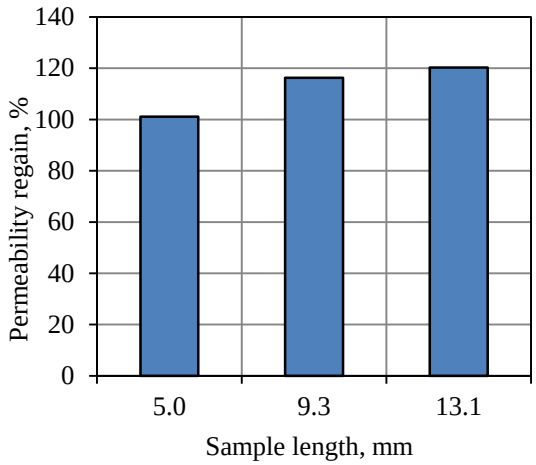

Figure 6.10. Breaker concentration effect on permeability regain

After sample flooded with FR and breaker, respectively, the permeability regain is higher for longer samples. And the formation damage to all samples is released. For the short sample, the 0.1 vol% FR was interacting with 0.024 wt% breaker fully. Therefore

the permeability regain is around 100%. However, for the longer samples, the injection of 0.1 vol% FR resulted in a high concentration of FR in the inlet side (near fracture matrix) and lower concentration in the outlet side (deep matrix). If the sample is simplified to be two parts, as shown in Figure 6.11, the left part has a high FR concentration a high breaker concentration, which has a 101.1% permeability regain. The other part has a low FR concentration. Due to the comparable emulsion particle size and tight sand pore size, the experiment observed the breaker did not fully degrade the FR filter cake. The injection pressure was constantly increasing. Then the breaker was probably blocked by the FR filter cake at the left part, and displayed a very minimal concentration in the right part, but the lower concentration FR there will generate a high permeability regain.

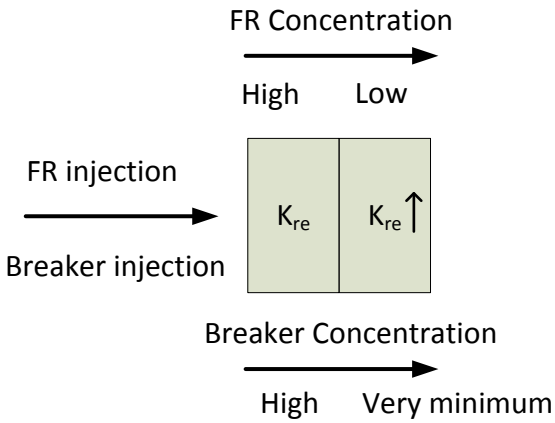

Figure 6.11. Simplified model for permeability regain with FR and breaker in long core

6.3.6. Gas Transportation in Tight Sand after Treated with Additives. 0.1 vol% FR were injected into three samples with different length, respectively, and then flooded by humidified Nitrogen. During Nitrogen flooding, sample weight was measured at certain time intervals, i.e. 1hr, as shown in Figure 6.12. Sample wet weight is defined by the weight after sample was measured with humidified Nitrogen before any additive

applied. The liquid saturation in the sample is the weight difference between its weight during flooding and the wet weight, divided by its pore volume:

$$S_L = \frac{w_L - w_{wet}}{PV} \times 100\% \quad (23)$$

where S_L=liquid saturation, %; w_L=sample weight at certain time, g; w_{wet}=sample weight after humidified Nitrogen flooding, g; PV= sample pore volume, cm^3;

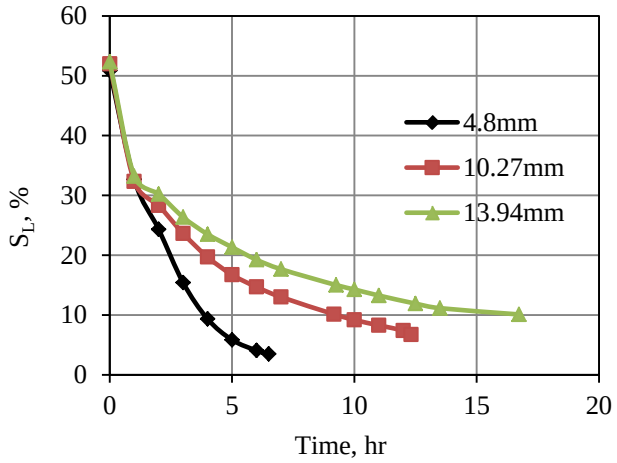

Figure 6.12. Liquid saturation during humidified Nitrogen flooding (not treated with breaker)

The initial liquid saturation is 50.9-52.3% for all length samples. After the humidified Nitrogen flooding, the remaining liquid saturation is lower (3.5%) for short sample and higher (10.1%) for long sample. With the same flooding strength, it is easier for the emulsion particle to be flooded out in the short sample. For the long sample, the emulsion particle has more chance to be flooded into deeper matrix. And for the same liquid saturation, it takes longer time for the long samples to achieve than the short ones.

0.1 vol% FR and 0.024 wt% breaker were injected into three samples with different length, respectively, and then flooded by humidified Nitrogen. The liquid saturation in samples is illustrated in Figure 6.13.

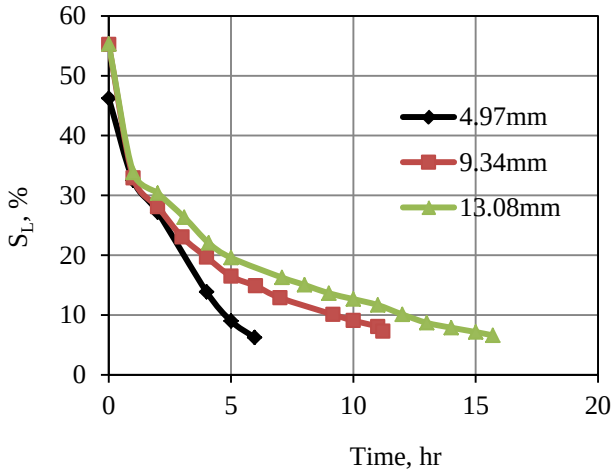

Figure 6.13. Liquid saturation during humidified Nitrogen flooding (treated with breaker)

The initial liquid saturation is 55.2-55.3% for medium and long samples, and 46.2% for short samples. After the humidified Nitrogen flooding at the same flooding strength, the final liquid saturation is almost the same for all length samples: 6.2-7.3%. This is probably because the breaker cut the polymer into short chain and smaller emulsion particle. It is easier to be flooded out. But due to the small pore size, some emulsion particles reside in the pore throat and cannot be reached by the gas flow.

6.4. CONCLUSIONS

1) Ammonium persulfate breaker does have a positive function with this FR. The over-balanced condition gets a full recovery of permeability. The balanced condition shows a better permeability regain than under-balanced condition;
2) In the short samples, lower concentration FR achieved a higher permeability regain, without the introduction of breaker. Its gas phase permeability is increased after flooded with low concentration FR;

3) After FR flooding, the formation damage is mostly happened in the near fracture matrix. But the permeability is almost recovered for the medium and long cores;
4) The permeability regain increases with the higher breaker concentration. 0.1 vol% (1 gpt) FR with 0.024 wt% (2 pptg) breaker is good enough;
5) After flooded by FR and breaker, respectively, the sample permeability regain is higher for longer samples. And the formation damage to all samples is released;
6) After FR and breaker flooding, respectively, the initial liquid saturation is very close for all length samples.
7) After flooded by FR and gas, it displays a lower remaining liquid saturation for short sample, and a higher remaining liquid saturation for long sample. After flooded by FR, breaker and gas, it indicates the remaining liquid saturation is almost the same for various length samples;
8) For the same liquid saturation, it takes longer time in the long sample to achieve than in short one.

7. SURFACTANT WETTABILITY IMPACT ON LIQUID INTAKE IN SHALE

7.1. INTRODUCTION

Shale gas has been proved to be economically viable through horizontal drilling and hydraulic fracturing. This technology will generate complex fracture networks, and expose shale matrix through these numerous micro-meter sized fractures. After hydraulic fracturing, fluid flowback is usually one of the major concerns, and it could be as little as 5% in the Haynesville shale to as much as 50% in areas of the Barnett and the Marcellus shales (King 2012).

Surfactant could reduce the water block in the matrix by providing a low surface tension. It can reduce the capillary pressure and increase the reservoir fluid phase permeability. After Berea sandstone soaking in surfactant (Kewen and Abbas 2000), the sample surface, which is initially strong water wet, could attain a contact angle of 120° with water drop and 60° with oil drop, which changed to be oil wet. Before the treatment, water could take in 0.56 PV, after treatment, water could only take in less than 0.05 PV. Wettability altered by surfactant gets a prominent impact on the spontaneous imbibition in Berea sandstone. In gas shale, the imbibition of surfactant also could result in a lower imbibition rate than that with deionized water at the very beginning several minutes (Lakatos, Bódi et al. 2013, Roychaudhuri, Tsotsis et al. 2013). Then with experiment continues, the imbibition rate is almost the same for both surfactant and water. The imbibition of liquid will also cause fractures and shale broken into pieces (Dehghanpour, Zubair et al. , Wang, Butler et al. 2011). And it is more significant in non-organic shales than organic shales.

However, the characteristic of these fractures in lab study, such as fractures quantities and distribution, is not seen. The quantified relation between the liquid intake and time in shale is also not clear. This present study investigates the imbibition behavior of shale impacted by fractures and surfactant. A new sample preparation method is developed. When liquid is introduced, its shape will be intact rather than fall apart, and the fractures are able to generate within it. We will first describe the fractures generated in shale with the introduction of brine. Then the cocurrent spontaneous imbibition is carried out to investigate the brine intake before and after the shale is treated with

surfactant. Imbibition rates from experiments result are analyzed at various conditions. The factors impact on imbibition rate, such as the existence of fractures, sample length, surfactant concentration and treatment method, are investigated in detail.

7.2. EXPERIMENTAL

7.2.1. Materials. Rock sample: Marcellus shale was prepared with previous coating and slicing method. 11 slices were used here. Detailed parameters are shown in Table 7.1. Most samples were sliced to be around 5mm (as short samples), some were around 10mm (as medium samples), and some were around 15mm (as long samples).

Fluids: Clay stabilizer: KCl is used to contact with shale and create fractures with concentration of 2%. Surfactant: Gasflo G, commonly used in shale gas fracturing is implemented in this study with three concentrations: 0.025, 0.05, and 0.1% according to the former field and lab experiments. In order to prevent the clay from swelling, surfactant is also prepared with 2% KCl.

Table 7.1. Shale sample parameters

Sample No.	Thickness	Cross-sectional area
	mm	cm^2
24	4.96	1.003
25	5.54	0.946
26	4.55	0.982
27	4.80	0.959
23	4.44	0.986
28	4.93	1.023
22	10.55	0.991
31	9.17	0.994
32	9.47	1.059
21	14.76	1.034
33	13.58	1.086

7.2.2. Equipment. Same coreflooding and fluid imbibition setup were used here, as showin Figure 7.1 and Figure 7.2.

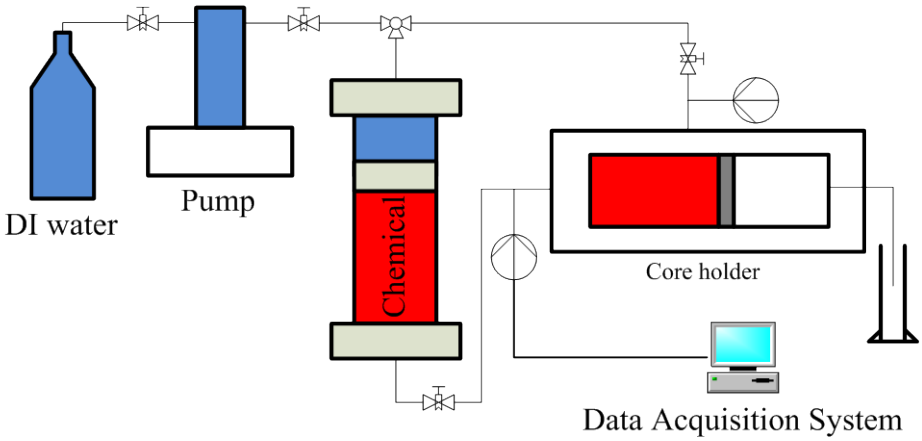

Figure 7.1. Coreflooding system

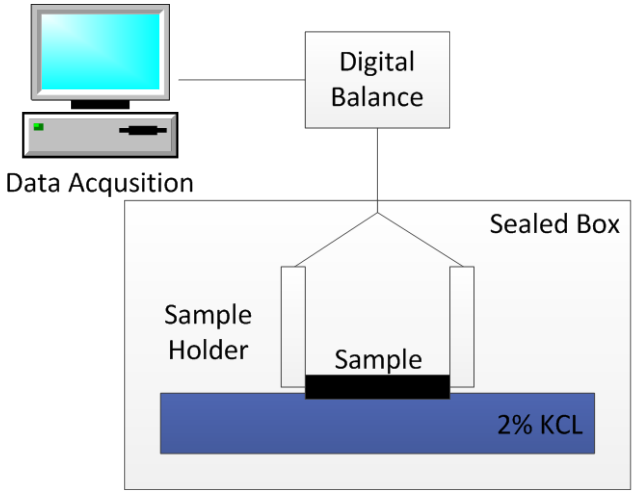

Figure 7.2. Spontaneous cocurrent imbibition system

7.2.3. Procedure. After oven dried to remove moisture attained in ambient condition during preparation, all samples were carried out the 1st imbibition, factures on sample both sides were generated and observed by the naked eyes. Then samples were putted in oven to vaporize the liquid, and carried out a 2nd time imbibition. After samples were dried, surfactant was used to treat the sample by flooding and soaking, respectively. After sitting still for 12 hrs, samples were oven dried again. 3rd imbibition was continued with these samples.

Therefore, a total of 3 time KCl imbibition experiments were performed on each sample.

A detailed flowchart is shown in Figure 7.3.

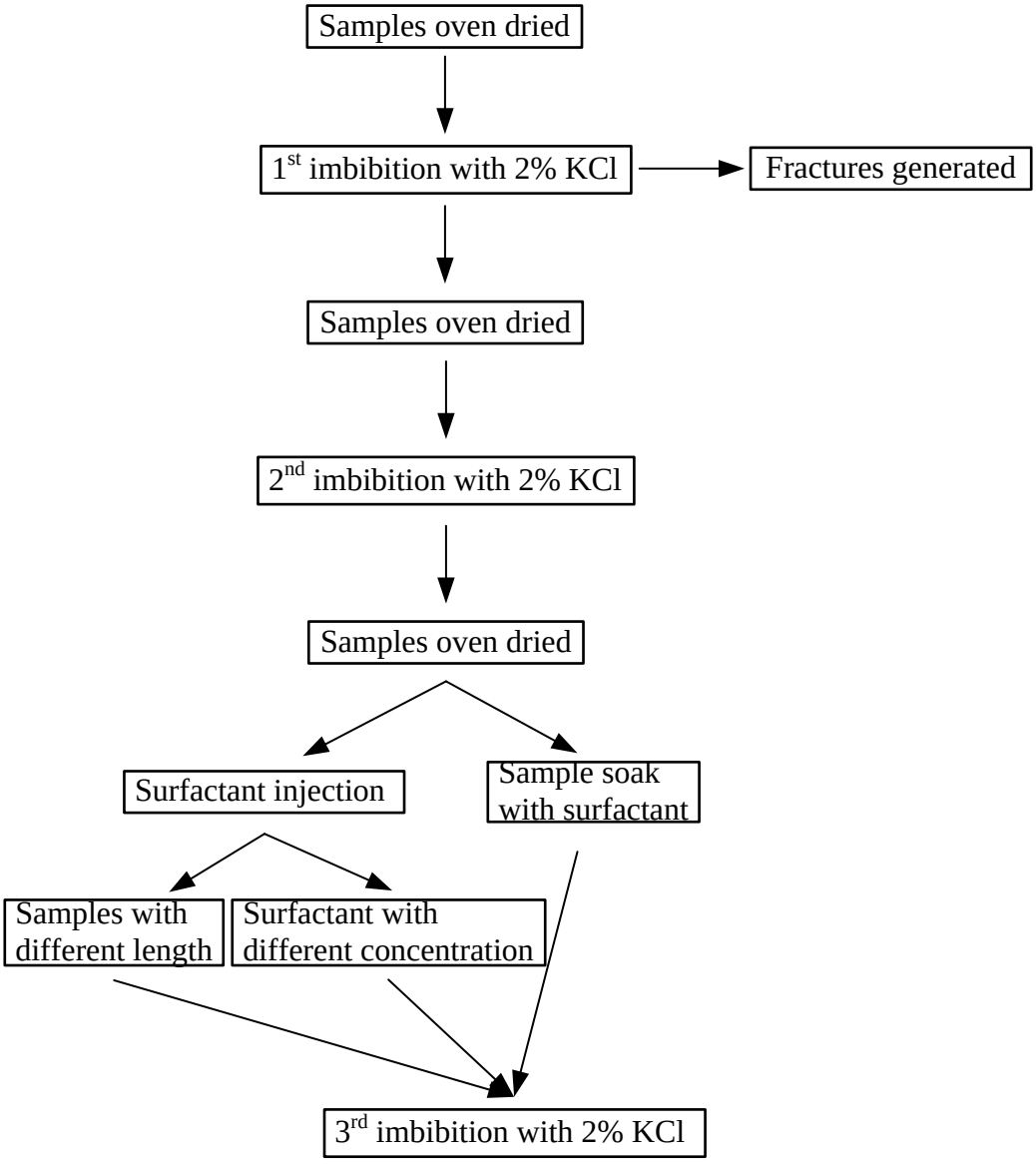

Figure 7.3. Experiment flow chart

7.3. RESULT AND DISCUSSION

7.3.1. Typical Imbibition Curve. A typical spontaneous cocurrent imbibition curve of gas shale with 2% KCl fluid is shown in Figure 7.4. The imbibition happened at early stage is very fast, and it becomes very slow at the later stage. At the early stage, the liquid took in is increasing very fast. At some point, it slows down and maintains at a

second rate. This phenomenon is also observed by previous researchers (Lakatos, Bódi et al. 2011, Roychaudhuri, Tsotsis et al. 2013). The two imbibition rates are very different from each other. Two straight lines were put on each part to fit with their data. Since capillary pressure is in reverse relation with the pores radius, and brine solution is the wetting phase. The line with high slope at early stage is defined as the 1st slope, where the liquid is supposed to enter the small pores close to fluid front. The other line at the later stage is defined as the 2nd slope, where the liquid is supposed to enter the large pores, and small pore far from the front. These two slopes were found extensively exist in all these experiments in this study. The quantities of these slopes are actually the imbibition rate of each sample at each stage. The slope was found comparable with each other is shown and discussed in the following part.

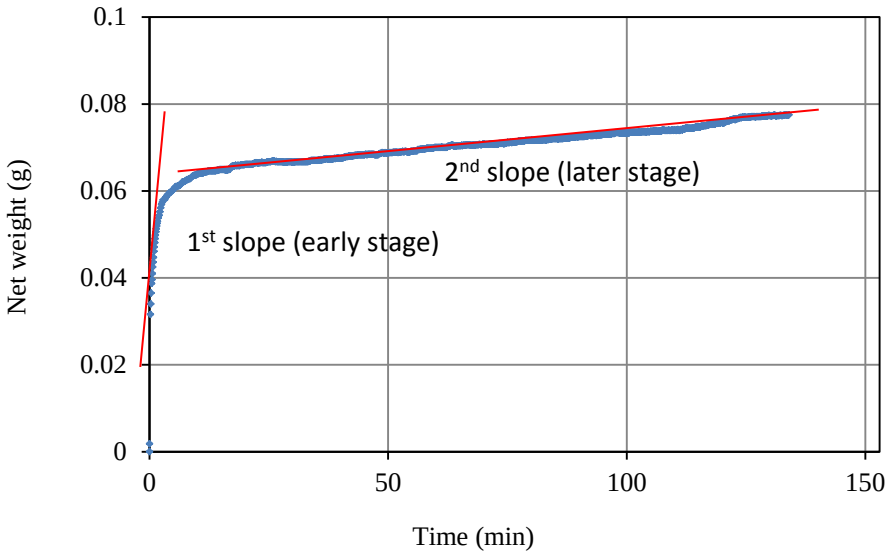

Figure 7.4. Typical imbibition curve (TS23)

7.3.2. Microfracture Impact on Imbibition Rate. To protect the samples from any influence or contamination such as fluid intrusion, for each sample, it had no chance to contact with any liquid before imbibition, except when it was cored from underground

as a 5 inch core. After samples were prepared and sliced with considerable attention, their surface was carefully examined. No fracture could be found with the naked eyes.

After 1st time imbibition was finished, sample was taken out, and the extra liquid on the sample surface was gently cleaned. Due to the high area by clay content in shale, sample surface will dry out in less than 1 minute and leave few channels wetted by the imbibed brine. These channels were identified as fractures generated during the imbibition process. After samples were oven dried, the fractures were still observable with the naked eyes. The fractures will go across the sample face, and distribute unevenly on both surfaces, as shown in Figure 7.5. Fracture width is in micrometer range. For the short samples, most of them could generate fractures extend throughout them, but this did not happen to medium and long samples. For long sample: No. 21, the fractures are very minor on the side contact with liquid, and not observable after dried.

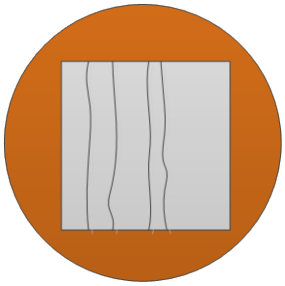

Figure 7.5. Demonstration of fractures on sample

Table 7.2. Statistical of the fractures on sample

Sample No	Length	No. of fractures	Fracture type
	mm		
23	4.49	6	
24	4.96	7	3 throughout
25	5.49	4	2 throughout
26	4.59	6	3 throughout

Table 7.2. Statistical of the fractures on sample (cont.)

Sample No	Length	No. of fractures	Fracture type
	mm		
27	4.84	7	1 throughout
28	4.96	6	1 throughout
22	10.64	6	
31	9.16	5	
32	9.44	6.5	
21	14.73	12	minor fracs
33	13.57	5	

After 1st time imbibition, samples were putted in oven to vaporize the liquid, and then carried out a 2nd time imbibition. Short and medium length samples with fractures show a lower data in the 1st slope figure where the liquid was taken in very fast, as shown in Figure 7.6. The sample with fractures could be considered as larger pores, compare with samples without fracture. Since capillary pressure is in reverse relation with the pores radius, and brine solution is the wetting phase, so the large pores will have a smaller capillary pressure than that in small pores. Therefore, sample containing fractures will have a lower imbibition rate at the beginning.

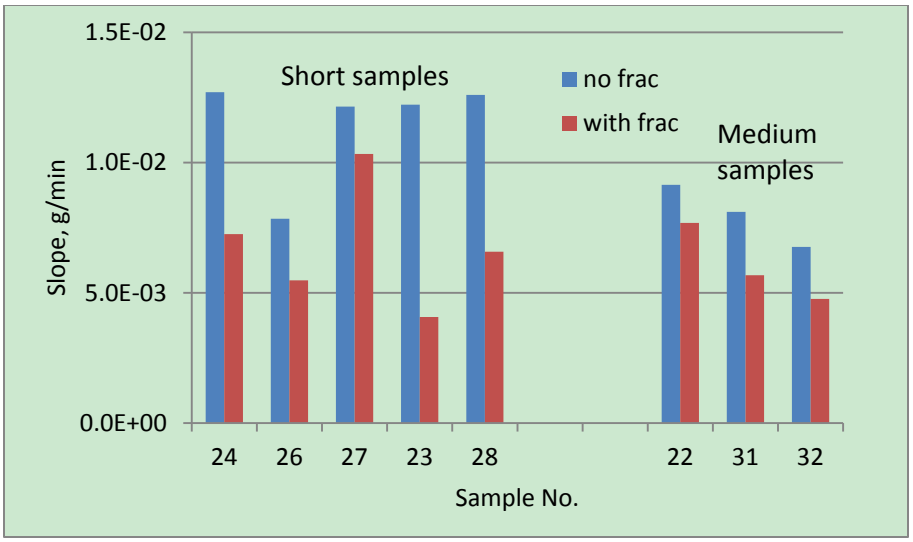

Figure 7.6. 1st slope of samples with and without fractures

The 2nd slope is controlled by large pores and small pore far from the front. For all samples, it is comparable before and after the fractures were created, as shown in Figure 7.7. Some samples with fracture have larger 2nd slope than before, while some slopes are lower than before.

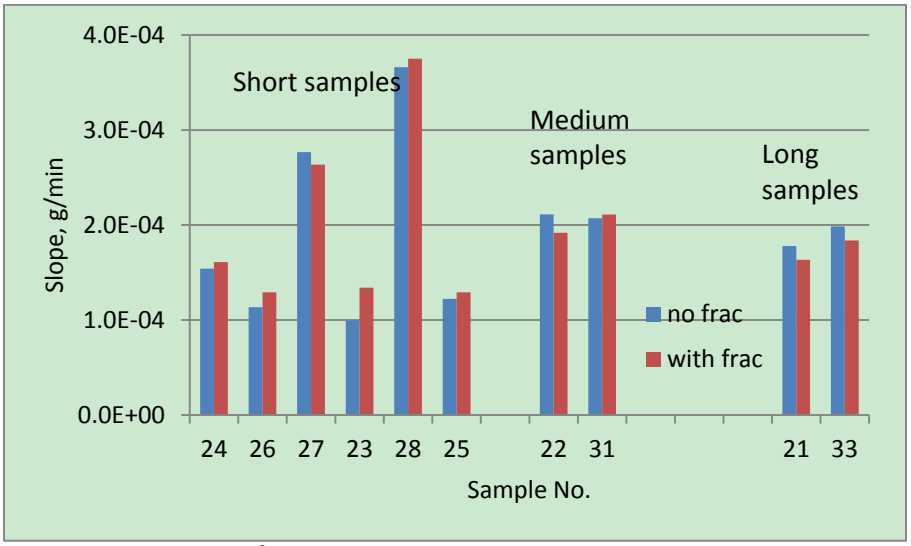

Figure 7.7. 2nd slope of samples with and without fractures

7.3.3. Length Effect on Imbibition Rate. After the 2nd imbibition, surfactant was injected into samples with different length, respectively. After dried in oven, a 3rd imbibition was conducted with these samples. No more fractures were found on the samples after the 3rd imbibition. So the fracture impact on the imbibition rate is avoided. Then the 2nd and 3rd imbibition curves were used to compare the surfactant impact on shale imbibition condition.

For the 1st slope, short sample shows a sharp decrease, medium samples decrease a little, and long sample almost does not change, as shown in Figure 7.8. However, for the 2nd slope, the short, medium and long samples all increase, as shown in Figure 7.9. The variation of these slope data was calculated and shown in Table 7.3. The shorter the sample, the more it decreases for the 1st slope, but the more it increases for the 2nd slope.

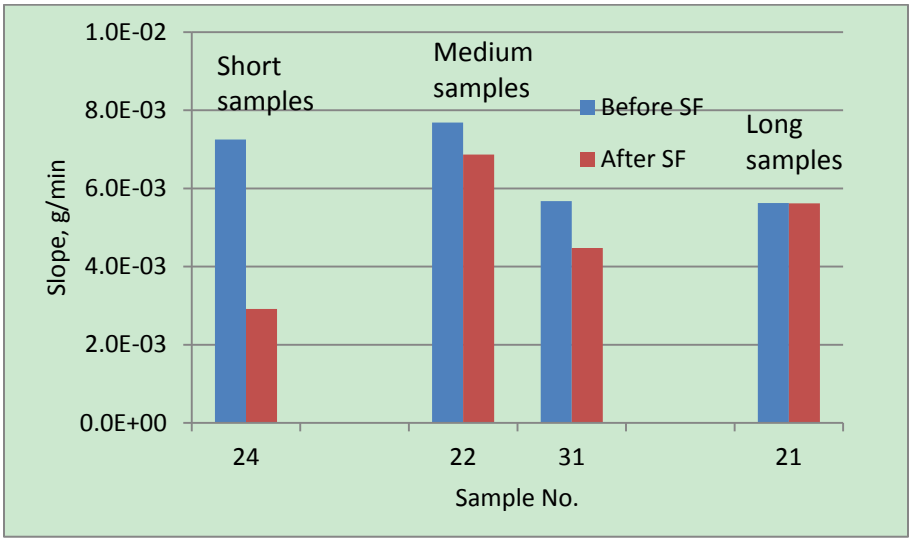

Figure 7.8. 1st slope of samples before and after surfactant treatment

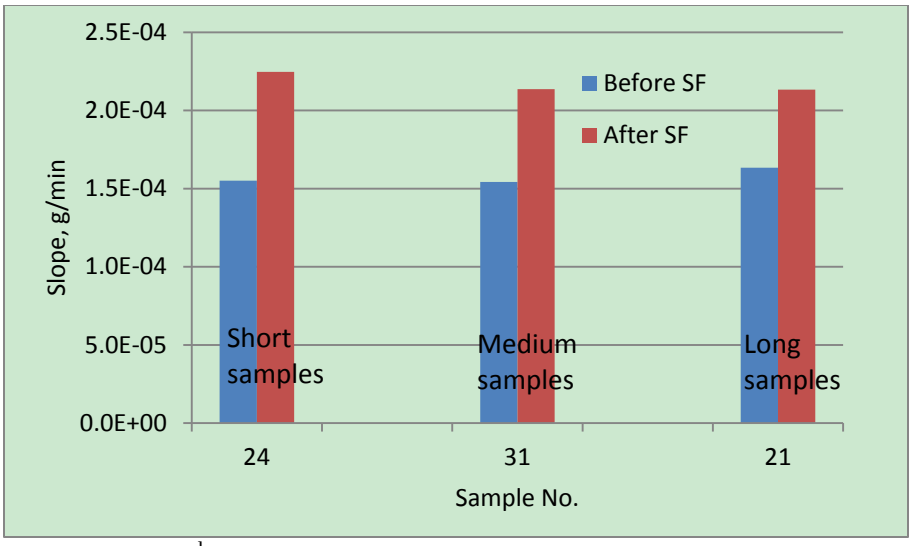

Figure 7.9. 2nd slope of samples before and after surfactant treatment

Table 7.3. Comparison of two slopes before and after surfactant treatment

Sample	Change of 1st slope	Change of 2nd slope,
	%	%
Short	- 59.8	31.0
Medium	- 10.6-21.1	27.8
Long	- 0.1	23.4

7.3.4. Surfactant Concentration Effect on Imbibition Rate. After fractures were created in the 2nd imbibition, the short samples were flooded with three concentrations of surfactant: 0.1, 0.05, and 0.025 vol%, then dried in oven, and conducted the 3rd imbibition.

After surfactant treatment, the 1st slope is found to be decreasing and 2nd slope is increasing than before the surfactant was introduced, as shown in Figure 7.10 and Figure 7.11. The lower the fluid concentration decrease, the smaller it decreases for the 1st slope, and the more it increases for the 2nd slope, as shown in Table 7.4.

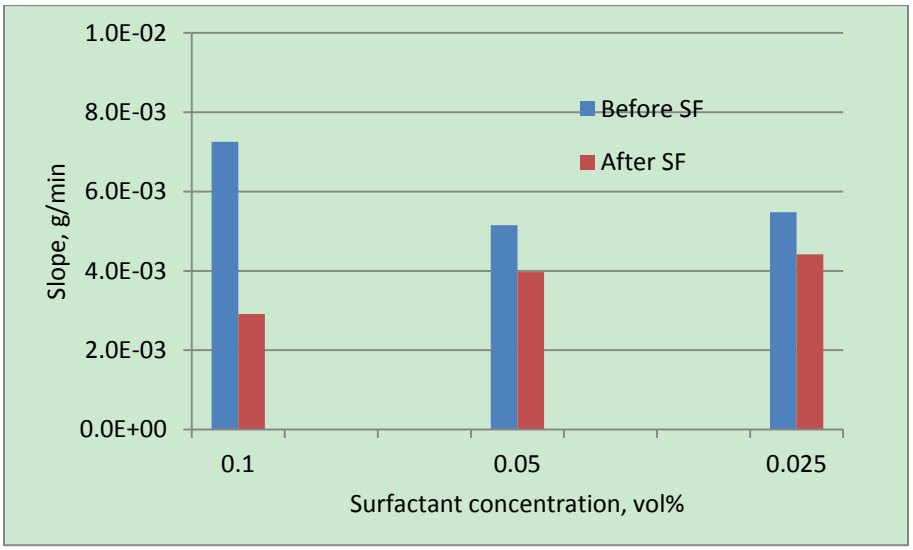

Figure 7.10. 1st slope of samples before and after surfactant treatment

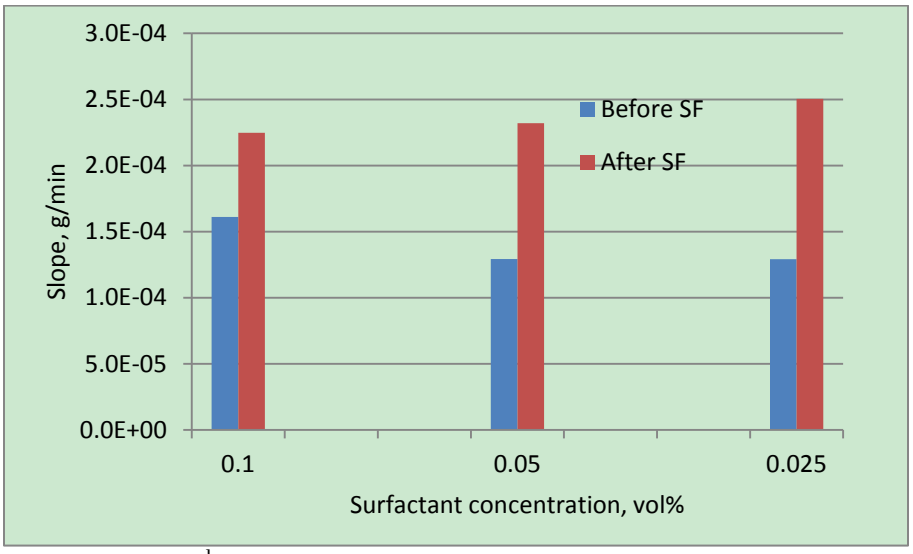

Figure 7.11. 2nd slope of samples before and after surfactant treatment

Table 7.4. Comparison of two slopes before and after surfactant treatment

Concentration	Decrease of 1st slope	Increase of 2nd slope
vol%	%	%
0.1	-59.8	28.3
0.05	-22.9	44.3
0.025	-19.4	48.4

7.3.5. Imbibition Rate Impact by Different Treatment Methods. All the samples mentioned before were treated by surfactant injection. Another condition, surfactant soaking was also studied by soaking Sample No. 27 into 0.1 vol% surfactant, with its one side contact with liquid, and the other side open to air, like imbibition. After soaking for 12 hrs, Sample No. 27 was oven dried and conducted the 3rd imbibition.

Compare with the injection treated sample No. 24 with the same concentration surfactant. Their slopes are shown in Figure 7.12 and Figure 7.13. Although two short samples were treated with same fluid, the decreasing of 1st slope and increasing of 2nd slope also happened. As shown in Table 7.5, compare with surfactant flooding, the sample treated with soaking displays a lower of decrease of 1st slope, and a high increase of 2nd slope. Results from the soaking are very much like the flooding with lower concentration surfactant.

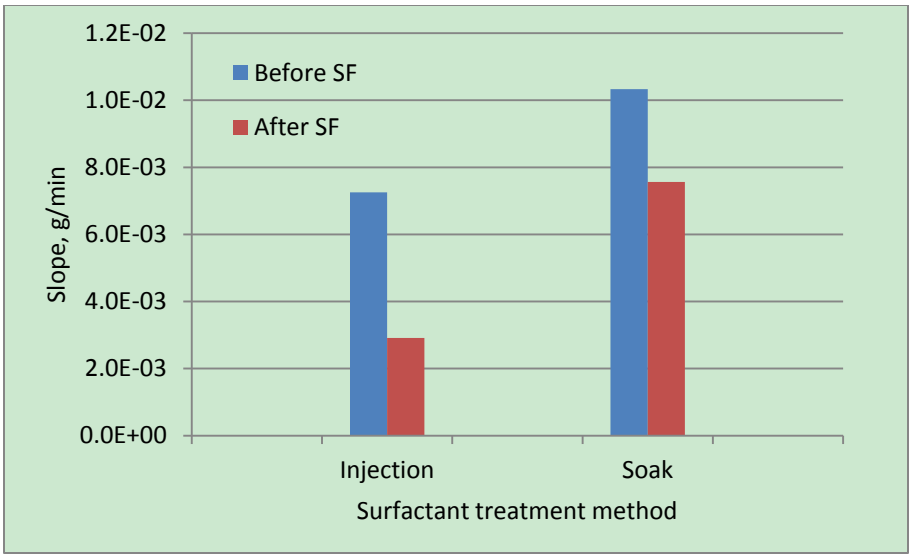

Figure 7.12. 1st slope of samples before and after surfactant treatment

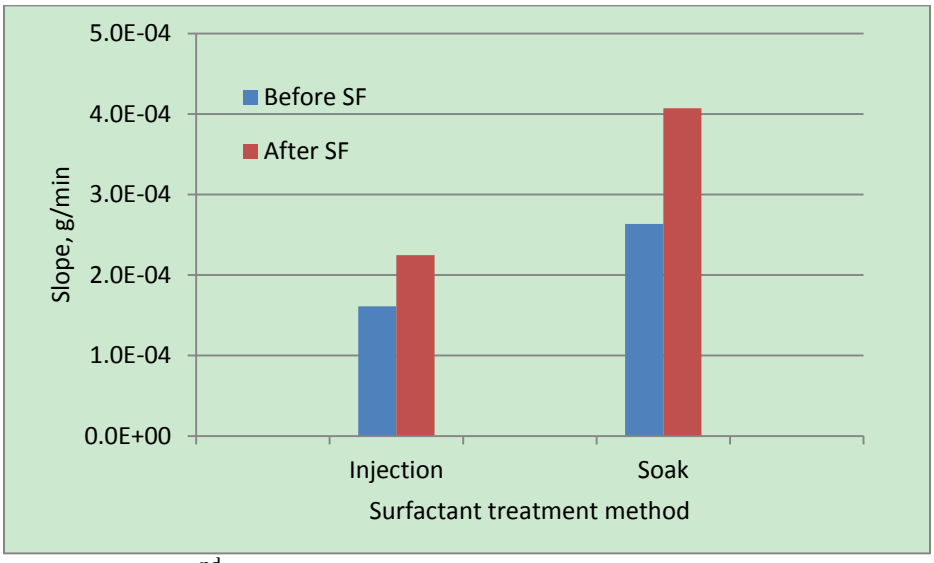

Figure 7.13. 2nd slope of samples before and after surfactant treatment

Table 7.5. Comparison of two slopes before and after surfactant treatment

Sample No.	Treatment method	Change of 1st slope, %	Change of 2nd slope, %
24	Flooding	-59.8	28.3
27	Soak	-26.8	35.3

7.4. CONCLUSIONS

1) A comprehensive experimental method is developed to study fluid imbibition with cocurrent imbibition method. The result is quantities, compared with other researcher's preparing method;
2) The imbibition happened at early stage is very fast, and it becomes very slow at the later stage. The two imbibition rates are very different from each other;
3) Microfracture will generate at the first time when shale encounter with brine. Around 5 fractures/cm^2 were found. After samples oven dried and contact with liquid again, no more fractures were found;
4) Samples containing fractures will have a lower imbibition rate at the early stage. But this impact at later stage is not obvious;
5) After surfactant treatment, the shorter the sample, the more the slope decreases at early stage, but the more it increases at the later stage;
6) After surfactant treated, the lower the fluid concentration, the smaller the slope decreases at early stage, and the more it increases at later stage;
7) Compare with surfactant flooding, the sample treated with soaking displays a lower of decrease at early stage, and a high increase at the later stage.

8. CONCLUSIONS AND RECOMMENDATIONS

8.1. CONCLUSIONS

The conclusions are sorted by each topic as followed.

8.1.1. Friction Reducer Transports in Microchannel and Microfracture.

1) This FR solution is a shear thinning fluid. The impact of FR solution concentration was more obvious at low velocities. Higher concentrations of FR solution displayed a larger pressure gradient than that of the lower concentration. The residual resistance factor to water is relatively low for this friction reducer;
2) This FR solution is not very sensitive to the surface wettability at high velocities, but this sensitivity increases in smaller microchannels and lower velocities;
3) Based on the analyzes of emulsion particle size and the typical gas shale pore size, this FR solution will not go into the matrix pores easily, but can block the pore entrance on fracture face to prevent the fluid from leak off, and help pressure build up and fracture extension during slickwater fracturing;
4) If the flow is already laminar, as in microchannel here, there is no turbulence for the friction reducer to suppress. Consequently, the addition of a polymer under these conditions can only increase the flow resistance and pressure drop (given a fixed flow rate), but its impact is not very significant.

8.1.2. Petrophysical Properties Impact of Multiple Additives Consecutively Treating on Tight Sand.

1) From the porosity data measured, this tight sand is relatively homogenous. But its absolute permeability test with tight sand shows it has some variation. The initial water saturation in these tight sand has a big impact on the gas phase permeability;
2) Due to the high content of quartz and clay, tight sand surface displays water wet. The introduction of friction reducer makes the tight sand become less water wet. The injection and soaking of breaker all turn the tight sand surface to be intermediate wet, and the contact angle is a little bit higher achieved by breaker injection. This surfactant did not change the surface wettability on this tight sand. The contact angle will remain the same after the sample treated with FR or FR and breaker, respectively;

3) At under-balanced and balanced condition, the pore radius decrease in tight sand resulted in a higher imbibition rate and amount than brine treated only. During over-balanced condition, where FR, breaker were injected into tight sand, respectively, the imbibition rate and amount are opposite. However, in the latter condition, the degraded FR polymer would possibility goes deep into the matrix, and cause near fracture damage. An equilibrate policy needs to be estimated between fluid imbibition and near fracture damage during hydraulic fracturing design;
4) For the humidified N_2 flooding, if FR and breaker enter the formation matrix first, the liquid saturation by gas flooding would be higher than the initial water saturation. The adding of surfactant could only decrease the liquid saturation by a very small fraction. Once the friction reducer, breaker, and surfactant enter tight sand matrix, certain contamination, such as water block or chemical residual will exist, and it is hard to remove by gas flooding;
5) If friction reducer degraded by breaker soaking at no pressure drop, the degraded polymer and broken emulsion particles would be released from the blocked pore throat, the remaining liquid saturation would not be impacted. The humidified N_2 flooding displayed similar liquid saturation with the initial water saturation.

8.1.3. Formation Damage of Friction Reducer and Breaker on Tight Sand.

1) When FR is degraded by breaker at over-balanced condition, it gets a full recovery of gas phase permeability. The balanced condition shows a better permeability regain than under-balanced condition;
2) In the short samples, lower concentration FR achieved a higher permeability regain, without the introduction of breaker. Its gas phase permeability is increased after flooded by low concentration FR. After FR flooding, the formation damage is mostly happened in the near fracture matrix. But the permeability is almost recovered for the medium and long cores;
3) The permeability regain increases with the higher breaker concentration. 0.1 vol% (1 gpt) FR with 0.024 wt% (2 pptg) breaker is good enough. After flooded by FR and breaker, respectively, the sample permeability regain is higher for longer samples. And the formation damage to all samples are released;

4) After FR and breaker flooding, respectively, the sample initial liquid saturation is very close for all length samples. After flooded by FR and gas, the sample displayed a lower remaining liquid saturation for short sample, and a higher remaining liquid saturation for long sample. If flooded by FR, breaker and gas, it indicates the remaining liquid saturation is almost the same for various length samples. For the same liquid saturation, it takes longer time in the long sample to achieve than in short one.

8.1.4. Surfactant Wettability Impact on Liquid Intake in Shale.

1) A new sample preparation method is successfully developed by coating and slicing. It is applicable to study liquid intake in shale, and featured to be faster permeability measurement, less rock consumption;
2) A comprehensive experimental method is developed to study fluid imbibition with cocurrent imbibition method. The result is quantities, compared with other researcher's preparing method;
3) Microfracture will generate at the first time when shale encounter with brine. After samples dried by oven and then contact with liquid again, no more fractures were found;
4) The imbibition happened at early stage is very fast, and it becomes very slow at the later stage. The two imbibition rates are very different from each other. Samples containing fractures will have a lower imbibition rate at the early stage. But this impact at later stage is not obvious;
5) After surfactant treatment, the shorter the sample, the more the slope decreases at early stage, but the more it increases at the later stage. After surfactant treated, the lower the fluid concentration, the smaller the slope decreases at early stage, and the more it increases at later stage. Compare with surfactant flooding, the imbibition slope of the sample treated with soaking is higher at both stages.

8.2. RECOMMENDATIONS

Several experiments can be continued to further the study:

1) A 3M surfactant can be used to investigate the wettability alteration in shale. It is widely used in the electronic industry to prevent water and oil contamination;

2) The formation damage of polymer or gel on unconventional gas rock can be studied. It will help to understand the permeability change during proppant carrying stage during hydraulic fracturing;
3) A screen out can be built based on various formation pore size and emulsion particle size of multiple friction reducers.

APPENDIX A.

RESISTANCE FACTOR V.S. VELOCITY OF XANTHAN

Resistance factor is defined as the ratio of the mobility of water to the mobility of polymer during polymer flooding (Sun, Saleh et al. 2012). Under the same experimental conditions, the resistance factor equals the apparent viscosity. Preview study reported that Xanthan produces a similar phenomenon as in this study, as shown in Figure A.1 (Seright, Fan et al. 2011). With 55 mD, 269 mD, and 5120 mD cores, at the same fluid velocity, the resistance factor is high in high-permeability rocks than that in low-permeability ones.

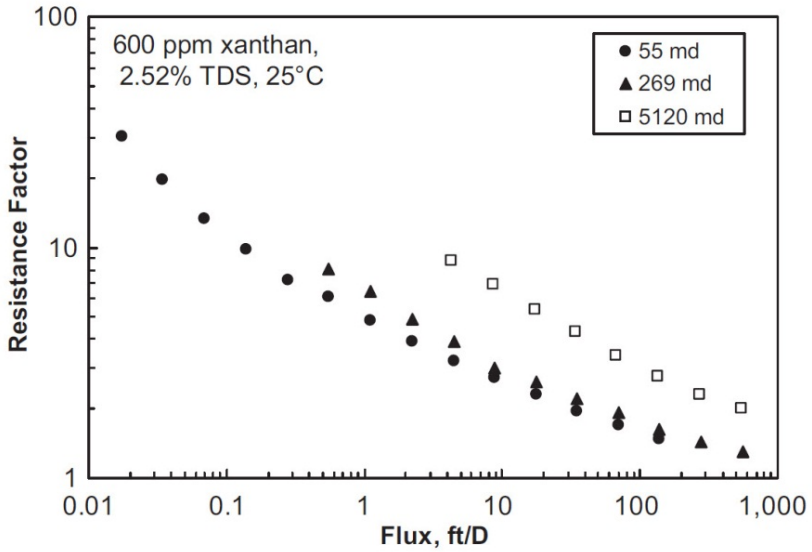

Figure A.1. Resistance factor vs. flux for 600 ppm Xanthan (Seright and Fan, 2011)

APPENDIX B.

RESISTANCE FACTOR V.S. SHEAR RATE OF XANTHAN

With the same experiment data in Appendix A, under the assumption that the rock is homogeneous, the pore size of each sample were converted to circular capillary diameters from permeability and porosity data, as shown in Table B.1. Then, the velocity was converted to shear rate. Figure B.1 shows the relationship between the shear rate and the resistance factor, indicating that at the same shear rate, the resistance factor in higher permeability sample is larger than that in low permeability sample.

Table B.1. Sample pore size conversion

K (mD)	Φ (%)	D (μm)
55	0.17	10.22
269	0.212	20.23
5120	0.35	68.69

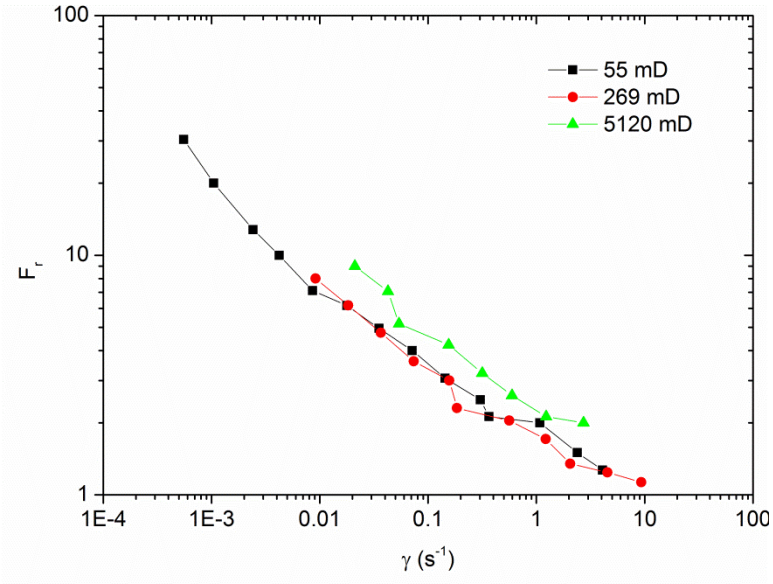

Figure B.1. Resistance factor vs. shear rate for 600 ppm Xanthan
(Modified from Seright and Fan, 2011)

APPENDIX C.

GAS PHASE PERMEABILITY MEASUREMENT

C.1. Gas phase permeability data before treated with additives

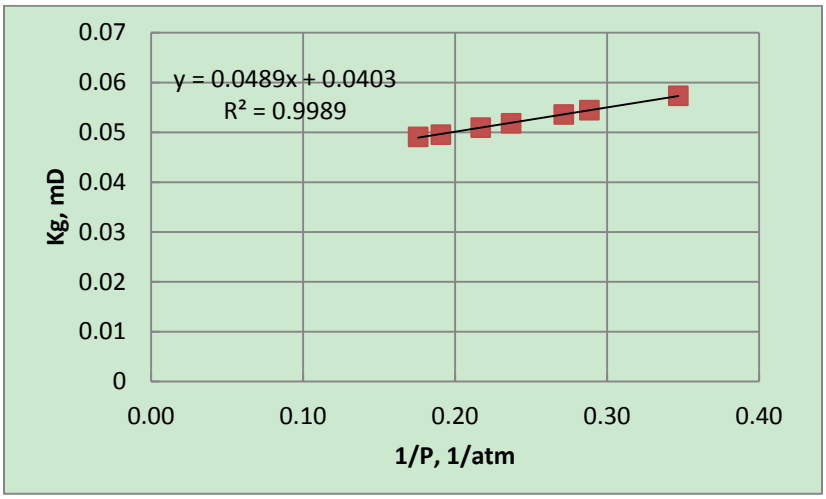

Figure C.1. TS11 gas phase permeability measured with humidified Nitrogen

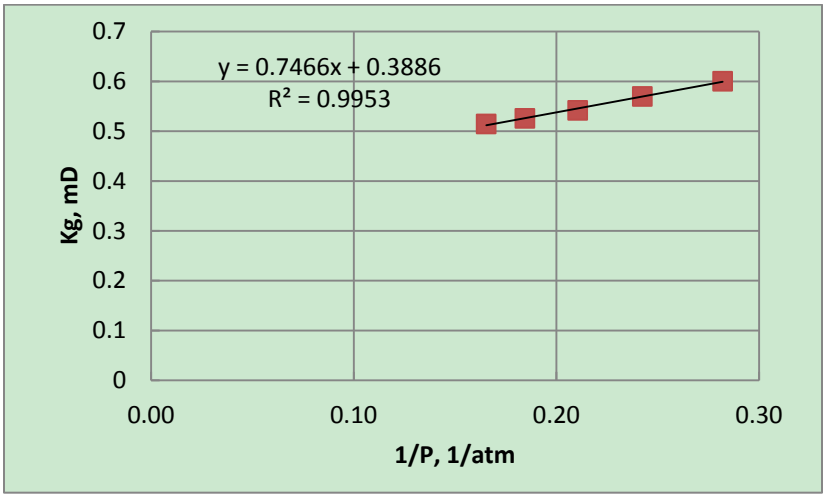

Figure C.2. TS20 gas phase permeability measured with humidified Nitrogen

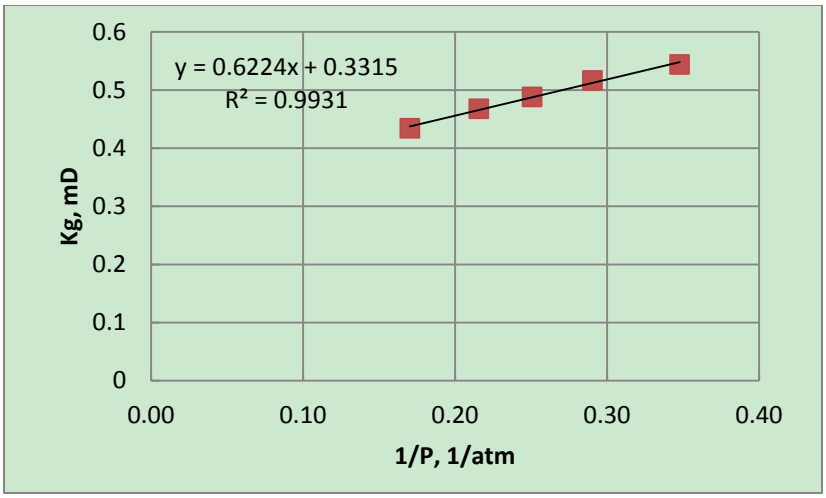

Figure C.3. TS21 gas phase permeability measured with humidified Nitrogen

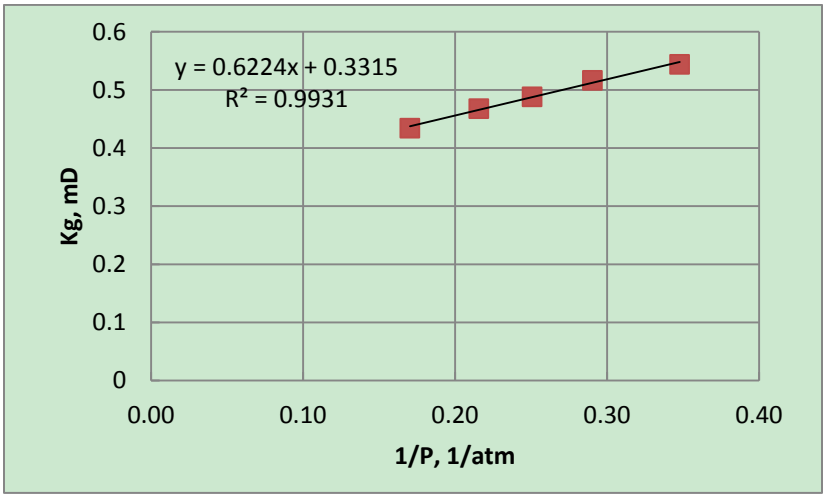

Figure C.4. TS22 gas phase permeability measured with humidified Nitrogen

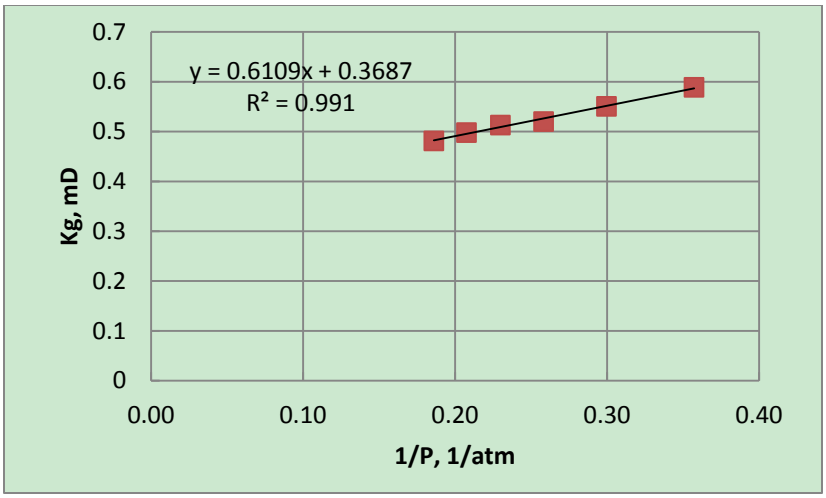

Figure C.5. TS26 gas phase permeability measured with humidified Nitrogen

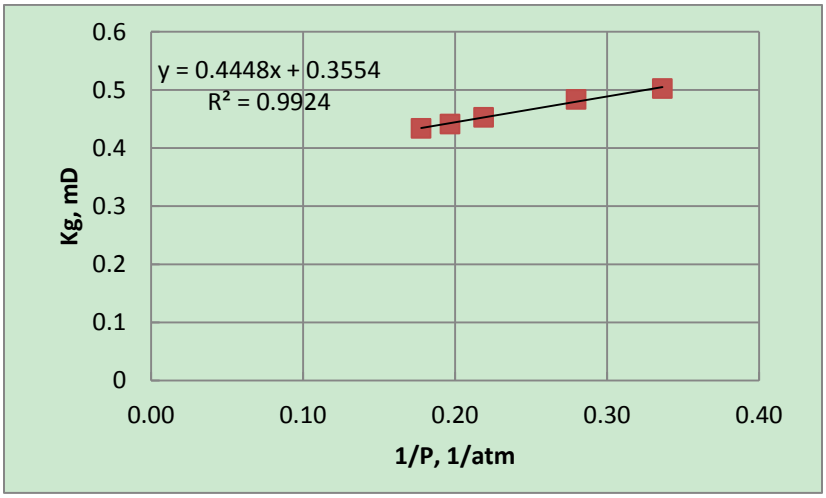

Figure C.6. TS27 gas phase permeability measured with humidified Nitrogen

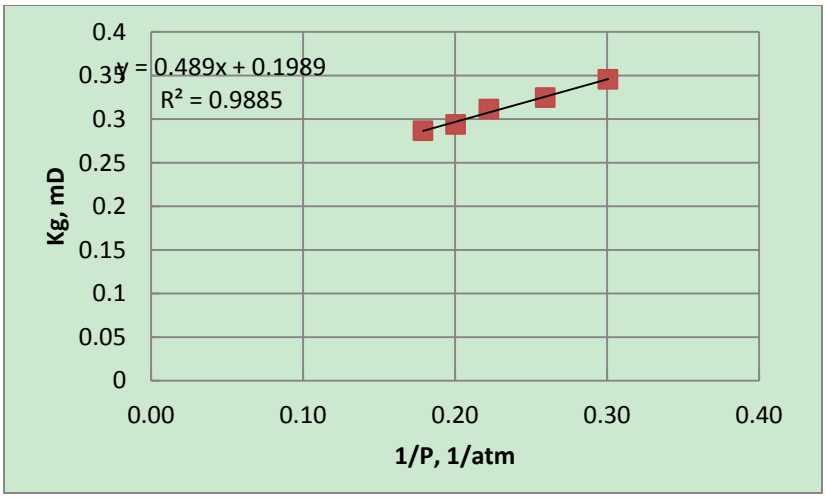

Figure C.7. TS29 gas phase permeability measured with humidified Nitrogen

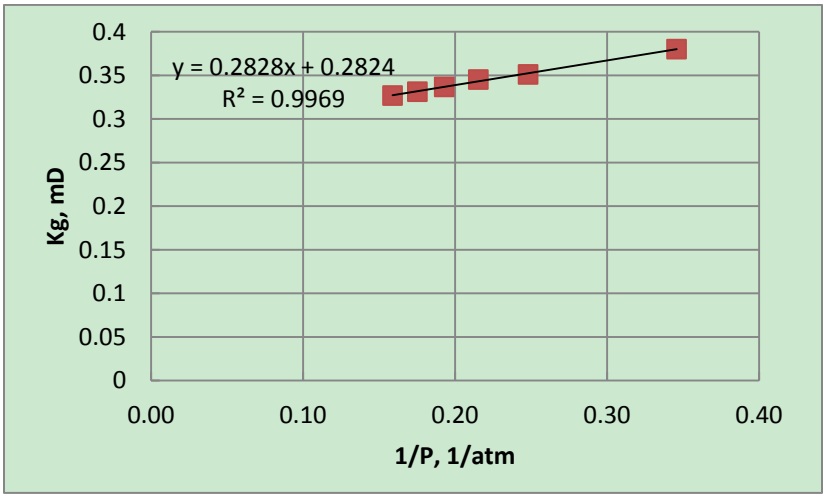

Figure C.8. TS30 gas phase permeability measured with humidified Nitrogen

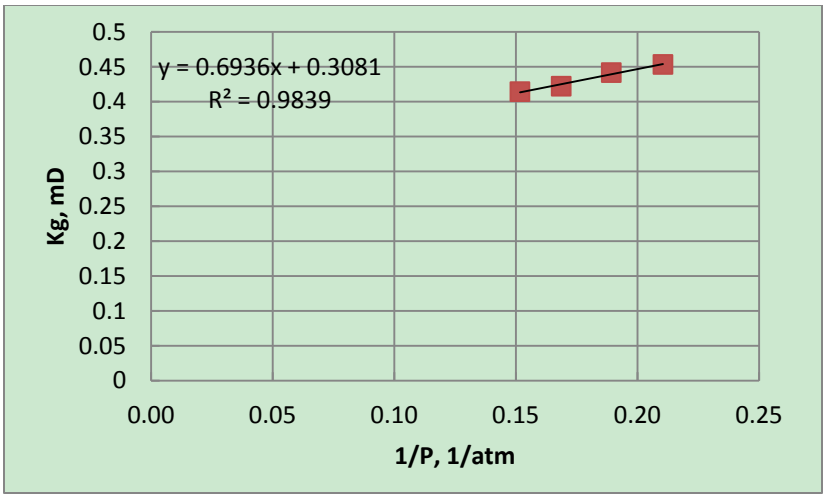

Figure C.9. TS33 gas phase permeability measured with humidified Nitrogen

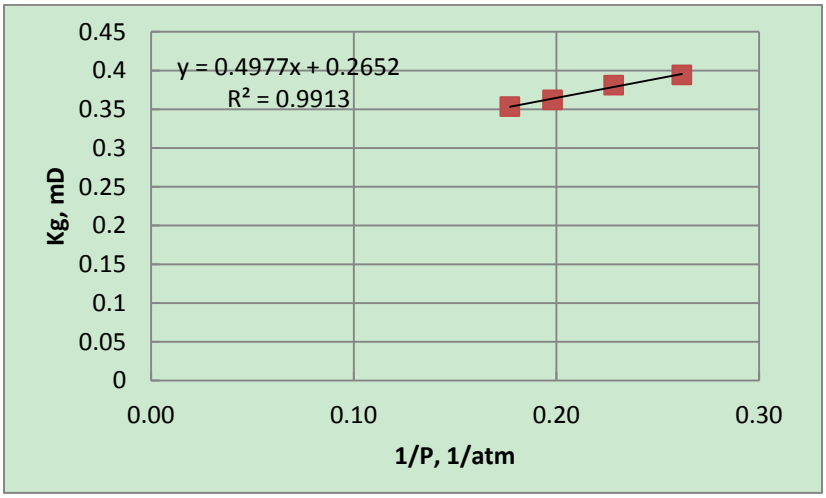

Figure C.10. TS35 gas phase permeability measured with humidified Nitrogen

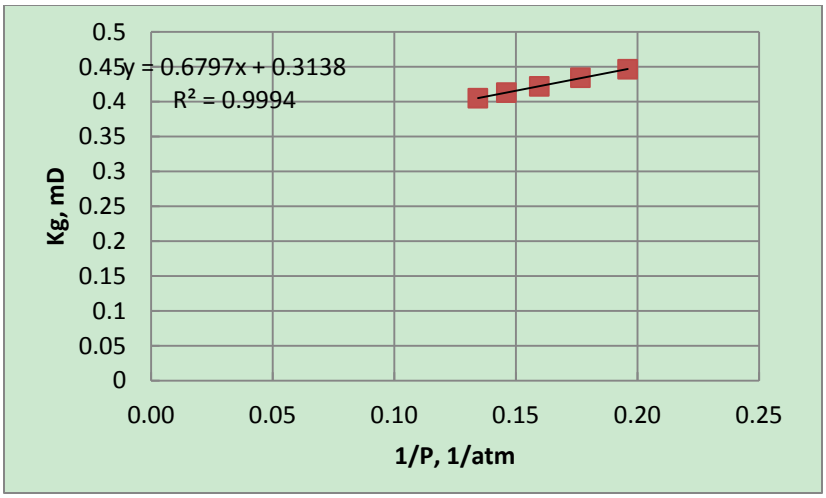

Figure C.11. TS34 gas phase permeability measured with humidified Nitrogen

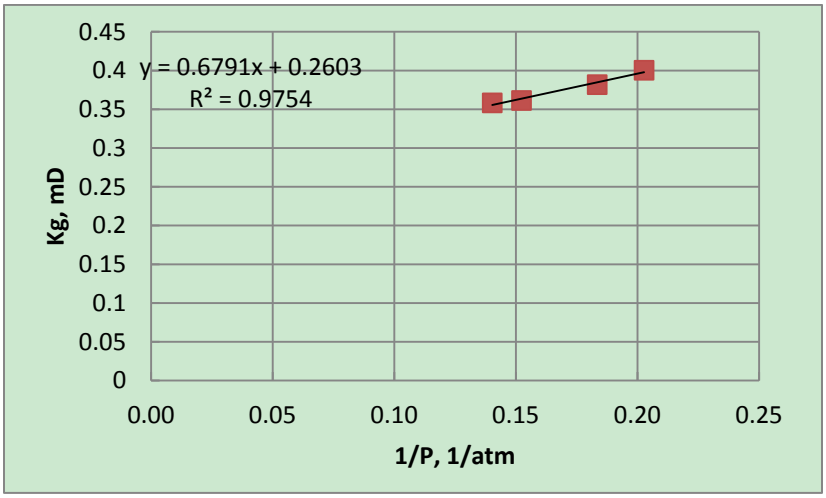

Figure C.12. TS25 gas phase permeability measured with humidified Nitrogen

C.2. Gas phase permeability data after treated with FR and/or breaker

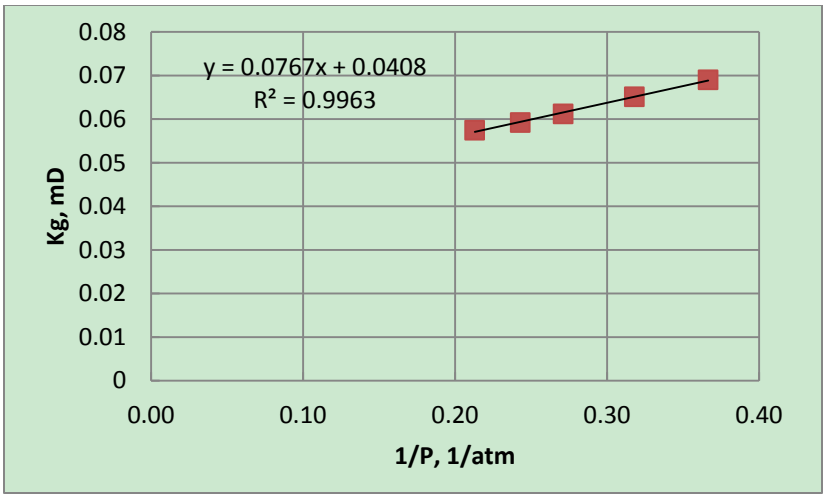

Figure C.13. TS11 gas phase permeability after treated with FR and/or breaker

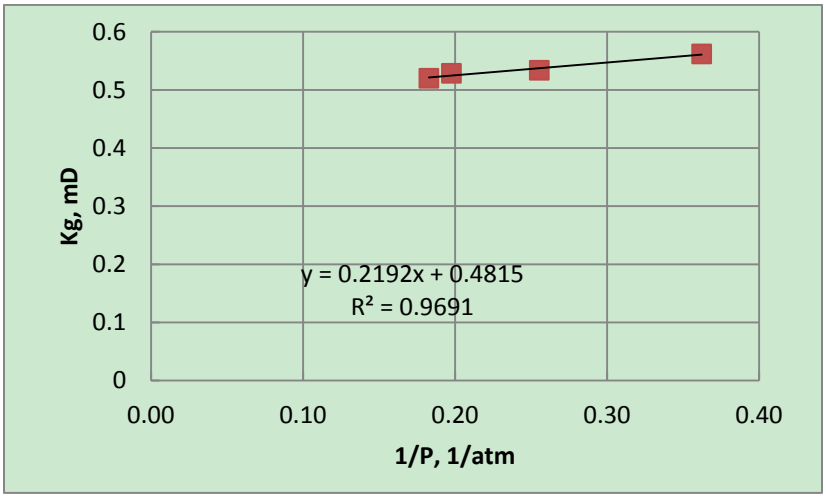

Figure C.14. TS20 gas phase permeability after treated with FR and/or breaker

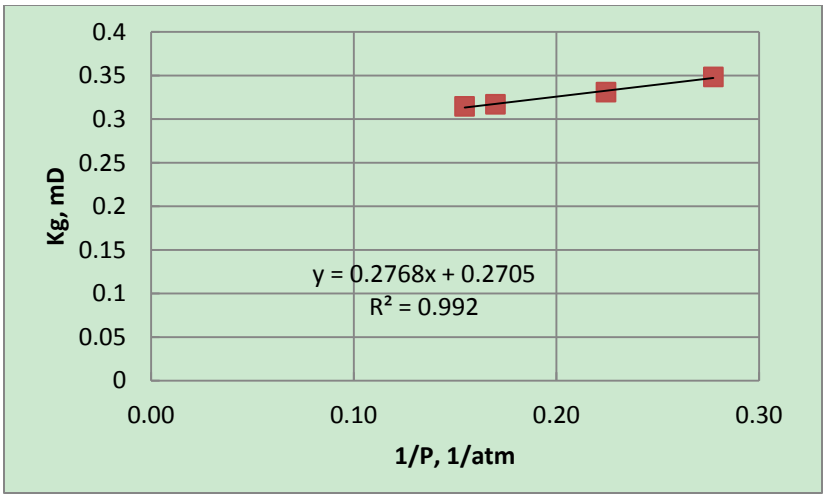

Figure C.15. TS21 gas phase permeability after treated with FR and/or breaker

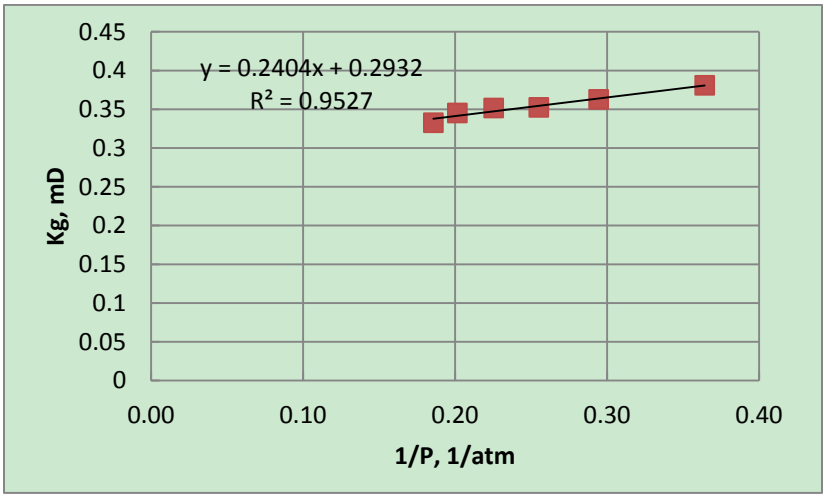

Figure C.16. TS26 gas phase permeability after treated with FR and/or breaker

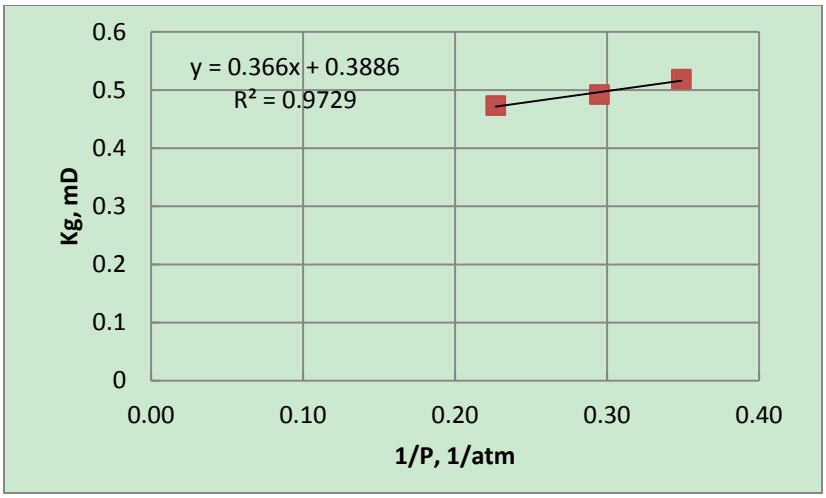

Figure C.17. TS27 gas phase permeability after treated with FR and/or breaker

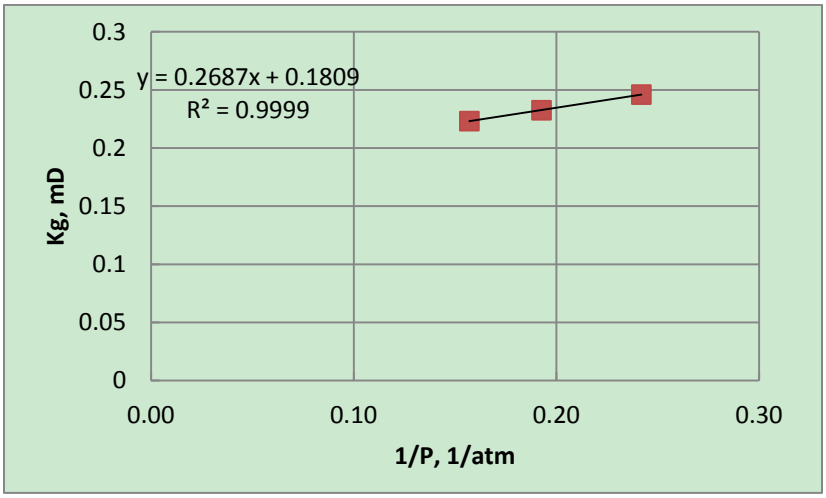

Figure C.18. TS29 gas phase permeability after treated with FR and/or breaker

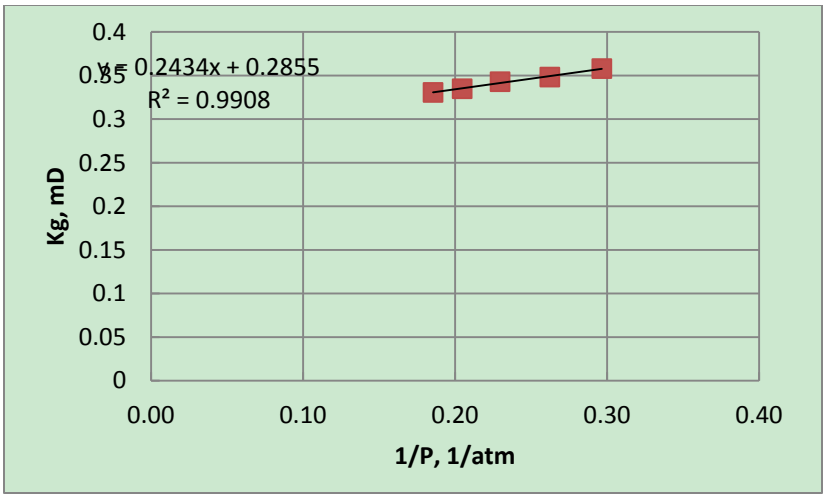

Figure C.19. TS30 gas phase permeability after treated with FR and/or breaker

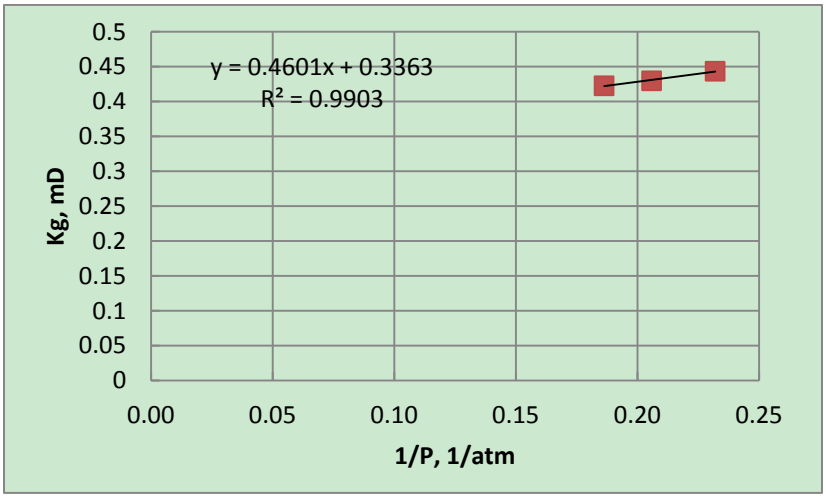

Figure C.20. TS33 gas phase permeability after treated with FR and/or breaker

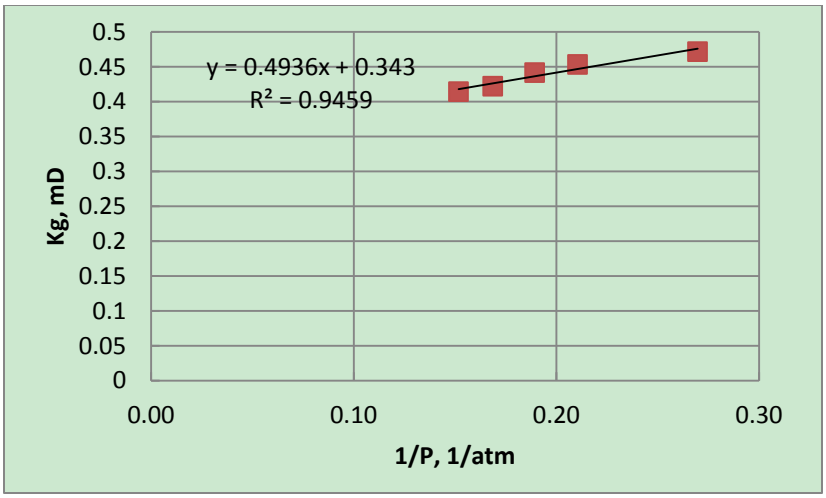

Figure C.21. TS35 gas phase permeability after treated with FR and/or breaker

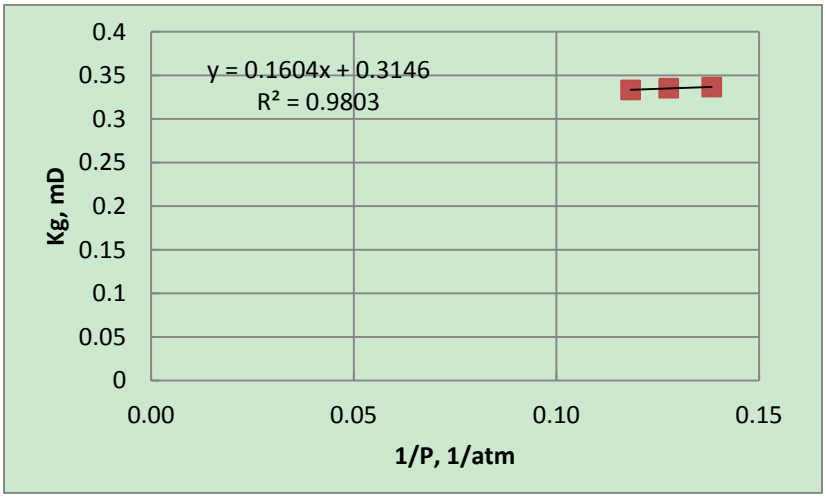

Figure C.22. TS34 gas phase permeability after treated with FR and/or breaker

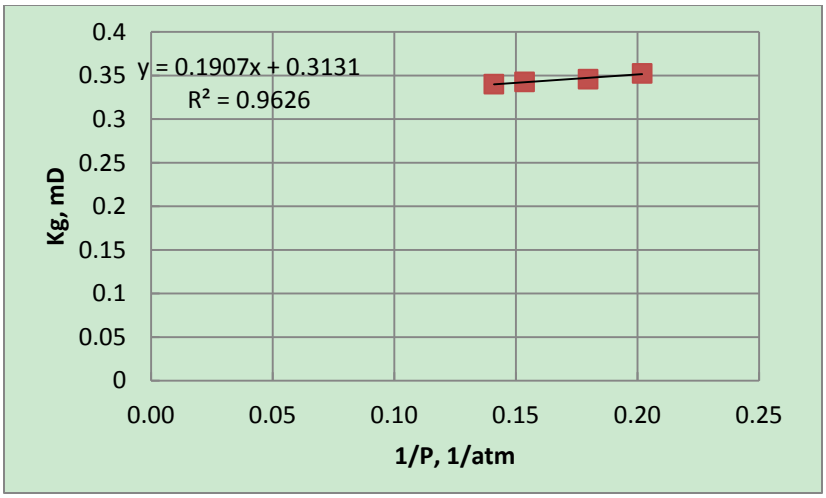

Figure C.23. TS25 gas phase permeability after treated with FR and/or breaker

BIBLIOGRAPHY

Abe, A. A. (2005). Relative Permeability and Wettability Implications of Dilute Surfactants at Reservoir Conditions, Idaho State University, Idaho, USA.

Abrams, A. and Vinegar, H. J. 1985. Impairment Mechanisms in Vicksburg Tight Gas Sands. Presented at the SPE/DOE Low Permeability Gas Reservoirs Symposium, Denver, Colorado, USA, 1985/1/1/. SPE-13883-MS. http://dx.doi.org/10.2118/13883-MS

Adibhatla, B., Mohanty, K., Berger, P. and Lee, C. 2006. Effect of surfactants on wettability of near-wellbore regions of gas reservoirs. *Journal of Petroleum Science and Engineering* 52 (1): 227-23610.1016/j.petrol.2006.03.026.

Aften, C. and Watson, W. P. 2009. Improved Friction Reducer for Hydraulic Fracturing. Presented at the SPE Hydraulic Fracturing Technology Conference, The Woodlands, Texas, USA, 19-21 January 2009. SPE-118747-MS. http://dx.doi.org/10.2118/118747-MS

Apaydin, O. G., Ozkan, E. and Raghavan, R. 2012. Effect of Discontinuous Microfractures on Ultratight Matrix Permeability of a Dual-Porosity Medium. *SPE Reservoir Evaluation & Engineering* 15 (4): pp. 473-485. SPE-147391-PA. http://dx.doi.org/10.2118/147391-PA.

Arthur, J., Bohm, B., Coughlin, B. J., Layne, M. and Cornue, D. 2009. Evaluating the environmental implications of hydraulic fracturing in shale gas reservoirs. Presented at the SPE Americas E&P Environmental and Safety Conference, San Antonio, Texas, USA, 23-25 March 2009. SPE-121038-MS. http://dx.doi.org/10.2118/121038-MS

Bai, B., Elgmati, M., Zhang, H. and Wei, M. 2012. Rock characterization of Fayetteville shale gas plays. *Fuel*

Baser, B., Shenoy, S., Gadiyar, B., Jain, S. and Parlar, M. 2010. An Alternative Method of Dealing With Pressure: Friction Reducer for Water Packing of Long Horizontal Open Holes in Low-Fracturing-Gradient Environments. *SPE Drilling & Completion* 25 (3): 300-308. SPE-123155-PA. http://dx.doi.org/10.2118/123155-PA.

Bird, R. B., Stewart, W. E. and Lightfoot, E. N. (2007). Transport phenomena, John Wiley & Sons.

Boyer, C., Kieschnick, J., Suarez-Rivera, R., Lewis, R. E. and Waters, G. 2006. Producing gas from its source. *Oilfield Review* 18 (3): 36-49

Byrnes, A. P., Sampath, K. and Randolph, P. 1979. Effect of pressure and water saturation on permeability of western tight sandstones. DOE Symposium on Enhanced Oil & Gas Recovery and Improved Drilling Technology, Tulsa, Oklahoma, USA, Aug 1979.

Carman, P. S. and Cawiezel, K. Successful Breaker Optimization for Polyacrylamide Friction Reducers Used in Slickwater Fracturing. Presented at the, 2007/1/1/. 10.2118/106162-MS

Celata, G., Cumo, M., McPhail, S. and Zummo, G. 2006. Characterization of Fluid Dynamic Behaviour and Channel Wall Effects In Microtube. *International Journal of Heat and Fluid Flow* 27 (1): 135-14310.1016/j.ijheatfluidflow.2005.03.012.

Chen, J.-H., Zhang, J., Jin, G., Quinn, T., Frost, E. and Chen, J. 2012. Capillary Condensation and NMR Relaxation Time in Unconventional Shale Hydrocarbon Resources. Presented at the SPWLA 53rd Annual Logging Symposium, Cartagena, Colombia, June 16-20 2012.

Chiquet, P., Broseta, D. F. and Thibeau, S. 2005. Capillary Alteration Of Shaly Caprocks By Carbon Dioxide. Presented at the SPE Europec/EAGE Annual Conference, Madrid, Spain, 13-16 June 2005. SPE-94183-MS. http://dx.doi.org/10.2118/94183-MS

Clark, R. A., Mullen, K. and Stevanus, K. Adopting North American, Multi-stage Fracturing and Horizontal Completion Technologies Starts to Unlock the Amin Tight Gas Formation in the Sultanate of Oman. Presented at the, 2013/1/28/. 10.2118/164008-MS

Clarkson, C. R., Solano, N., Bustin, R., Bustin, A., Chalmers, G., He, L., Melnichenko, Y. B., Radliński, A. and Blach, T. P. 2012. Pore structure characterization of North American shale gas reservoirs using USANS/SANS, gas adsorption, and mercury intrusion. *Fuel*

Conway, M. W., Venditto, J. J. J., Reilly, P. B. and Smith, K. W. 2011. An Examination of Clay Stabilization and Flow Stability in Various North American Gas Shales. Presented at the SPE Annual Technical Conference and Exhibition, Denver, Colorado, USA 30 October-2 November 2011. SPE-147266-MS. http://dx.doi.org/10.2118/147266-MS

Curtis, J. B. 2002. Fractured shale-gas systems. *AAPG bulletin* 86 (11): 1921-1938doi: 10.1306/61EEDDBE-173E-11D7-8645000102C1865D

Dehghanpour, H., Zubair, M. H. A., Chhabra, A. and Ullah, A. Liquid Intake of Organic Shales. *Energy & Fuels*

Ding, W., Li, C., Li, C., Xu, C., Jiu, K., Zeng, W. and Wu, L. 2012. Fracture Development in Shale and Its Relationship to Gas Accumulation. *Geoscience Frontiers* 3 (1): 97-10510.1016/j.gsf.2011.10.001.

EIA. (2011). "Review of Emerging Resources: U.S. Shale Gas and Shale Oil Plays."

Elgmati, M. M., Zhang, H., Bai, B., Flori, R. E. and Qu, Q. 2011. Submicron-Pore Characterization of Shale Gas Plays. Presented at the North American Unconventional Gas Conference and Exhibition, The Woodlands, Texas, USA, 14-16 June 2011. SPE-144050-MS. http://dx.doi.org/10.2118/144050-MS

Ford, W. G. F., Penny, G. S. and Briscoe, J. E. 1988. Enhanced Water Recovery Improves Stimulation Results. *SPE Production Engineering* 3 (4): 515 - 521. SPE-15851-PA. http://dx.doi.org/10.2118/15851-PA.

Fredrich, J., Greaves, K. and Martin, J. 1993. Pore geometry and transport properties of Fontainebleau sandstone. *International journal of rock mechanics and mining sciences & geomechanics abstracts* 30 (7): 691-69710.1016/0148-9062(93)90007-Z.

Gas, T. I. (2001). Tight Gas Resource Map of the United States.

Gasparik, M., Ghanizadeh, A., Bertier, P., Gensterblum, Y., Bouw, S. and Krooss, B. M. 2012. High-Pressure Methane Sorption Isotherms of Black Shales from the Netherlands. *Energy & Fuels* 26 (8): 4995-500410.1021/ef300405g.

Georgi, D. T., Jin, G., Li, B., Mehmani, A. and Chen, J. 2013. The Condition of Capillary Condensation and Its Effects on Adsorption Isotherms of Unconventional Gas Condensate Reservoirs. Presented at the SPE Annual Technical Conference and Exhibition, New Orleans, Louisiana, USA 30 Sept.-2 Oct. 2013. SPE-166162-MS. http://dx.doi.org/10.2118/166162-MS

Grieser, B., Hobbs, J., Hunter, J. and Ables, J. 2003. The Rocket Science Behind Water Frac Design. Presented at the SPE Production and Operations Symposium, Oklahoma City, Oklahoma, USA, 22-25 March 2003. SPE-80933-MS. http://dx.doi.org/10.2118/80933-MS

Henares, T. G., Mizutani, F., Sekizawa, R. and Hisamoto, H. 2008. “Drop-and-Sip” Fluid Handling Technique for the Reagent-Release Capillary (RRC)-based Capillary-Assembled Microchip (CAs-CHIP): Sample Delivery Optimization and Reagent Release Behavior in RRC. *Analytical Sciences* 24 (1): 127-13210.2116/analsci.24.127.

Hjertén, S. and Kiessling-Johansson, M. 1991. High-Performance Displacement Electrophoresis in 0.025-To 0.050-Mm Capillaries Coated With a Polymer To Suppress Adsorption And Electroendosmosis. *Journal of Chromatography A* 550: 811-82210.1016/S0021-9673(01)88584-8.

Humphrey, M., Istok, J., Flint, L. and Flint, A. 1996. Improved method for measuring water imbibition rates on low-permeability porous media. *Soil Science Society of America Journal* 60 (1): 28-3410.2136/sssaj1996.03615995006000010007x.

Kaufman, P. B., Penny, G. S. and Paktinat, J. 2008. Critical Evaluation of Additives Used in Shale Slickwater Fracs. Presented at the SPE Shale Gas Production Conference, Fort Worth, Texas, USA, 16-18 November 2008. SPE-119900-MS. http://dx.doi.org/10.2118/119900-MS

Kelland, M. A. (2012). Production Chemicals for the Oil and Gas Industry, Taylor & Francis.

Kewen, L. and Abbas, F. 2000. Experimental Study of Wettability Alteration to Preferential Gas-Wetting in Porous Media and Its Effects. *SPE Reservoir Evaluation & Engineering* 3 (2): 139 - 14910.2118/62515-PA.

King, G. E. 2010. Thirty Years of Gas Shale Fracturing: What Have We Learned? Presented at the SPE Annual Technical Conference and Exhibition, Florence, Italy, 19-22 September 2010. SPE-133456-MS. http://dx.doi.org/10.2118/133456-MS

King, G. E. 2012. Hydraulic Fracturing 101: What Every Representative, Environmentalist, Regulator, Reporter, Investor, University Researcher, Neighbor and Engineer Should Know About Estimating Frac Risk and Improving Frac Performance in Unconventional Gas and Oil Wells. Presented at the SPE Hydraulic Fracturing Technology Conference, The Woodlands, Texas, USA 6-8 February 2012. SPE-152596-MS. http://dx.doi.org/10.2118/152596-MS

Krishnamoorthy, C. and Ghajar, A. J. 2007. Single-Phase Friction Factor in Micro-Tubes: A Critical Review of Measurement, Instrumentation and Data Reduction Techniques From 1991-2006. Presented at the ASME 2007 5th International Conference on Nanochannels, Microchannels, and Minichannels, Puebla, Mexico 18–20 June 2007

Kundert, D. P. and Mullen, M. J. 2009. Proper Evaluation of Shale Gas Reservoirs Leads to a More Effective Hydraulic-Fracture Stimulation. Presented at the SPE Rocky Mountain Petroleum Technology Conference, Denver, Colorado, USA, 14-16 April 2009. SPE-123586-MS. http://dx.doi.org/10.2118/123586-MS

Lakatos, I., Bódi, T., Lakatos-SzabC, J. and Szentes, G. 2011. PVT Properties, Wettability and Capillary Forces in Unconventional Gas Reservoirs: Topics Rarely Visited. Presented at the SPE Reservoir Characterisation and Simulation Conference and Exhibition, Abu Dhabi, UAE 9-11 October 2011. SPE-148157-MS. http://dx.doi.org/0.2118/148157-MS

Lakatos, I. J., Bódi, T., Lakatos-Szabó, J. and Szentes, G. 2013. Detrimental Effect of Capillary Forces in Extreme Low Permeable Unconventional Gas Reservoirs. Presented at the 17th European Symposium on Improved Oil Recovery, St. Petersburg, Russia, 16 April 2013.

Leahy-Dios, A., Das, M., Agarwal, A. and Kaminsky, R. D. 2011. Modeling of Transport Phenomena and Multicomponent Sorption for Shale Gas and Coalbed Methane in an Unstructured Grid Simulator. Presented at the SPE Annual Technical Conference and Exhibition, Denver, Colorado, USA, 30 October-2 November 2011. SPE-147352-MS. http://dx.doi.org/10.2118/147352-MS

Li, K., Chow, K. and Horne, R. N. 2002. Effect of Initial Water Saturation on Spontaneous Water Imbibition. Presented at the SPE Western Regional/AAPG Pacific Section Joint Meeting, Anchorage, Alaska, USA, 20-22 May 2002. SPE-76727-MS. http://dx.doi.org/10.2118/76727-MS

Li, K. and Horne, R. N. 2000. Characterization of Spontaneous Water Imbibition into Gas-Saturated Rocks. Presented at the SPE/AAPG Western Regional Meeting, Long Beach, California 19-22 June 2000. SPE-62552-MS. http://dx.doi.org/10.2118/62552-MS

Li, K. and Liu, X. 2007. Prediction of Recovery by Spontaneous Imbibition in Gas/Liquid/Rock Systems. Presented at the EUROPEC/EAGE Conference and Exhibition, London, U.K., 11-14 June 2007. SPE-107355-MS. http://dx.doi.org/10.2118/107355-MS

Li, K. and Zhao, H. 2012. Fractal prediction model of spontaneous imbibition rate. *Transport in porous media* 91 (2): 363-37610.1007/s11242-011-9848-0.

Lindsay, S. D., Mcneil, F., Sackash, M. J. and Bryant, J. E. 2011. Use of Salt-Tolerant Friction Reducer for Coiled-Tubing Applications in Unconventional Shale Formations. Presented at the SPE/ICoTA Coiled Tubing & Well Intervention Conference and Exhibition, The Woodlands, Texas, USA, 5-6 April 2011. SPE-142064-MS. http://dx.doi.org/10.2118/142064-MS

Luffel, D. L. and Guidry, F. K. 1992. New Core Analysis Methods for Measuring Reservoir Rock Properties of Devonian Shale. *Journal of Petroleum Technology* 44 (11): 1,184 - 181,190. SPE-20571-PA. http://dx.doi.org/10.2118/20571-PA.

Luffel, D. L., Hopkins, C. W. and Schettler, P. D., Jr. 1993. Matrix Permeability Measurement of Gas Productive Shales. Presented at the SPE Annual Technical Conference and Exhibition, Houston, Texas, USA, 3-6 October 1993. SPE-26633-MS. http://dx.doi.org/10.2118/26633-MS

MacBeth, C. and Schuett, H. 2007. The stress dependent elastic properties of thermally induced microfractures in aeolian Rotliegend Sandstone. *Geophysical Prospecting* 55 (3): 323-33210.1111/j.1365-2478.2007.00601.x.

Malayalam, A., Faz, I., Gangopadhyay, A. K., Liu, S., Plemons, P. and Rodrigues, V. Multidisciplinary Insights From Analysis of Borehole Microseismic Data From the Cotton Valley Tight Gas Formation in East Texas, U.S.A. Presented at the, 2013/1/28/. 10.2118/163970-MS

Malpani, R. V. 2007. Selection of fracture fluid for stimulating tight gas reservoirs.

Mayerhofer, M. J. and Meehan, D. N. Waterfracs - Results from 50 Cotton Valley Wells. Presented at the, 1998/1/1/. 10.2118/49104-MS

Nelson, P. H. 2009. Pore-Throat Sizes in Sandstones, Tight Sandstones, and Shales. *AAPG bulletin* 93 (3): 32910.1306/10240808059.

Odusina, E. O., Sondergeld, C. H. and Rai, C. S. 2011. An NMR Study of Shale Wettability. Presented at the Canadian Unconventional Resources Conference, Alberta, Canada, 30 October-1 November 2012. SPE-147371-MS. http://dx.doi.org/10.2118/147371-MS

Paktinat, J., O'Neil, B. J., Aften, C. W. and Hurd, M. D. 2011. Critical Evaluation of High Brine Tolerant Additives Used in Shale Slick Water Fracs. Presented at the SPE Production and Operations Symposium, Oklahoma City, Oklahoma, USA, 27-29 March 2011. 141356. http://dx.doi.org/10.2118/141356-ms

Paktinat, J., O'Neil, B. J., Aften, C. W. and Hurd, M. D. 2011. High Brine Tolerant Polymer Improves the Performance of Slickwater Frac in Shale Reservoirs. Presented at the North American Unconventional Gas Conference and Exhibition, The Woodlands, Texas, USA, 14-16 June 2011. SPE-144210-MS. http://dx.doi.org/10.2118/144210-MS

Paktinat, J., O'Neil, B. J. and Tulissi, M. G. 2011. Case Studies: Impact of High Salt Tolerant Friction Reducers on Freshwater Conversation in Canadian Shale Fracturing Treatments. Presented at the Canadian Unconventional Resources Conference, Alberta, Canada, 15-17 November 2011. SPE-149272-MS. http://dx.doi.org/10.2118/149272-MS

Paktinat, J., Pinkhouse, J. A., Little, J. B., Lash, G. G. and Penny, G. S. 2007. Investigation of Methods to Improve Utica Shale Hydraulic Fracturing in the Appalachian Basin. Presented at the Eastern Regional Meeting, Lexington, Kentucky USA 17-19 October 2007. SPE-111063-MS. http://dx.doi.org/10.2118/111063-MS

Palisch, T., Vincent, M. and Handren, P. 2010. Slickwater Fracturing: Food for Thought. *SPE Production & Operations* 25 (3): 327-344. SPE-115766-PA. http://dx.doi.org/10.2118/115766-PA.

Perez, R., Benish, T. G., Boyer, M., Adeyeye, A. and Wieland, D. Multizone Tight Gas Completions in the Piceance Basin: Over a Decade of Learnings. Presented at the, 2013/3/26/. 10.2523/17129-MS

PSU. (2008). "Unconventional natural gas reservoir could boost U.S. supply." Retrieved July, 3, 2014, from http://news.psu.edu/story/191364/2008/01/17/unconventional-natural-gas-reservoir-could-boost-us-supply.

Qi, Z. Y., Wang, Y. F. and Xu, X. L. 2014. Effects of Interfacial Tension Reduction and Wettability Alteration on Oil Recovery by Surfactant Imbibition. *Advanced Materials Research* 868: 664-66810.4028/www.scientific.net/AMR.868.664.

Rae, P. and Di Lullo, G. 1996. Fracturing Fluids and Breaker Systems - A Review of the State-of-the-Art. Presented at the SPE Eastern Regional Meeting, Columbus, Ohio, USA, 23-25 October 1996. SPE-37359-MS. http://dx.doi.org/10.2118/37359-MS

Ram, A., Finkelstein, E. and Elata, C. 1967. Reduction of Friction in Oil Pipelines by Polymer Additives. *Industrial & Engineering Chemistry Process Design and Development* 6 (3): 309-31310.1021/i260023a009.

Rimassa, S. M., Howard, P. and Arnold, M. O. 2009. Are You Buying Too Much Friction Reducer Because of Your Biocide? Presented at the SPE Hydraulic Fracturing Technology Conference, The Woodlands, Texas, USA, 19-21 January 2009. SPE-119569-MS. http://dx.doi.org/10.2118/119569-MS

Rimassa, S. M., Howard, P. R. and Blow, K. A. 2009. Optimizing Fracturing Fluids From Flowback Water. Presented at the SPE Tight Gas Completions Conference, San Antonio, Texas, USA, 15-17 June 2009. SPE-125336-MS. http://dx.doi.org/10.2118/125336-MS

Ross, D. J. and Marc Bustin, R. 2007. Impact of mass balance calculations on adsorption capacities in microporous shale gas reservoirs. *Fuel* 86 (17): 2696-2706

Roychaudhuri, B., Tsotsis, T. and Jessen, K. 2013. An experimental investigation of spontaneous imbibition in gas shales. *Journal of Petroleum Science and Engineering* 111: 87-9710.1016/j.petrol.2013.10.002.

Roychaudhuri, B., Tsotsis, T. T. and Jessen, K. 2011. An Experimental and Numerical Investigation of Spontaneous Imbibition in Gas Shales. Presented at the SPE Annual Technical Conference and Exhibition, Denver, Colorado, USA 30 October-2 November 2011. SPE-147652-MS. http://dx.doi.org/10.2118/147652-MS

Rushing, J. A., Newsham, K. E. and Blasingame, T. A. 2008. Rock Typing: Keys to Understanding Productivity in Tight Gas Sands. Presented at the SPE Unconventional Reservoirs Conference, Keystone, Colorado, USA 10-12 February 2008. SPE-114164-MS. http://dx.doi.org/10.2118/114164-MS

Sarwar, M. U., Cawiezel, K. E. and Nasr-El-Din, H. A. 2011. Gel Degradation Studies of Oxidative and Enzyme Breakers to Optimize Breaker Type and Concentration for Effective Break Profiles at Low and Medium Temperature Ranges. Presented at the SPE Hydraulic Fracturing Technology Conference, The Woodlands, Texas, USA 24-26 January 2011. 10.2118/140520-MS

Schlichting, H. and Gersten, K. (2004). Boundary-layer theory, Springer.

Seright, R., Fan, T., Wavrik, K. and Balaban, R. 2011. New Insights into Polymer Rheology in Porous Media. *SPE Journal* 16 (1): 35-42. SPE-129200-PA. http://dx.doi.org/10.2118/129200-PA.

Shah, S. N. and Kamel, A. H. A. 2010. Investigation of Flow Behavior of Slickwater in Large Straight and Coiled Tubing. *SPE Production & Operations* 25 (1): 70-79. SPE-118949-PA. http://dx.doi.org/10.2118/118949-PA.

Sharp, K. V. and Adrian, R. J. 2004. Transition from laminar to turbulent flow in liquid filled microtubes. *Experiments in Fluids* 36 (Compendex): 741-747

Sheng, J. (2010). Modern Chemical Enhanced Oil Recovery: Theory and Practice, Gulf Professional Publishing.

Sondergeld, C. H., Ambrose, R. J., Rai, C. S. and Moncrieff, J. 2010. Micro-Structural Studies of Gas Shales. Presented at the SPE Unconventional Gas Conference, Pittsburgh, Pennsylvania, USA 23-25 February 2010. SPE-131771-MS. http://dx.doi.org/10.2118/131771-MS

Sondergeld, C. H., Newsham, K. E., Comisky, J. T., Rice, M. C. and Rai, C. S. 2010. Petrophysical Considerations in Evaluating and Producing Shale Gas Resources. Presented at the SPE Unconventional Gas Conference, Pittsburgh, Pennsylvania, USA 23-25 February 2010. SPE-131768-MS. http://dx.doi.org/10.2118/131768-MS

Song, F.-Q., Wang, J.-D. and Liu, H.-L. 2010. Static Threshold Pressure Gradient Characteristics of Liquid Influenced by Boundary Wettability. *Chinese Physics Letters* 27: 02470410.1088/0256-307X/27/2/024704.

Sun, H., Stevens, R. F., Cutler, J. L., Wood, B., Wheeler, R. S. and Qu, Q. 2010. A Novel Nondamaging Friction Reducer: Development and Successful Slickwater Frac Applications. Presented at the Tight Gas Completions Conference, San Antonio, Texas, USA, 2-3 November 2010. SPE-136807-MS. http://dx.doi.org/10.2118/136807-MS

Sun, H., Wood, B., Stevens, R. F., Cutler, J., Qu, Q. and Lu, M. 2011. A Nondamaging Friction Reducer for Slickwater Frac Applications. Presented at the SPE Hydraulic Fracturing Technology Conference, The Woodlands, Texas, USA, 24-26 January 2011. SPE-139480-MS. http://dx.doi.org/10.2118/139480-MS

Sun, Y., Saleh, L. and Bai, B. (2012). Measurement and Impact Factors of Polymer Rheology in Porous Media. Rheology. Croatia, InTech: 187-202.

Sun, Y., Wu, Q., Bai, B. and Ma, Y. 2013. The Flow Behavior of Friction Reducer in Microchannels During Slickwater Fracturing. Presented at the SPE Production and Operations Symposium, Oklahoma City, Oklahoma, USA SPE-164476-MS. http://dx.doi.org/10.2118/164476-MS

Tang, G.-Q. and Firoozabadi, A. 2002. Relative Permeability Modification in Gas/Liquid Systems Through Wettability Alteration to Intermediate Gas Wetting. *SPE Reservoir Evaluation & Engineering* 5 (6): 427 - 43610.2118/81195-PA.

Tiab, D. and Donaldson, E. C. (2011). Petrophysics: theory and practice of measuring reservoir rock and fluid transport properties, Gulf professional publishing.

Tinni, A., Fathi, E., Agarwal, R., Sondergeld, C. H., Akkutlu, I. Y. and Rai, C. S. (2012). Shale permeability measurements on plugs and crushed samples. SPE Canadian Unconventional Resources Conference. Calgary, Alberta, Canada, Society of Petroleum Engineers.

Tjon-Joe-Pin, R., Brannon, H. D. and Rickards, A. R. 1993. Remedial Treatment for Polymeric Damage Removal Provides Improved Well Productivity. Presented at the SPE Asia Pacific Oil and Gas Conference, Singapore 8-10 February 1993. SPE-25385-MS. http://dx.doi.org/10.2118/25385-MS

Tschirhart, N. R. (2005). The evaluation of waterfrac technology in low-permeability gas sands in the East Texas basin, Texas A&M University.

Van Gijtenbeek, K. A. W., Neyfeld, A. P. and Prudnikova, A. 2006. One Molar Salt Solutions used for Clay Control in Waterbased Frac Fluids in West Siberia. Presented at the SPE Russian Oil and Gas Technical Conference and Exhibition, Moscow, Russia 2006/1/1/. SPE-101203-MS. http://dx.doi.org/10.2118/101203-MS

Wang, D., Butler, R., Liu, H. and Ahmed, S. 2011. Flow-rate behavior and imbibition in shale. *SPE Reservoir Evaluation & Engineering* 14 (04): 485-492

Wang, D., Butler, R., Liu, H. and Ahmed, S. 2011. Flow-Rate Behavior and Imbibition in Shale. *SPE Reservoir Evaluation & Engineering* 14 (04): 485 - 49210.2118/138521-PA.

Wang, F., Yue, X. A., Xu, S. L., Zhang, L. J., Zhao, R. B. and Hou, J. R. 2009. Influence of Wettability on Flow Characteristics of Water through Microtubes and Cores. *Chinese Science Bulletin* 54 (13): 2256-226210.1007/s11434-009-0167-6.

Wang, F. P. 2008. Production Fairway: Speed Rails in Gas Shales. Presented at the 7th Annual Gas Shales Summit, Dallas, TX, USA, 6-7 May, 2008.

Wang, F. P. and Reed, R. M. 2009. Pore Networks and Fluid Flow in Gas Shales. Presented at the SPE Annual Technical Conference and Exhibition, New Orleans, Louisiana, USA, 4-7 October 2009. SPE-124253-MS. http://dx.doi.org/10.2118/124253-MS

Wang, G., He, D., Wang, S. and Cheng, L. 2013. Characteristics of the pore structure and storage capability of Sulige tight sandstone gasfield. *ACTA PETROLEI SINICA* 34 (4): 660-66610.7623/syxb201304005.

Wells, J. D. and Amaefule, J. O. 1985. Capillary Pressure and Permeability Relationships in Tight Gas Sands. Presented at the SPE/DOE Low Permeability Gas Reservoirs Symposium, Denver, Colorado, USA, 19-22 March, 2003. SPE-13879-MS. http://dx.doi.org/10.2118/13879-MS

White, C. M. and Mungal, M. G. 2008. Mechanics and Prediction of Turbulent Drag Reduction with Polymer Additives. *Annual Review of Fluid Mechanics* 40: 235-25610.1146/annurev.fluid.40.111406.102156.

White, G. L. 1964. Friction Pressure Reducers in Well Stimulation. *Journal of Petroleum Technology* 16 (8): 865 - 86810.2118/802-PA.

Woodworth, T. R. and Miskimins, J. L. Extrapolation of Laboratory Proppant Placement Behavior to the Field in Slickwater Fracturing Applications. Presented at the, 2007/1/1/. 10.2118/106089-MS

Wu, S. and Firoozabadi, A. 2011. Simultaneous Increase in Gas and Liquid Relative Permeabilities and Reduction of High-Velocity Coefficient From Wettability Alteration. *Journal of Canadian Petroleum Technology* 50 (2): 17 - 2310.2118/144637-PA.

Wyant, R. E., Perkins, T. K. and Moore, T. F. (1964). Borate-gum gel breakers. United States, Google Patents.

Yang, Y., Hu, G. and Kremer, A. Using Prefrac Test Information to Predict and Avoid Screenout Associated With Slickwater Frac in Tight Gas Sands at the Wattenberg Field in the Denver-Julesburg Basin. Presented at the, 2008/1/1/. 10.2118/115214-MS

Yu, M. and Lau, H.-C. 2013. Production Technology Challenges of Tight and Shale Gas Production in China. Presented at the International Petroleum Technology Conference, Beijing, China 26-28 March 2013. 10.2523/17096-MS

Zelenev, A. S., Gilzow, G. A. and Kaufman, P. B. 2009. Fast Inverting, Brine and Additive Tolerant Friction Reducer for Well Stimulation. Presented at the SPE International Symposium on Oilfield Chemistry, The Woodlands, Texas, USA, 20-22 April 2009. SPE-121719-MS. http://dx.doi.org/10.2118/121719-MS

Zhang, S., Klimentidis, R. E. and Barthelemy, P. 2011. Porosity and Permeability Analysis on Nanoscale FIB-SEM 3d Imaging of Shale Rock. Presented at the International Symposium of the Society of Core Analysts, Austin, Texas, USA, 18-21 September 2011.

Zhou, J., Sun, H., Stevens, R. F., Qu, Q. and Bai, B. 2011. Bridging the Gap between Laboratory Characterization and Field Applications of Friction Reducers. Presented at the SPE Production and Operations Symposium, Oklahoma City, Oklahoma, USA, 27-29 March 2011. SPE-140942-MS. http://dx.doi.org/10.2118/140942-MS

VITA

Yongpeng Sun was born on Jan, 30, 1985 in Jilin, China. He received his Bachelor of Science degree in Petroleum Engineering from Southwest Petroleum University at Sichuan, China in 2007. Then he studied at China University of Petroleum at Beijing, China, and received Master of Science degree in Hydrodynamic in 2010. In Aug 2014, he will receive his Doctor of Philosophy in Petroleum Engineering from Missouri University of Science and Technology at Rolla, Missouri.